POLYTECHNIQUE MONTRÉAL
affiliée à l'Université de Montréal

Simultaneous Data Communication and Power Transfer Technique with Multiport Interferometric Receiver

TONGFENG GUO
Département de Génie électrique

Mémoire présenté en vue de l'obtention du diplôme de *Maîtrise ès sciences appliquées*

Génie Électrique

Août 2020

POLYTECHNIQUE MONTRÉAL
affiliée à l'Université de Montréal

Ce mémoire intitulé :

Simultaneous Data Communication and Power Transfer Technique with Multiport Interferometric Receiver

présenté par **Tongfeng GUO**
en vue de l'obtention du diplôme de *Maîtrise ès sciences appliquées*
a été dûment accepté par le jury d'examen constitué de :

Mohammad SHARAWI, président
Ke WU, membre et directeur de recherche
Djerafi TAREK, membre

DEDICATION

To my family

ACKNOWLEDGEMENTS

First of all, I would like to express my gratitude to my supervisor Dr. Ke Wu who gave me the opportunity to pursue the master studies at École Polytechnique de Montréal. His passion for research, patience, and innovative ideas have impressed me and driven me to explore new space in our field and accomplish this thesis research.

I would like to thank all the jury members of my dissertation committee for their time and efforts in reviewing my thesis and providing me valuable comments.

I would also like to thank all the personnel at the Poly-Grames Research Center, in particular the technical staff including Mr. Jules Gauthier, Mr. Steve Dubé, Mr. Maxime Thibault, and Mr. Traian Antonescu, for their great work in circuit fabrication and measurement. My gratitude is extended to Mrs. Rachel Lortie and Nathalie Lévesque for their administrative services and to Mr. Jean- Sébastien Décarie for his IT support.

I am indebted to all my student colleagues for their professional advice, in particular Xiangqiang Gu, Kai Wang, Wentao Lin, Ben You, Dongze Zheng, Desong Wang, Ruizhi Liu and Chunmei Liu. It is a great pleasure to study and work with them. I am grateful to all the advice and help from my friends. They gave me the feeling of being at home when I was staying in Montreal.

Last but not least, I would like to thank my parents, who gave me the birth and brought me up. They have always been supporting me, listening to me and loving me.

RÉSUMÉ

Le problème de la communication est généralement présenté comme un problème de transmission d'un message généré d'un point a un autre. Certains systèmes de communication modernes souffrent de contraintes énergétiques sévères. Avec le développement rapide des systèmes électroniques sans fil de faible puissance, d'innombrables activités de recherche ont été menées en vue d'explorer la faisabilité d'une alimentation à distance ou sans fil de ces systèmes. Par conséquent, la transmission d'énergie sans fil (WPT) est en cours de développement en tant que technique prometteuse pour alimenter des appareils électroniques à distance et pour prolonger la durée de vie des réseaux sans fil à contrainte d'énergie. Parmi les énergies renouvelables récoltées dans l'environnement, les signaux RF rayonnés par les émetteurs peuvent être une ressource viable pour le transfert d'énergie sans fil, tandis que les signaux RF ont été largement utilisés comme véhicule pour la transmission d'informations sans fil (WIT). Par conséquent, le transfert simultané d'informations et la plateforme de transfert de puissance sans fil (SWIPT) deviennent bénéfiques, car il réalise les deux utilisations utiles des signaux RF en même temps et il offre ainsi potentiellement une grande commodité aux utilisateurs mobiles.

L'antenne redresseuse, qui combine des fonctionnalités du redresseur et de l'antenne, est un élément clé pour la transmission et la récolte d'énergie sans fil. L'efficacité de conversion du circuit de redressement détermine les performances globales de l'antenne redresseuse. Par conséquent, pour concevoir une antenne redresseuse à haute efficacité qui peut garantir la qualité d'un système WPT, il convient de se concentrer davantage sur l'investigation, l'analyse et le développement de redresseurs axés sur les performances en référence à une efficacité de conversion radio fréquence à courant continu. D'un autre côté, les circuits redresseurs peuvent simplement récupérer l'énergie et ils ne peuvent pas décoder le signal transmis pour fins de communication. Cependant, la transmission de données est une exigence essentielle des systèmes de communication sans fil. Par conséquent, si la capacité de détection et de traitement du signal peut être ajoutée à une architecture antenne redresseuse, un récepteur avec transmission de puissance sans fil et communication de données simultanées peut être réalisé.

Ce mémoire vise à étudier et à démontrer un récepteur de multifonction et de multiport qui a la capacité de collecter simultanément l'énergie sans fil et les données de communication fonctionnant à la fréquence des microondes. Pour atteindre ces objectifs, il devient intéressant lorsqu'une seule chaine de récepteurs est capable à la fois de convertir l'énergie radiofréquence

en courant continu, tout en convertissant en même temps le signal modulé RF en bande de bases (BB) signe. Par conséquent, la méthodologie fondamentale pour recevoir le signal RF et convertir le signal en BB tout en récoltant simultanément la puissance est dérivée et analysée. L'objectif peut être atteint potentiellement en utilisant un signal à deux tones avec un redresseur-récepteur intégré (IRR) proposé dans ce mémoire.

De plus, l'architecture du récepteur sans fil est étudiée, conçue et démontrée afin d'accomplir la transmission d'énergie simultanée anticipée sans fil et la communication de données. Compte tenu des caractéristiques souhaitables pour le développement de récepteurs sans fil, telles qu'une faible consommation d'énergie, une structure simple et des structures à faible coût, l'interféromètre multisport est sélectionné comme une approche appropriée pour développer un tel récepteur. Pour ce faire, différentes structures d'une jonction à six ports sont étudiées et une configuration appropriée de jonction à six ports microruban fonctionnant à 2,45 GHz est conçue et prototypée. De plus, un IRR spécifique à haut rendement fonctionnant à faible puissance d'entrée avec la capacité d'extraire complète de la génération de puissance en courant continu et de décodage du signal modulé de réception est conçu et connecté à la jonction à six ports pour réaliser la communication à six ports et le récepteur d'alimentation.

Enfin, la simulation ADS du récepteur à six ports avec fonction de récupération d'énergie et de détection de données est présentée et ses performances en diagramme de constellation et en taux d'erreur par bit sont comparées à celles de l'homologue conventionnel.

ABSTRACT

The problem of communication is usually cast as one of transmitting a message generated at one point to another point. Some modern communication systems are known to suffer from severe energy constraints and power consumptions. With the rapid development of low power wireless electronic systems, countless research activities have been carried out to explore the feasibility of a remote or wireless powering of those systems. Therefore, wireless power transmission (WPT) is being developed as a promising technique, for powering electronic devices over distance and for prolonging the lifetime of energy constrained wireless networks. Among the renewable energy harvested from the environment, the RF signals radiated by transmitters can be a viable resource for wireless power transfer, while RF signals have been widely used as a vehicle for wireless information transmission (WIT). Therefore, simultaneous wireless information and power transfer (SWIPT) platform becomes appealing since it realizes both useful utilizations of RF signals at the same time, and thus potentially offers great convenience to mobile users.

The rectenna, combining the functionalities of rectifier and antenna, is a key element for wireless power transmission and harvesting. The conversion efficiency of the rectifying circuit determines the overall performance of the rectenna. Therefore, to design a high-efficiency rectenna that can guarantee the quality of a WPT system, more focus should be concentrated on the investigation, analysis and development performance-driven rectifiers with reference to high RF-to-DC conversion efficiency. On the other hand, rectenna circuits can just scavenge energy and they cannot decode the transmitted signal for communication purpose. However, the data transmission is an essential requirement of wireless communication systems. Therefore, if the ability of signal detection and processing can be added to a rectenna architecture then a multi-function receiver with simultaneous wireless power transmission and data communication can be realized.

This dissertation aims to investigate and demonstrate a multi-function and multi-port receiver with the capability of simultaneous wireless energy harvesting and data communication operating at microwave frequency. To achieve these goals, it becomes interesting when a single receiver chain is able to convert the RF power to DC power, while at the same time converting the RF modulated signal to BaseBand (BB) signal. Therefore, the fundamental methodology to receive and convert the RF signal to BB while simultaneously harvesting power is derived and analyzed in this work. The aforementioned aim can be achieved theoretically by utilizing a two-tone signal with an Integrated Rectifier-Receiver (IRR) proposed

in this dissertation.

Furthermore, a wireless receiver architecture is studied, designed and demonstrated to achieve the anticipated simultaneous wireless power transmission and data communication. Considering the underlying desirable features for developing such wireless receivers as low-power consumption, simple structure, and low-cost structures, multiport interferometers are selected as a proper approach to developing such a receiver. To do so, various structures of a six-port junction are investigated and an appropriate configuration of microstrip six-port junction operating at 2.45 GHz is designed and prototyped. In addition, a special high efficiency IRR operating at low input power with the ability of fully extracting generated DC power and decoded modulated signal is designed and connected to the six-port junction to realize the proposed six-port communication and power receiver.

Finally, the ADS simulation of the six-port receiver with the features of power harvesting and data detection is presented and its performances in terms of constellation points and BER are then compared to the conventional counterpart.

TABLE OF CONTENTS

LIST OF TABLES

LIST OF FIGURES

LIST OF SYMBOLS AND ACRONYMS

ADS	Advanced Design System
AGC	Automatic Gain Control
AMPH	Ambient Microwave Power Harvesting
BB	BaseBand
BER	Bit Error Rate
BPSK	Binary Phase Shift Keying
CDMA	Code-Division Multiple Access
CMOS	Complementary Metal Oxide Semiconductor
CW	Continuous Wave
DC	Direct current
EM	Electromagnetic
FMCW	Frequency Modulation Continuous Wave
GSM	Global System for Mobile Communications
HB	Harmonic Balance
IRR	Integrated Rectifier-Receiver
LED	Light-Emitting-Diode
LNA	Low-Noise Amplifier
LO	Local Oscillator
MHMIC	Miniaturized Hybrid Microwave Integrated Circuit
MIM	Metal-Insulator-Metal
MMIC	Monolithic Microwave Integrated Circuit
OFDM	Orthogonal Frequency Division Multiplexing
PAPR	Peak to Average Power Ratio
QAM	Quadrature Amplitude Modulation
QPSK	Quadrature Phase Shift Keying
RF	Radio-Frequency
SDR	Software Defined Radio
SIW	Substrate Integrated Waveguide
SWIPT	Simultaneous Wireless Information and Power transfer
VSWR	Voltage Standing Wave Ratio
VNA	Vector Network Analyzer
WEH	Wireless Energy Harvesting
SSPS	Space Solar Power Systems

WSN	Wireless Sensing Networks
WPT	Wireless Powering Transmission
WIT	Wireless Information Transmission
ISM	Industrial-Scientific-Medical

CHAPTER 1 INTRODUCTION

1.1 Background

After Heinrich Hertz first demonstrated that electromagnetic wave could propagate in free space, radio-frequency(RF) based wireless technology has gone through a rapid development since then, acting as one of the key foundations of nowadays information society. Wireless technology can be categorized into three basic functions, namely, wireless communication, wireless sensing and wireless powering [1].

Compared to other two applications, wireless power transfer(WPT) is less known to people although it could date back to Nikola Tesla's attempt to demonstrate the feasibility of WPT using resonant coupling during his pioneering experiment more than one century ago [2].

The invention of Klystron tube and microwave cavity magnetron successfully broke the restriction of limited power source issues, thus laying a solid foundation of WPT. The modern history of power transmission has began since 1950's not only thanks to the development of WPT technology itself but also heavily due to various applications. Experiment carried out by Goubau et al., to transmit microwave power using a beam waveguide gave a theoretical direction for the WPT research afterwards [3]. The development of WPT technology led to the creation of a new term rectenna including the words of rectifier and antenna which was patented by W. C. Brown in 1969 [4]. He successfully showed that by using a rectenna attached on a model helicopter, which could receive and be driven by wireless energy coming from the ground.

Another important milestone is the solar-power satellite concept (SPS) introduced by P. Glaser in 1968, in which the energy is obtained in orbit and converted into microwave power and finally beamed to earth. Later silicon Schottky barrier diodes were proved to have better efficiency and larger power handling capability than conventional point-contact semiconductor diodes, making Schottky diodes still popular nowadays.

Presently, a large number of power-constrained wireless communication systems are used in various applications from portable entertainment systems to health care devices and wireless infrastructures. These systems are typically powered by batteries that have a limited operation time and they have to be replaced or recharged in order to guarantee the operation of a network for a certain period of time. However, the procedure of battery replacement or recharging may create an undesired expenditure and sometimes is not practical or readily unavailable (e.g., implant devices inside human bodies or for sensors embedded in building

structures). Hence, harvesting energy wirelessly from the environment can be a promising solution in providing long-lasting energy supplies for energy-constraint power-limited wireless communication systems. Usually, solar and wind are the well-known renewable energy sources for energy harvesting which may not be available continuously according to the environment, location and weather conditions. Therefore, scavenge energy from ambient RF signals can be a potential alternative in generating clean and renewable power source [5].

On the other hand, wireless communication in the past century has relied primarily on nonlinear devices to modulate and demodulate signal for wireless services. It is therefore well known that one of the most important concerns in communication systems is their power consumption so that extensive research activities are being focused to reduce the required power level of wireless communication systems through the design of low-power receiver techniques. Moreover, to develop wireless communication systems, simple structure, compact-sized, low-cost and wideband transceivers are also points of interest. Considering those mentioned requirements, multiport receiver techniques based on the principle of interferometer seem to be more practical compared to the other existing receiver configurations since their simple architectures can address most of the above-mentioned issues [6].

Besides, RF techniques have been instrumental for WIT. Since these signals that carry energy can at the same time be used as a vehicle for wirelessly transporting information, simultaneous WPT and data communication platform becomes an interesting new area of research that attracts increased attention toward the development of self-powered receivers [5]. Consequently, in this thesis we have conducted research on the far-field WPT and developed rectennas and wireless receivers with the capability of energy harvesting and data demodulation at the same time in such a way to use the same transmitted EM wave to transport both energy that is harvested at the receiver, and information that is decoded by the receiver.

1.2 Research Objectives and Methodology

1.2.1 Research objectives

The overall objective of this dissertation is to develop a wireless receiver for simultaneous wireless power transmission and data communication using the multiport technique. To be more specific, there are three main objectives as follows:

1. To investigate different configurations of a rectifier circuit and to propose a simple architecture with high RF-to-DC conversion efficiency operating at microwave frequency under low/medium RF power level;

2. To analyze different configurations of six-port junction and design one of them with minimum passive loss to transfer as much as possible RF power to detectors.

3. To propose an innovative structure of six-port receiver with the capability of simultaneous wireless power transmission and data communication.

   Besides the system design, a theoretical analysis of conversion efficiency of thermionic nonlinear devices will be investigated and a set of simplified conversion efficiency prediction techniques will be proposed. Low loss transmission line will also be considered and an optimum choice of transmission line structure could be introduced.

1.2.2 Methodology and strategy

To complete the objectives of this dissertation, we have used the following steps:

1. The required conditions to design the rectifier circuits (using Schottky diode) with high RF-to-DC conversion efficiency are examined in terms of basic diode model and circuit design. It is well known that the maximum efficiency of Schottky diode rectifiers is limited by the physical intrinsic features and the loss of the system. Therefore, the internal analysis of Schottky diodes dealing with rectifying element characteristics as well as the external analysis considering the component modeling and matching effects are investigated in detail.

2. To validate the idea of a system with the capability of simultaneous wireless power transmission and data communication, different configurations of wireless receiver are studied. Considering the desirable requirements of a wireless receiver such as low power consumption, compact-sized and low-cost, the use of a multiport technique is an appropriate solution that addresses all the above-mentioned concerns.

3. Since the designed six-port junction is used in a power harvesting structure, it has to have the minimum passive loss to transfer as much as possible RF power to detectors. To do so, one with the lowest loss is selected among the different configurations of sixport junction, designed and optimized to operate at the desirable frequency

4. The detector of interest has to generate more DC power; therefore it should act as a rectifier with a high RF-to-DC conversion efficiency. This rectifier is designed considering the required conditions such as low-power frequency with the ability of dividing the generated DC power with a specific ratio.

5. After the detection module, some part of the DC voltage is transferred to a set of the differential amplifiers to realize the I and Q data detection [7] (analog signal detection [37]) while another part of DC power is harvested.

1.3 Original Contributions

The original contributions of this dissertation can be summarized in the following:

- A novel energy harvesting system which includes a very simple rectifier with a relatively high efficiency at the low power level. To the best of our knowledge, the designed rectenna has the highest efficiency reported to date compared to the previous studies for the same level of input power.
- A new wireless receiver architecture of simultaneous wireless energy harvesting and data communication is presented. The proposed system is based on the six-port technique in connection with special modules of rectification circuit which acts as a detector and also a rectifier both to achieve data extraction and high efficient RF-to-DC rectifying functions.
- The concept of average energy harvesting efficiency is presented. This concept provides a method to calculate energy harvesting efficiency for the framework of simultaneous wireless energy harvesting and data communication

In summary, this dissertation addresses the design issues from system-level analysis to component-level design, from CAD simulation to experimental validation, as well as from original idea to prototype implementation.

1.4 Dissertation Outline

This dissertation works on the nonlinear analysis of rectifier and detector circuit, multi-port design issues for wireless receiver, and finally a system of simultaneous wireless energy harvesting and data communication. The dissertation is organized as follows:

Chapter 2 provides a general description of wireless receiver capable of energy harvesting and wireless receiver with multiport technique. It begins with the basic concept of WPT, and further concentrates on RF-to-DC conversion system. And then, the multi-port techniques and applications are introduced. In the end, wireless six-port receiver and the comparison between six-port receiver and traditional receiver are presented.

In Chapter 3, the integration problem between the rectifier and the detector is tackled to realize a system for simultaneous wireless energy harvesting and data communication. The nonlinearity of diodes is studied, and the frequency conversion characteristics of Schottky diode are analyzed. Then, the RF-to DC conversion efficiency of the rectifier and the operating mechanism of the diode detector are analyzed, respectively. Finally, the integration of rectifier and detector based on a diode using multi-tone signals is introduced.

Chapter 4 describe the design of six-port junction and rectifying circuit. Firstly, the six-port circuit theory is presented. The review of different configurations of six-port junction and extraction of the related S-parameters of each configuration are presented. Also, the design and fabrication process of a six-port junction operating at 2.45 GHz are explained and the measurement results are presented. In addition, a high-efficiency rectifier structure that operates at low input energy is designed and connected to a six-port junction so to implement a receiver. The operating principle of six-port receiver is provided and the baseband signal is recovered.

In Chapter 5, an idea of simultaneous wireless energy harvesting and data communication system based on multi-port interferometer technology is proposed. This chapter first briefly reviews the different configurations of wireless receivers and explains the reasons for choosing multi-port technology to design such systems. Based on the designed six-port network and the proposed rectifier circuit in Chapter 4, the design process of a special detector module with high RF-DC conversion efficiency is introduced. Next, the designed integrated rectifier and detector is connected to the six-port output to implement the receiver. Finally, the ADS simulation of a six-port receiver with power collection and data detection functions is introduced, and its performance in constellation diagram and BER is compared with traditional receivers. The simulation starts with the ideal component model provided in ADS and ends with a more realistic model obtained in EM simulation and measurement.

Chapter 6 summarizes the thesis work with a concise conclusion and gives some future directions of our research in this interesting area of microwave engineering.

CHAPTER 2 LITERATURE REVIEW

WPT could be categorized into three main types: Near-field WPT (inductive, capacitive and resonant reactive coupling), far-field directive power beaming WPT, and low power far-field nondirective WPT or ambient microwave power harvesting(AMPH) [8]. Near-field WPT is mainly used when the distance between power source and devices are close. And commercial products based on inductive charging has been released years ago, such as cell phone charge pad [9], and vehicle charging system [10]. This kind of WPT requires the dimension of coil is much smaller compared to the wavelength of operating frequency, and spacing between the coils is smaller than $2D^2/\lambda$, where D is the diameter of coil. So the distance between coils and position alignments will have a significant influence on the transmission efficiency [8]. Far-field directive power beaming WPT technology could date back to decades ago. A common schematic of this kind technology could be a power consuming device receiving energy from a narrow-beam antenna which is transmitting in a well-defined direction pointing to the receiver [11,12]. While power can also be transferred by a propagating electromagnetic wave, radiated and received by antennas that do not load each other because they are in each other's far fields; the efficiency of low power far-field nondirective WPT is lower but does not necessarily depend critically on placement or location [8].

2.1 Wireless receiver capable of energy harvesting

2.1.1 Far-field wireless power transmission

Far-field directive power beaming WPT, and low power far-field nondirective WPT or AMPH are completely different from near-field WPT and this dissertation work focuses on far-field wireless power transmission with the features of both directive power and lower power. Far-field power transmission is mostly related to the development of rectennas. The rectenna, or the rectifying circuit integrated with an antenna, is the most important module in long-range WPT, whose development has been reviewed in [1, 13–15].

The overall performance of a WPT system is normally determined by the efficiency of both the antenna and the related rectifier circuit. Then, it is essential to design high-efficiency rectennas to guarantee the quality of the WPT system.

In general, wireless rectennas are studied from two points of view, namely, operating frequency and RF-to-DC conversion efficiency. Most rectenna elements and rectenna arrays have been developed for frequencies below 10 GHz, especially for the ISM bands and Wi-

Fi bands which are mostly related to traditional wireless communication. For example, a rectenna with 84.4% and 82.7% RF-to-DC conversion efficiency operating at 2.45 and 5.8 GHz, respectively, was presented in [16]. The rectennas operating at low frequencies normally aim at harvesting the ambient energy from abundant Wi-Fi and other wireless signal sources. For low frequency operation, the antenna structure may be limited by its physical and aperture size although ambient electromagnetic power density is relatively high at commonly used wireless frequencies due to its wide-spread deployment for commercial applications and its relatively low-cost wireless power source generation [5].

2.1.2 RF-to-DC conversion system

In order to simplify the analysis and clearly demonstrate the power loss of each part in the wireless receiver, an efficiency chain was developed and demonstrated [17]. The total efficiency is determined by antenna efficiency, matching network efficiency, parasitic efficiency, RF-DC conversion efficiency and source-to-load efficiency [18].

Antenna efficiency

High efficient antenna design:

In [19],a high-efficiency broadband antenna was introduced for a relatively low input power scenario. This dual-polarized cross-dipole antenna covers 1.8 to 2.5 GHz and has harmonic rejection property which could further improve the efficiency by rejecting higher harmonics. Compared to rectennas with a similar size, the proposed rectenna has a higher output power under the same injecting input power condition.

Antenna array:

As another key solution to maximizing the energy reaching diode, a microstrip rectangular patch antenna array was adopted at millimeter-wave frequency [20]. In the near field measurement, the conversion efficiency of around 67% was achieved at 35.7 GHz with a 4×4 patch antenna array.

High impedance antenna:

In order to reduce the loss of matching network between an antenna and a diode commonly with a relative high impedance, high-impedance antennas were introduced in [21]. Based on the design procedures and the developed equivalent circuit, two different shaped folded diploe antennas were demonstrated, namely straight-type and card type. At the operating frequency of 535 MHz (Japanese digital TV broadcasting frequency), antennas have a characteristic

impedance of 2000 Ω with the VSWR=2 criterion.

Multiband antenna:

A broadband rectenna covering CDMA, GSM900, GSM1800 and 3G bands was demonstrated to absorb main RF energy available in the air [22]. With input impedance of 300 Ω, the folded dipole antenna was designed together with matching networks to reach a gain of 1.5 dBi over the entire band of interest.

Broadband antenna:

A broadband bent triangular omnidirectional antenna covering frequency band from 850 MHz to 1.94 GHz was demonstrated by M. Arrawatia [23]. This antenna has a VSWR $\leqslant 2$ over the covering band and designed to receive both horizontal and vertical polarized waves. A voltage of 3.76 V for open circuit and 1.38 V across a load of 4.3 $K\Omega$ could be attained when receiving energy from a cell site of 25 m away. A broadband rectifier was reported by D. Wang with a relatively bandwidth of 57% [24]. With a commercial diode HSMS 2820, efficiency performance greater than 50% was obtained when measured from 1.25 to 2.25 GHz. Furthermore, input power dynamic range greater than 14 dB which is from 12 dBm to 26 dBm was measured.

Matching networking efficiency

Adding inductors:

In a low input power level, energy harvesting efficiency becomes difficult partially due to high matching network loss. Simply placing inductors in series with the diode would help reduce the VSWR and further reduce the transmission line loss [25,26]. By adding 3 inductors between the transmission line and the diode, the power conversion efficiency rises from 22.5% to 35%. But note that an optimal number of inductors exists as adding more inductors introduce more inductor resistance loss which will reduce transmission line efficiency. In addition, one novel architecture has recently been develped to realize a broadband rectifier which operates at microwave frequencies without introducing any matching network [27]. With a high impedance inductor, such rectifier has 40% efficiency with dynamic input power range from 20 to 25 dBm over more than two decades of bandwidth.

Low loss transmission line:

For the application of millimeter wave systems, substrate integrated waveguide (SIW) technology is particularly suitable because of its natural features, such as compact size, high isolation, low radiation and leaky losses. A novel compact rectenna with a patch antenna and a schottky diode based rectifier circuit integrated inside an SIW resonator was first in-

troduced by Ana Collado [28]. But inevitable loss is generated due to reflections in the SIW cavity and discontinuity of transmission between patch antenna and rectifier circuit.

Extending input power range:

In order to extend the input power range of a rectifier but still with an acceptable matching efficiency, researchers in Singapore developed a novel dual-band rectifier [29]. By using a pHEMT, more than 30% power conversion efficiency was achievable under input power ranging from -15 to 20 dBm condition. Another approach to overcomeing the degradation of system performance with varying incident power level is using transmission line resistance compression networks (TLRCNs). T. W. Barton has derived analytical formulas for TLRCNs and developed both single and multistage rectifiers based on it [30]. This technology helps to maintain RF input impedance a constant over a wide input power range despite of variations of resistive loads. Operating at 2.45 GHz, a 4 way system has more than 50% conversion efficiency over a variation of input power level of more than 10 dB. S. H. Abdelhalem proposed a solution to extend dynamic range input matching based on varactor diodes [31]. Simply using two varactor diodes to compensate for the variations of impedance due to the change of input power and resistive loads, the authors could attain a peak efficiency of 60% with $S_{11} < -20$ dB over a more than 12 dB dynamic input power range.

Parasitic efficiency

As part of RF energy injecting diode goes through parasitic junction capacitance which will not contribute to RF-DC conversion and is dissipated in the series resistance, using spindiodes would be an alternative to minimize parasitic loss [17]. The external bias dependent resistance of such diodes could not only benefit the matching network design, but also reduce parasitic loss. Another factor helping lower the loss is that junction capacitance could be reduced and further improving the frequency performance.

RF-DC conversion efficiency

Different nonlinear components:

As we can see in [17], a well-defined analytical expression states that using diodes with higher junction resistance and lower series resistance will lead to higher RF-DC conversion efficiency. But one needs to note that such topology would bring difficulty in matching network design, further causing a decrease of overall efficiency due to matching network losses. Again spindiodes show the potential to produce stronger nonlinearity as they take advantage of both charge and spin of the electron compared to those which only use the electron charge.

Another attractive approach to using herterostructure backward tunnel diodes in rectifier design has been proved to be highly efficient in low power case [32]. Having the feature of interband tunneling which means high curvature, this diode also enables to maximize the second order nonlinearity during fabrication without any bias. It has been demonstrated that this zero-bias second-order nonlinearity is superior to the any best schottky diode could achieve. Researchers in Georgia Institute of Technology has made a breakthrough in optical rectenna which convert electromagnetic wave at optical frequency to DC [33]. The coupling between antenna and diode is realized by putting an electrode in a metal-insulator-metal (MIM) diode with a junction capacitance of around 2 aF. Stable performance of the diode was verified by exposing it to solar illumination with temperature changes from 5 to 77 °C.

Enlarge available input power:

Larger power reaching the diode will bring a higher conversion efficiency. A hybrid harvester consisting of both RF radiation and mechanical vibration power was introduced by Polytechnique Montreal [34–36]. This work proved that the combination of uncorrelated signals from RF and vibration into a diode would dramatically improve the efficiency. The experiments show up to 6 dB gain can be achieved by hybrid harvester compared to the single source harvesting. Integrated cooperative harvester capable of collecting both electromagnetic [(principally RF] and kinetic energy simultaneously was also proposed [37–39]. Besides mechanical vibration power, a solar electromagnetic rectenna was demonstrated by F. Giuppi et al. from Spain [40]. Based on a flexible substrate, both solar cells and an antenna are nicely placed although solar cells could directly obtain DC current without any rectifier. Thermal energy is also mentioned to be a potential recycling source by adopting a thermoelectric [41–43]. Harmonic wave of nonlinear device also can be employed to increase RF-to-DC conversion efficiency and achieve passive harmonic transponder [44–46]

High peak to average power ratio (PAPR) signals:

Spanish researchers showed the improvement of RF-DC efficiency, which could also benefit from pre-generated signal waveforms [47]. After testing several kinds of signal waveforms, they found that high peak to average power ratio (PAPR) signals contribute to increasing RF-DC conversion efficiency. Furthermore, researchers in Portugal developed two schemes to address the issue of amplifying large multi-sine PAPR signals simply by adopting spatial power combination [48]. One highlighted that the design is to use synchronization in mode-locked oscillators to set a phase reference for high PAPR multi-sine waveforms. This enables to maximize the RF-DC conversion efficiency.

Self-synchronous feature:

By using a self-synchronous and self-biased E-pHEMT rectifier, an extremely high efficiency peak of 88% was obtained at 16 dBm by University of Cantabria [49]. With a self-resonant drain terminating coil, this approach is used in the development of 900 MHz wireless powering links. M. Litchfield has shown that a GaN X-Band power amplifiers could operate as self-synchronous rectifiers [50]. The self-synchronous feature is realized by the finite gate-to-drain nonlinear capacitance in the intrinsic GaN HEMT providing as the feedback and further making the transistor generating RF power at the gate port possible. A RF-to-DC efficiency of 64% was obtained when the MMICs work in rectifier mode. An Enhancement-mode Pseudomorphic High Electron Mobility Transistor (E-pHEMT) based self-biased and self-synchronous class E rectifier was proposed by M.N. Ruiz in Spain [51]. The self-synchronous feature is again realized by the device gate-to-drain coupling capacitance, further shrinking the size of the design. And gate-to-source Schottky junction makes self-biasing possible to enhance the efficiency. A high-efficiency zero-voltage-switching (ZVS) AC-DC light-emitting-diode (LED) driver was proposed by J.-W. Yang [52]. By using a self-synchronous rectifier instead of an output diode, the conduction loss is reduced dramatically and circuit schematic is simplified thus reducing the cost as no additional circuit is needed due to its self-driven feature.

DC to load transfer efficiency

Detailed mathematical derivation shows the best load choice in a low power harvesting case is equal to the diode resistance [53]. At a low input power level, this is approximately considered as the junction resistance.

Boosting efficiency

In order to power post-circuitry using rectified DC current, a boost DC-DC converter is necessary to lift the magnitude of the voltage to meet the requirement under different input voltage levels with a good efficiency. Such DC-DC converter modules are commercialized for quite a long time. For example, Texas Instruments has released DC-DC converter products including a low power converter [54]. This low power converter allows voltage boosting from 1.5 V to 7.5V. Japanese researchers have proposed a buck-boost DC-DC converter in discontinuous conduction mode (DCM) which has a boosting efficiency of more than 80% for variations of loads ranging from 400 to 4000 Ω at a low input voltage of 0.8 V [55]. Integrating this boost converter with a class-F rectifier has an overall efficiency of 60% with loads changing from 100 to 5000 Ω. Similar improvement has been made by Shanghai Jiaotong University on cascaded boost-buck converter [7]. With a conversion efficiency of about 90%, such converter

is suitable for an intermediate or large input power range as switching loss will be dominant in a low power level.

2.2 Wireless receiver with multiport technique

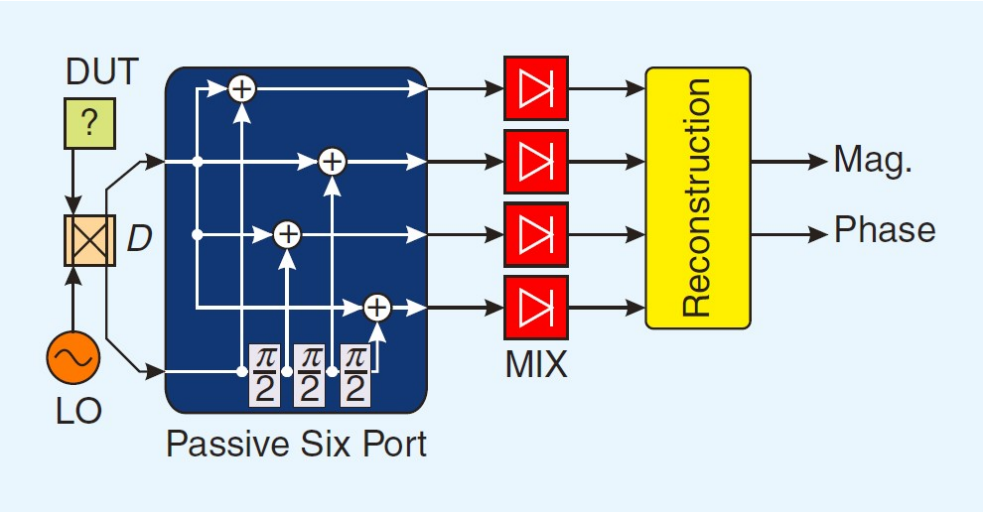

Figure 2.1 Multiport concept for use as a vector network analyzer [86].

2.2.1 Multiport technique

Engen first introduced multiport interferometer technology in the 1970s to develop accurate power measurement devices. The original work was presented in [56, 57], as shown in Figure 2.1. Soon after the first release, the principle was extended to the characterization of voltage, current, impedance, and phase, forming another network analyzer method [57]. Based on these concepts, various applications have been proposed to prove the universality of the basic multi-port concept [58].

2.2.2 Multiport applications

Because multi-port circuit technology can provide low-cost amplitude and phase measurement, it can be used for microwave network measurement. In addition, the multi-port can not only obtain network parameters, but also realize power measurement. Multi-port technology provides simultaneous power flow and impedance measurement without phase measurement. In [59] and [60], the microwave network measurement is described in detail. In addition, multi-port technology has many other applications in microwave and millimeter wave systems, where the phase and amplitude of the signal need to be measured, such as directional

instruments, reflectometers and antenna measurements. In [56], a multiport reflectometer for measuring the reflection coefficient of a load has been described. Similarly, the application potential of radar is great, especially in the automotive industry that requires low-cost, high-performance radar [61]. In addition, because multi-port architectures have low cost, long-term stability and up to 50 dB dynamic range, they seem to be suitable for antenna measurements including near-field and polarization [62,63]. Multiport technology is also used to perform non-destructive dielectric constant measurements. This technique is suitable for measuring relatively high loss dielectric liquids. In addition, multi-port technology has applications in optical systems. Early research on the use of multi-port architectures in optics was an optical reflectometer for measuring the optical complex reflection coefficient [65]. Compared with other technologies, an important advantage of this architecture is the ability to process high-power signals, so that large-signal analysis systems can be built for power amplifiers or semiconductor circuits [66].

2.2.3 Multiport receiver

The concept of a multiport receiver was first proposed in 1994, and it inspired important developments in wireless receiver design [67, 68]. The basic working principle of a multiport receiver is that the additive mixing of RF and LO or coherent interference through a passive network. Passive networks can provide two controlled relative phase and amplitude outputs for direct down conversion through diode power detectors or power readings. Therefore, because a power detector is used instead of a mixer, a multi-port receiver can increase the upper frequency limit and reduce the required power.

A millimeter-wave application of six-port demodulator in connection with homodyne and heterodyne receivers were introduced in [69].Since then, extensive research has been conducted on multiport technology and used as an alternative method of directly converting transmitters and receivers to modulate and demodulate in different modulation schemes such as BPSK, QPSK and QAM signal.

2.2.4 Comparison between Multiport Receivers and Conventional Receivers

Compared with the traditional six-port receiver, the six-port receiver has several advantages. First of all, broadband specifications can be easily obtained by constructing passive components. In addition, the homodyne technology based on power detection ensures relatively low power consumption due to relatively low driving power levels. In addition, its hardware architecture is simple and cost-effective. Therefore, a multi-port-based receiver is a convenient enhancement to a set of available receiving topologies. Especially for high frequency

and large bandwidth, they have proven to be an excellent alternative to general architecture [70]. In order to carefully verify the multi-port technology, from multiple perspectives, a benchmark has been established between the six-port receiver and the existing receiver architecture [71, 72].

RF Performance

Phase accuracy: In a conventional receiver, the phase noise of the LO is directly converted to the phase noise in the complex baseband. This phase noise causes adjacent channel interference due to mutual mixing, thereby reducing receiver selectivity. In the case of a direct conversion receiver and a six-port receiver, additional phase inaccuracies will be introduced due to inaccurate calibration. Due to the inevitable phase imbalance, phase distortion will occur [73].

Noise figure:The noise figure is usually defined by the receiver's LNA level. If no LNA is used in the structure of the receiver, the noise of the mixer can be compared with the noise of the power detector. For frequencies above 50 GHz, Schottky diodes are usually used to establish both. The noise figure of a diode mixer is close to its conversion loss, and its conversion loss is usually about 7 dB [74]. Simulations of microwave power detectors using beam-lead GaAs Schottky diodes show that for input powers less than -20 dBm, the noise figure can be less than 4.8 dB.

LO power: For most mixers, in order to obtain good conversion loss, the LO power should be in the range of 0 to 10 dBm [74]. In a six-port receiver, the appropriate condition is the LO power within the receiver input power range, which is much lower in practical applications (less than -10 dBm).

In-band dynamic range: The dynamic range of the six-port receiver is mainly determined by the accuracy of the calibration and the sensitivity of the detector. Preliminary tests show that the dynamic range is 40 dB [75, 76]. The dynamic range of mixer-based receivers is limited by linearity and a 1 dB compression point of -10 dBm to 10 dBm. For a signal bandwidth of 10 MHz, this will result in a dynamic range of approximately 90 to 100 dB. Using the AGC inserted in the LNA can increase the dynamic range of the receiver to 70 dB [69].

Self-mixing effects: Direct coupling and external reflections will produce DC offsets in direct conversion receivers and six-port receivers, because the required baseband signals and unwanted DC offsets are centered on DC and cannot be separated by filtering. The six-port receiver is less sensitive to DC offset, because this problem can be alleviated by calibration

procedures, but the direct conversion receiver needs to include some signal processing units to deal with this effect [72].

Constraints

Size: Most of the mixer-based receiver is occupied by active components and filters. The active components and filters are relatively large in size and cannot be integrated on a chip. Usually, the size of six ports is about $\frac{3}{4}\lambda$ in square. The higher the frequency, the smaller the passive six-port structure and the easier the integration in the MMIC design. For V, W and D band applications, six ports can be integrated on the chip. *Cost*: The cost of the direct conversion receiver is related to the frequency range. At high frequencies, especially in the D and W bands, mixers are expensive and rare in some cases, and power detectors can be used at higher frequencies. For the generation of millimeter wave signals, a frequency multiplier is usually followed by a lower frequency LO, which generates a smaller LO power. The six-port receiver will have a cost advantage by reducing the LO power requirements.

Based on the above comparison and discussion, it is clear that a six-port receiver is a suitable and cost-effective alternative to existing systems. In addition, it has been proven that the six-port receiver architecture is less sensitive to LO power changes and phase errors than anti-parallel diode receivers. [72].

2.3 Conclusion

This chapter has briefly review wireless receiver capable of energy harvesting and wireless receiver with multiport technique, respectively. For a WPT system, The total efficiency is determined by antenna efficiency, matching network efficiency, parasitic efficiency, RF-DC conversion efficiency and source-to-load efficiency. To realize a high efficiency rectifier, a key factor is developing low-loss diodes with higher junction resistance and low series resistance. Then six-port receiver has several advantages, such as simple structure, low power consumption, compact, low cost and broadband, which are helpful to build a WPT platform.

CHAPTER 3 INTEGRATED RECTIFIER AND RECEIVER

A diode is a two-terminal semiconductor device having a nonlinear V-I relationship. This nonlinearity can be exploited for the useful functions of signal detection, demodulation, switching, frequency multiplication, and oscillation [77]. RF and microwave diodes can be packaged as axial or beam lead components or as surface mountable chips, or be monolithically integrated with other components on a single semiconductor substrate.We first consider detector diodes and circuits, then discuss PIN diodes and control circuits, varactor diodes, and a summary of other types of diodes. Typical nonlinear relationship of diode is shown in

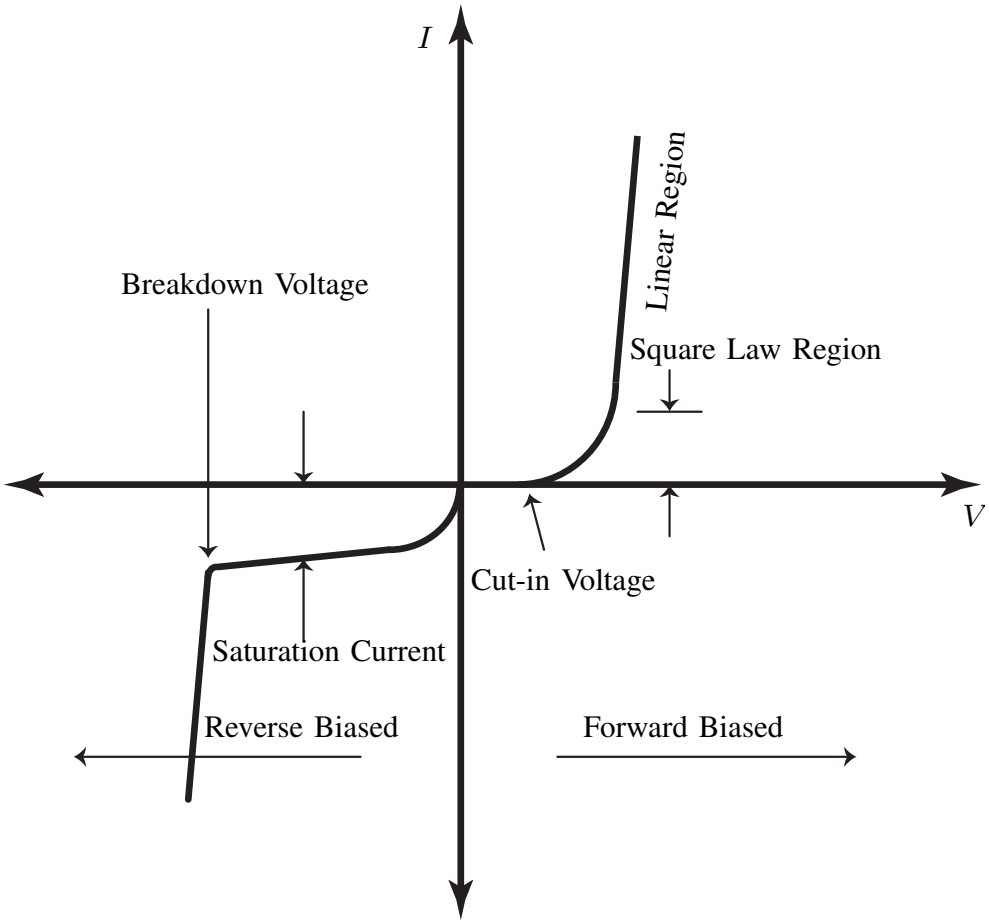

Figure 3.1 Electrical characteristics of diode

Figure 3.1. When the diode is reversely biased, very little current passes through unless the reverse breakdown voltage is exceeded. When forward biased and after exceeding the cut-in voltage, the diode begins to conduct. At low voltages, it first operates in a square law region.

Diodes operating in this region are known as small signal type. If the voltage is higher, the diode operates in a linear region, and is known as the large signal type.

3.1 Schottky Diodes

The classical PN junction diode commonly used at low frequencies has a relatively large junction capacitance that makes it unsuitable for high frequency application. The Schottky barrier diode, however, relies on a semiconductor–metal junction that results in a much lower junction capacitance [78, 79], allowing operation at higher frequencies. Commercially available microwave Schottky diodes generally use n-type gallium arsenide (GaAs) material, while lower frequency versions may use n-type silicon. Schottky diodes are often biased with a small DC forward current, but can be used without bias [80].

Generally, a Schottky diode can be applied to three basic frequency conversion operation in designing mixer, detector and rectifier circuits. However, the required features for a detector Schottky diode differ from the required specifications for a rectifier Schottky diode. Moreover, microwave rectification using Schottky diode has been widely discussed in the context of energy harvesting and WPT. In this chapter, therefore, we intend to have a closer look at Schottky barrier structure by itself in order, to integrate the detectors in rectifier for better operations.

In 1904, the first practical semiconductor device was introduced and in fact it was a metal semiconductor contact which showed a certain rectifying behavior. In 1938, Schottky suggested that the rectifying behavior could arise from a potential barrier [81]. This was later named as Schottky diode, which plays an important role in the development of high frequency electronics as rectifier. In the following, the diode operation as a rectifier is described and the design parameters for rectifier and operating mechanism of the diode detector are given. Consequently, the integration of rectifier and detector based on a diode using multi-tone signals is concluded.

A typical equivalent circuit for an RF diode is shown in Figure 3.2. The leads or contacts of the diode package are modeled as a series inductance, L_s , and shunt capacitance,C_p. Series resistor, R_s , accounts for contact and current-spreading resistance. Junction capacitance, C_j , and junction resistance, R_j , are bias dependent.

A junction diode can be modeled as a nonlinear resistor. according to [82], with a small-signal current and voltage relationship(V–I) expressed as

$$I(V) = I_s(e^{\alpha V} - 1) \tag{3.1}$$

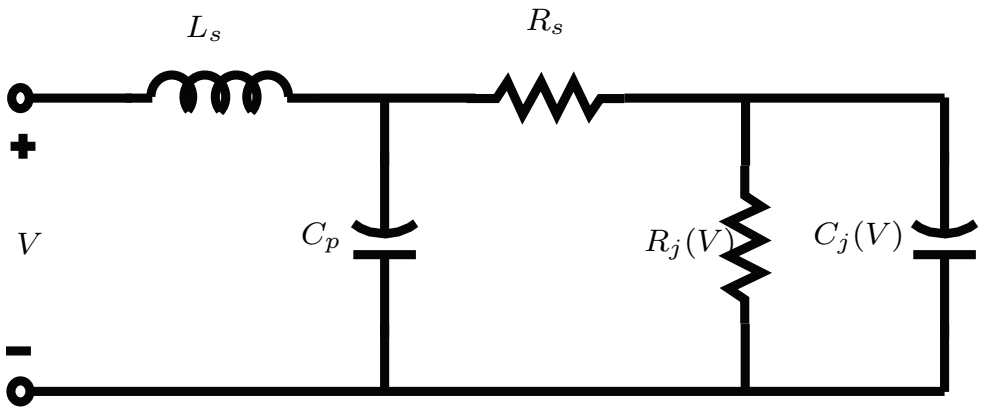

Figure 3.2 Equivalent AC circuit model for a Schottky diode.

where $\alpha = q/nkT$, and q is the charge of an electron, k is Boltzmann's constant, T is temperature, n is the ideality factor, and I_s stands for the saturation current [83, 84]. Typically, I_s is between 10^{-6} and $10^{-15}A$, and $\alpha = q/nkT$ is approximately $1/(25mV)$ for $T = 290K$. The ideality factor, n, depends on the structure of the diode, and can vary from about 1.05 for Schottky barrier diodes to about 2.0 for point-contact silicon diodes [80].

3.2 RF-to DC Conversion for Diode

At low-power level, the nonlinear part of a rectifying device cannot be considered as a simple switch, instead needs to be modeled by a variable resistance [17]. The nonlinearity of a device is inherently described by the dc voltage–current relationship. This can be expanded in power series about I_{bias}.

$$v(i) - v(I_{bias}) = \frac{v'(I_{bias})}{1!} \cdot (i - I_{bias}) + \frac{v''(I_{bias})}{2!} \cdot (i - I_{bias})^2 + \cdots \tag{3.2}$$

where v', v'', $\cdots$ are derivative of with respect to i. The three-term approximation for the diode current in (3.2) is called the small-signal approximation, and will be adequate for most of our purposes in low power range. If an RF current of magnitude A and frequency $\omega_\circ$

$$i_{\omega_\circ}(t) = A \cdot \cos(\omega_\circ t) \tag{3.3}$$

is injected into the diode, the output voltage can be calculated by replacing i by $i_{f_\circ}(t)$ in (3.2), and output diode current will be

$$v = v_{bias} + v' \cdot A \cdot \cos(\omega_\circ t) + \frac{v''}{2} \cdot (A \cdot \cos(\omega_\circ t))^2 + \cdots \tag{3.4}$$

and keeping only the term for which $\omega_\circ = 0$

$$v_{rec} = \frac{A^2}{4} \cdot \frac{d^2v}{di^2} \tag{3.5}$$

In (3.5), it is considered that no power goes to the harmonics (ideal harmonic terminations). Keeping the term depending on $\omega_\circ$ will give the RF voltage across the junction

$$v_{\omega_\circ}(t) = A \cdot \cos(\omega_\circ t) \cdot \frac{dv}{di} \tag{3.6}$$

which can be used to calculate the RF power absorbed by the junction, if we consider the later one as an integral of the product of the RF current and voltage over period T

$$P_{\omega_\circ} = \frac{1}{T} \int_0^T v_{\omega_\circ}(t) \cdot i_{\omega_\circ}(t)\, dt = \frac{A}{2} \cdot \frac{dv}{dt} \tag{3.7}$$

The ratio of the output dc voltage to the input RF power is

$$\Re = \frac{v_{rec}}{P_{\omega_\circ}} = \frac{1}{2} \cdot \frac{\frac{d^2v}{di^2}}{\frac{dv}{di}} \tag{3.8}$$

which is also called voltage responsivity [17]. Once the bias point of diode is definite, the voltage sensitivity is constant. Therefore, the output voltage of diode is always proportional to input power at the low power level(small signal input).

The open circuit voltage responsivity can be linked to the short-circuit current responsivity by the differential junction resistance [85]

$$\Re_v = \Re_i \cdot R_j \tag{3.9}$$

with $R_j = dv/di$ being the differential junction resistance depending on I_{bias}.

According to (3.1), the first derivative of 3.2 can be evaluated as

$$v' = \left.\frac{dV}{dI}\right|_{V_{bias}} = \frac{1}{\alpha(I_{bias} + I_s)} = R_d = R_j \tag{3.10}$$

where $V_{bias} = V(I_{bias})$ is the DC bias voltage. Similarly, the second derivative is

$$v'' = \left.\frac{d^2V}{dI^2}\right|_{V_{bias}} = \left.\frac{dR_d}{dI}\right|_{V_{bias}} = \frac{-1}{\alpha(I_{bias} + I_s)^2} = R_d^{'} = -\alpha R_j^2 \tag{3.11}$$

3.3 Rectifying Conversion Efficiency of Rectifier

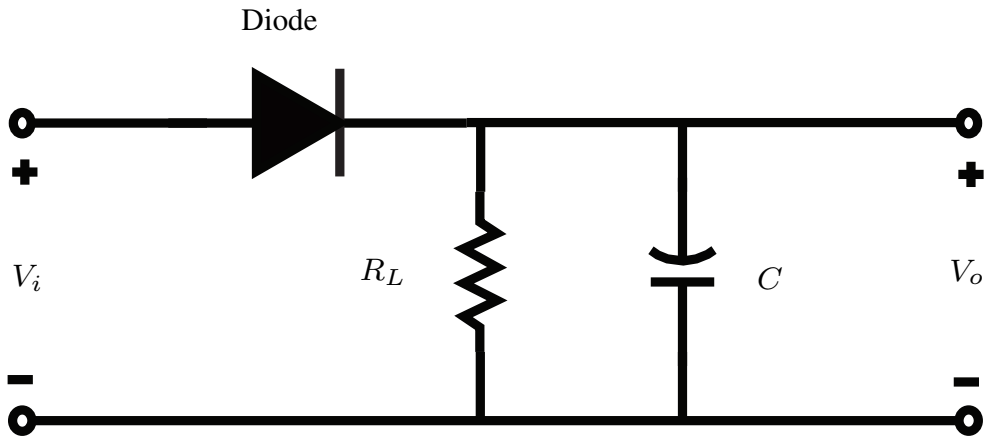

Figure 3.3 Typical rectifying circuit.

A typical but simplistic circuit for diode is shown in Figure 3.3. According to (3.5), with the RF signal passing through the diode, the generated DC power that will be dissipated in the load resistor R_L. Considering the DC circuit loop based on the small signal model in Figure 3.2, the generated DC power can then be calculated,

$$P_{DC} = \frac{v_{rect}^2}{R_v + R_L} \tag{3.12}$$

where $R_v = R_j + R_s$ is called video resistance. Combining formula (3.5), (3.7), (3.9), and (3.12), the conversion efficiency can now be calculated by the formula about junction resistance,

$$\eta_\circ = \frac{P_{\omega_\circ} \cdot \Re_{I_\circ}^2 \cdot R_j^2}{R_L + R_s + R_j} \tag{3.13}$$

We can see the rectification efficiency varies widely over the range of input voltage.Figure 3.4 gives the RF-to-DC rectification efficiency of common commercial diodes. Here, rectifiers do not contain matching circuit losses [17]. From (3.13), the conversion efficiency increases with power, which can be verified by the measured conversion efficiency of rectifier in Figure 3.4. When the input RF energy becomes higher, the nonlinearity of the diode will appear stronger. In the extreme case, if the input RF energy is high enough, the diode will operate beyond the range of small signal model. In this case, the I–V relationship curve will be described by linear range shown in Figure 3.1. In the linear operating range of diode, (3.5) will be expressed as a function of input voltage, accordingly the RF-to-DC rectification efficiency is higher. In this research work, we are primarily concerned about input RF signal at the low power level.

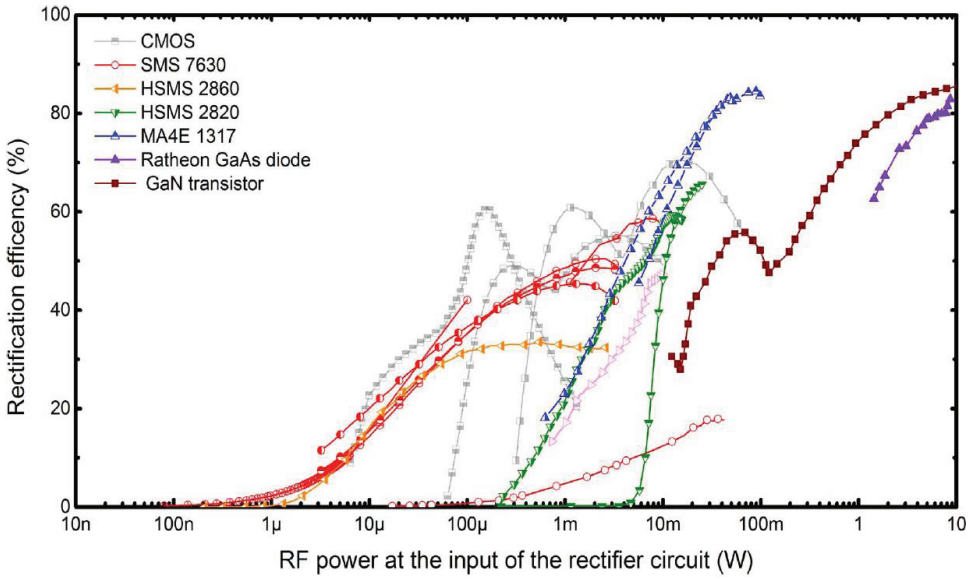

Figure 3.4 RF-to-DC conversion efficiency of state-of-the-art microwave rectifier circuits [17].

Because the signal we can employ is always relatively weak for the ambient electromagnetic energy, whatever the RF signal for communication or the waves for wireless sensor, after passing through lossy or attenuating propagation channel. Normally, the junction technology has an essential influence on the current responsivity. Therefore, one can try to select a diode with low series resistance and high junction resistance to gain optimal conversion efficiency from (3.13). From the standpoint of maximum power transmission of DC circuit loop, it is also better to use a load that is small compared to the junction resistance in order to enhance conversion efficiency.

3.4 Operating Principle for Diode Detector

Figure 3.5 show a typical diode detector circuit. A detector is used in receiver circuits to recognize the presence of signals. Typically a diode or similar device is used as a detector. Since this type of detector is unable to distinguish frequency, they may be preceded by a narrow band-pass filter which generally can be achieved by capacitance.

At very low RF voltage, say, below the knee of the diode characteristic shown in Figure 3.1, the diode exhibits the characteristics of small signal. As for diode detector, it is mainly used to demodulate an amplitude modulated RF carrier signal. Assuming a typical amplitude

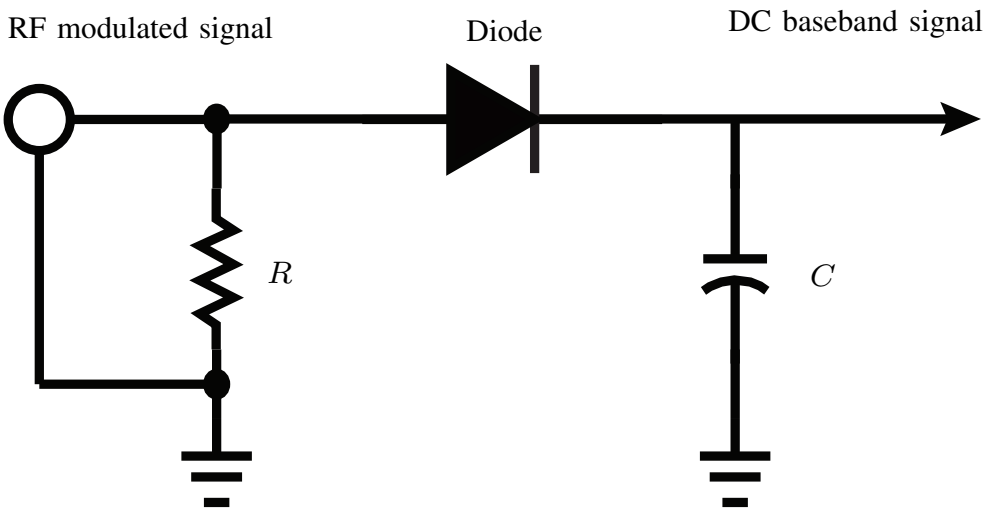

Figure 3.5 Block program of diode detector.

modulation signal in the form of a current can be expressed as

$$i(t) = i_0(1 + m\cos\omega_m t)\cos\omega_\circ t \tag{3.14}$$

where ω_m is the modulation frequency, $\omega_\circ$ is the RF carrier frequency ($\omega_\circ \gg \omega_m$), and m is defined as the modulation index ($0 \leqslant m \leqslant 1$).

For this case, the amplitude of input signal in (3.3) will become

$$A = i_0(1 + m\cos\omega_m t) \tag{3.15}$$

and put (3.15) into (3.5),we can get

$$\begin{aligned} v_{rec}^{AM} &= \frac{i_0^2}{4}\cdot\frac{d^2v}{di^2}\left[1 + \frac{m^2}{2} + 2m\cos\omega_m t + \frac{m^2}{2}\cos 2\omega_m t\right] \\ &= \frac{i_0^2}{4}\cdot R_d^{'}\left[1 + \frac{m^2}{2} + 2m\cos\omega_m t + \frac{m^2}{2}\cos 2\omega_m t\right] \end{aligned} \tag{3.16}$$

Here, the rectification voltage going through diode is calculated with respect to the carrier frequency of the modulated signal. In reality, when it comes to demodulation, the desired demodulated output of frequency ω_m is $mi_0^2R_d^{'}/2$. that is approximately proportional to the voltage square of the input RF signal, and hence the input signal power. This square-law behavior is the usual operating condition for detector diodes, but it can be obtained only over a restricted range of input power [80]. If the input power is too large, small-signal conditions will not apply, and the output will become saturated and approach a linear, and

then a constant, i versus v characteristic. On the other hand, in (3.16), the generated DC

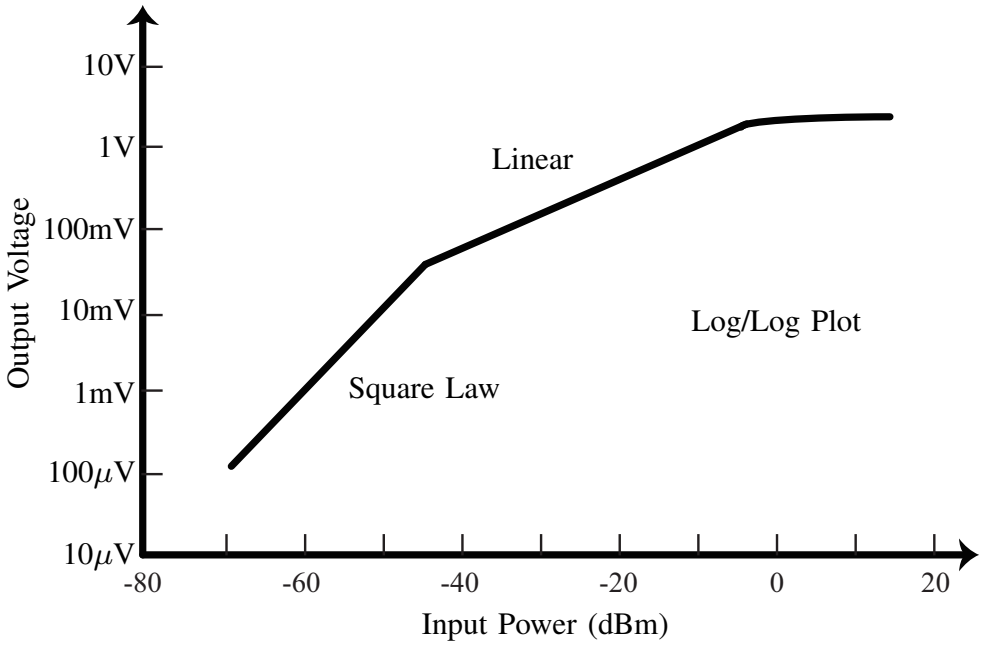

Figure 3.6 Diode Power/Voltage Characteristic.

voltage with respect to zero frequency is

$$v_{rec}^{DC} = \frac{i_0^2}{4} \cdot R_d^{'}(1 + \frac{m^2}{2}) \tag{3.17}$$

where m represents the power from the modulation while this part of power is very weak in practice. Therefore, the detector diode also can be applied to function as a rectifier. This conclusion paves the theoretical way to integrate rectifier into receiver which is the key to achieve multi-functional wireless system.

As a summary, the voltage versus power characteristics for a typical diode circuit is shown in Figure (3.6).

- Square law region (small signal)

  For very low RF voltage, below the knee of the diode characteristic, the output voltage V_o is proportional to the square of the input voltage V_i, thus V_o is proportional to the input power.

  $$P_i \propto V_o$$

- Linear region (large signal)

For higher RF voltage, above the knee, the output voltage is approximately the peak of the RF voltage, proportional to the square root of the power. In the linear detection region, the output voltage is given by:

$$P_i \propto V_o^2$$

Therefore, when a diode operates in the linear region, the diode can be used to design a rectifier to maximize the RF-to-DC conversion efficiency; when the input signal of a diode is at the lower level, the diode can be employed to design the detector to demodulate receiving communication signal as well as rectifer to harvest the receiving energy. In this research work, we are interested in the fact that at the low power level, the diode can operate as rectifier and detector simultaneously.

In reality, the square-law detection is only valid for input signals below about -20dBm. At -20dBm, input voltage across the 50-ohm resistor will only be 63.24 millivolts, peak-to-peak. DC detector output voltage will be even lower, and smaller input signals yield ever-smaller output (square-law at work). So the range of detectable signal limits input dynamic range.

3.5 Information Transmission

3.5.1 Multi-tone signal excitation

In order to analyze the nonlinear characteristics of diode with multi-tone signal excitation, we assume diode has an input voltage v_i and an output voltage v_o. In the most general case, the output response of a diode can be modeled as a Taylor series in terms of the input signal voltage [80]

$$v_o = a_o + a_1 v_i + a_2 v_i^2 + a_3 v_i^3 + a_4 v_i^4 + \cdots \tag{3.18}$$

where a_o, a_1, a_2 , ... are expansion factors which are determined by the physical electrical parameters of a diode. We assume that the excitation signal of a diode is a multi-tone signal with n number of tones defined as

$$v_{in} = \Sigma_{i=1}^{n} V_i \cos x_i \tag{3.19}$$

where $x_i = \omega_i t + \phi_i$, is determined by the frequency and the phase of the ith tone and V_i is the magnitude of the ith tone. With v_{in} exciting a diode, we can apply (3.19) into (3.18) to

get the output response of an arbitrary tone excitation for one diode:

$$\begin{aligned} v_{out} = &\sum_{i=1}^{n} \frac{a_2}{2} V_i^2 + \sum_{i=1}^{n} (a_1 V_i + \frac{3a_3}{4} V_i^3) \cos x_i \\ &+ \sum_{i=1}^{n} \frac{a_2}{2} V_i^2 \cos(2x_i) + \sum_{i=1}^{n-1} \sum_{j=1}^{n-i} a_2 V_i V_{i+j} \cdot [\cos(x_i + x_{i+j}) + \cos(x_i - x_{i+j})] + \cdots \end{aligned} \tag{3.20}$$

where standard trigonometric identities are used to expand the initial expression. We see that the output response consists of harmonics in the form of $m \cdot x_i + n \cdot y_j$ with $m, n = 0, \pm 1, \pm 2, \pm 3, \cdots$. These combinations of arbitrary two input frequencies are called intermodulation products. Actually, intermodulation products come from the nonlinear characteristics of device. We can use intermodulation products of diode with multi-tone signal excitation to modulate signal or demodulate receiving communication signal.

3.5.2 Two-tone signal excitation

In this dissertation, we primarily focus on the usage of two-tone signals where different input signals are constructed using V and ϕ. Subsequently, our analysis and simulation will focus on two-tone multisine signals.

We assume that the excitation signal of the diode is the combination of two signals operating at different frequencies, which is the simplistic form of receiving signals after passing through complicated propagation channel.

$$v_{in} = V_1 \cos x_1 + V_2 \cos x_2 \tag{3.21}$$

where $x_1 = \omega_1 t + \phi_1$ and $x_2 = \omega_2 t + \phi_2$ are determined by magnitude and phase at frequencies $\omega_1/2\pi$ and $\omega_2/2\pi$, respectively.

As shown in Figure 3.7, two additive signals together excite the diode. By employing (3.18), the signal after the nonlinear diode without any filtering, can be related to the input as follows

$$\begin{aligned} v_{out} = &\frac{a_2}{2}(V_1^2 + V_2^2) + (a_1 V_1 + \frac{3a_3}{4} V_1^3) \cos x_1 + (a_1 V_2 \\ &+ \frac{3a_3}{4} V_2^3) \cos x_2 + \frac{a_2}{2}[V_1^2 \cos(2x_1) + V_2^2 \cos(2x_2)] \\ &+ a_2 V_1 V_2 [\cos(x_1 + x_2) + \cos(x_1 - x_2)] + \cdots \end{aligned} \tag{3.22}$$

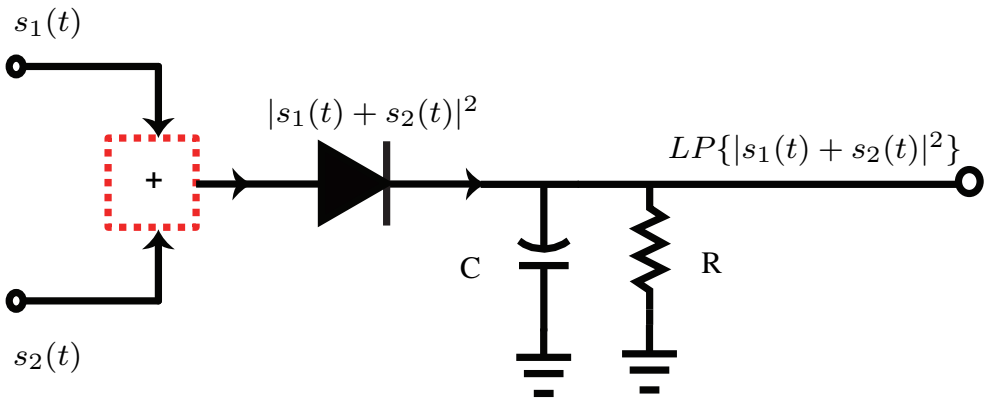

Figure 3.7 Mixing characteristics of two-tone signal excitation

where $x_1 = \omega_1 t + \phi_1$ and $x_2 = \omega_2 t + \phi_2$. By applying a lowpass filter and some simplifications, the filtered signal $V_o(t)$ reaching the output can be written as

$$\begin{aligned} V_o =& LP\{v_{out}\} \\ =& 0.5a_2V_1^2 + 0.5a_2V_2^2 + a_2V_1V_2 \cdot \cos[(\omega_1 - \omega_2)t + \phi_1 - \phi_2] \end{aligned} \tag{3.23}$$

We can define DC as the mean value of (3.23) in the corresponding envelope signal period of receiving symbol(if input excitation signal is received modulated signal). We also can define AC as the component of the first intermodulation, i.e., the coefficient of $\cos[(\omega_1 - \omega_2)t + \phi_1 - \phi_2]$. Based on our definition, DC and AC of this receiving system are

$$V_{DC}(t) = 0.5a_2V_1^2 + 0.5a_2V_2^2 \tag{3.24a}$$

$$V_{AC}(t) = a_2V_1V_2 \cdot \cos[(\omega_1 - \omega_2)t + \phi_1 - \phi_2] \tag{3.24b}$$

From the receiver's decoder point of view, AC of (3.24) can be able to contain magnitude, frequency, or phase modulation information and can be used to demodulate the received information. On the other hand, DC of (3.24) can be used to determine the magnitude of receiving signal, namely input power, and can be used to harvest received energy in term of rectifier.

3.6 Conclusion

This chapter has theoretically tackled the integration problem between the rectifier and the detector. To realize a system with the capability of simultaneous wireless energy harvesting and data communication, The nonlinearity of diodes is studied and the frequency conversion

characteristics of Schottky diode are analyzed. Then, the RF-to DC conversion efficiency of the rectifier and the operating mechanism of the diode detector are presented, respectively. Finally, the integration of rectifier and detector based on a diode using multi-tone signals is concluded.

CHAPTER 4 MULTI-PORT RECEIVER

4.1 Six-Port Technology Review

Multi-port circuits have been studied and developed since the 1970s [86–90]. It was first used by Cohn and Weinhouse to measure the phase of a microwave signal, and then developed by Engen and Hoer to obtain the complex reflection coefficients of a signal in microwave analysis. One typical multiport circuit is six-port junction. The six-port technology was further developed by Professor R. G. Bosisio and collaborators, used as a microwave and millimeter-wave demodulator [67].

A Six-Port is a passive circuit originally designed for the measurement of the microwaves circuits. A example of the early application of the Six-Port was the reflectometer [91]. The Six-Port system which has six ports(as namesake), namely two inputs and four outputs, mostly consist of three hybrid couplers and a Wilkinson power divider The outputs are connected to four power detectors. When the six port behavior is linear, the input-output relations can be analytically derived, and phase and amplitude measurements can be accurately performed.

Since the Li's discovery [67] of the application of six-port in direct conversion receiver in 1993, many other researches [69, 92–94] which are based on the similar architecture have shown that the Six-Port architecture is a promising candidate to be used in various direct PSK and QAM modulation and demodulation.

4.2 Six-port Junction Circuit Theory

When the six-port circuits work as modulators, the outputs of the hybrid couple are connected to two pairs of mono-ports, having adjustable reflection coefficients. Different modulation signals (such as QPSK, 8PSK, and 16QAM) can be obtained by using different reflection coefficients that are only real part values. For example, the QPSK signal is produced if the pair of reflection coefficients is 1 and -1 (open and short circuits, respectively). Our work is focused on how to demodulate the received RF signal by six-port circuit.

When six-port circuits work as demodulators, there are three configurations of block diagrams to design and apply the six-port circuits according to the design situation as follows:

- Three couplers + power divider
- Two couplers + two power dividers 90° phase shifter

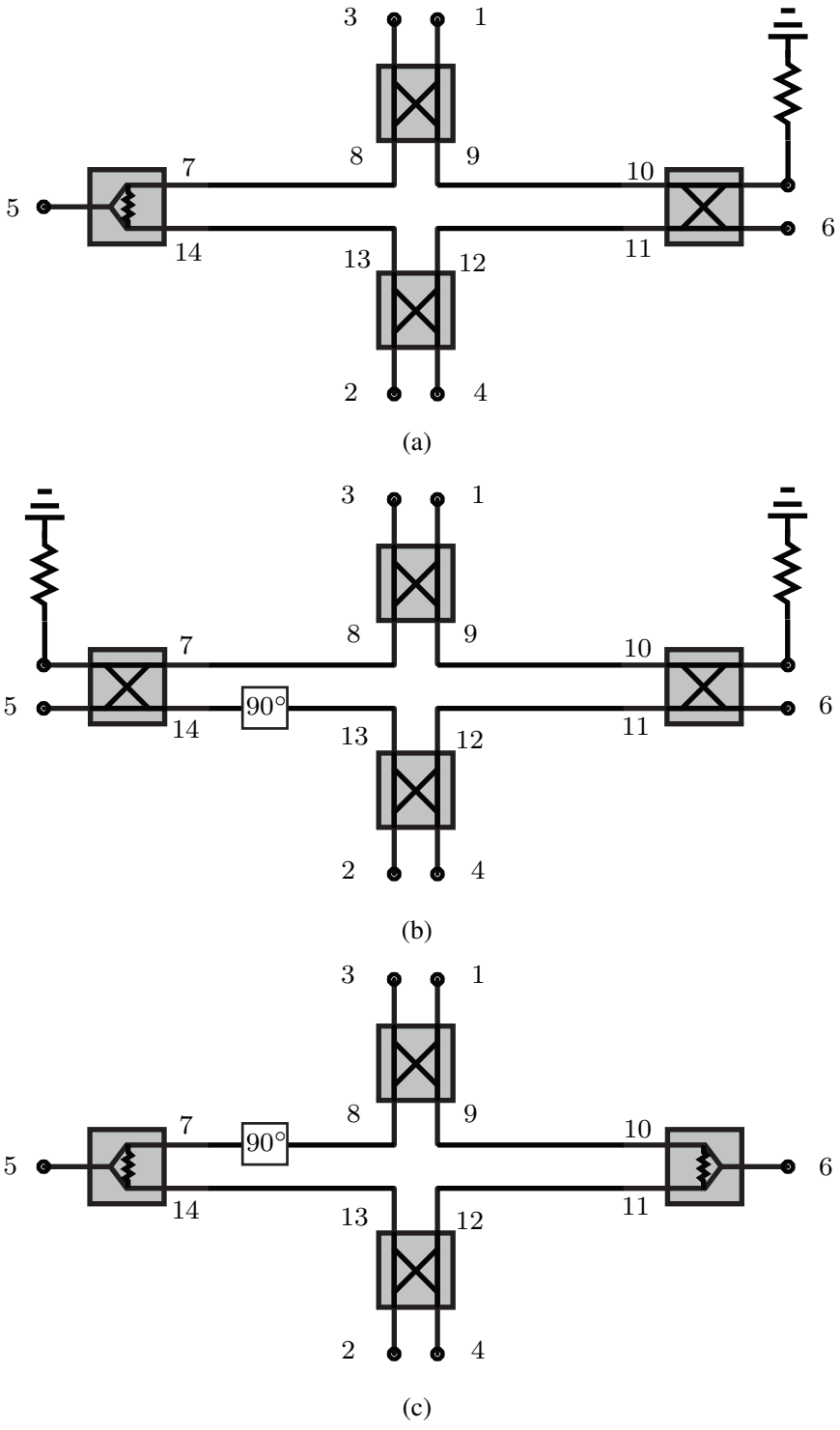

Figure 4.1 Block diagram of three configurations of six-port circuit

- Four couplers + 90° phase shifter

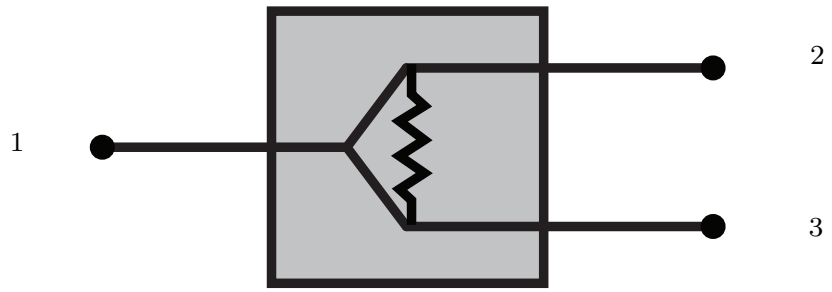

Figure 4.2 Block diagram of power divider of six-port circuit

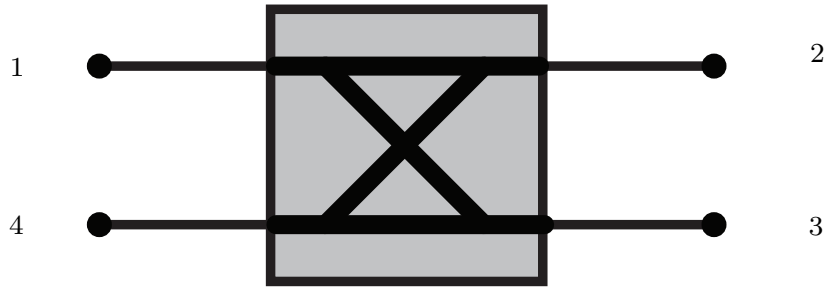

Figure 4.3 Block diagram of hybrid coupler of six-port circuit

The three configurations of six-port circuit have been widely applied at microwave and millimeter-wave frequency. Each of them has its own features, including advantages and disadvantages:

- For the configuration in Figure 4.1(a), no phase shifter is required.
- For the configuration in Figure 4.1(b), no power divider is required.
- For the configuration in Figure 4.1(c), no additional matching load is required.

The block diagrams of different configurations of six-port circuit are shown in Figure 4.1.

The analysis of the six-port circuit is shown by calculating the S parameter matrix of the first type. The other two configurations of six-port junctions can be analyzed through the similar process.

The S parameter matrix of ideal power divider shown in Figure 4.2 is given in (4.1):

$$S = -j\frac{1}{\sqrt{2}}\begin{bmatrix} 0 & 1 & 1 \\ 1 & 0 & 0 \\ 1 & 0 & 0 \end{bmatrix} \tag{4.1}$$

The S parameter matrix of ideal 90° hybrid coupler shown in Figure 4.3 is given in (4.2):

$$S = -j\frac{1}{\sqrt{2}}\begin{bmatrix} 0 & j & 1 & 0 \\ j & 0 & 0 & 1 \\ 1 & 0 & 0 & j \\ 0 & 1 & j & 0 \end{bmatrix} \tag{4.2}$$

To obtain the S parameter matrix of the entire six-port junction, all the input ports, the intermediate ports and the output ports are numbered, as shown in Figure 4.1 (a). The incident wave and reflected wave at each port are defined as a_n and b_n, $n = 1, 2, \cdots, 10$.

From (4.1) and (4.2), the incident waves at port 8, port 9, port 12 and port 13 can be correspondingly expressed as:

$$\begin{aligned} b_7 &= -j\tfrac{1}{\sqrt{2}}a_1 \\ b_{10} &= -\frac{1}{\sqrt{2}}a_2 \\ b_{11} &= -j\frac{1}{\sqrt{2}}a_2 \\ b_{14} &= -j\frac{1}{\sqrt{2}}a_1 \end{aligned} \tag{4.3}$$

where they act as incident wave of other two hybrids in Figure 4.1 (a), we apply (4.3) into (4.2). Then the reflected waves at port 1 to port 6 can be expressed as:

$$\begin{aligned} b_1 &= \frac{1}{2}(ja_1 + ja_2) \\ b_2 &= \frac{1}{2}(-a_1 + ja_2) \\ b_3 &= \frac{1}{2}(-a_1 + a_2) \\ b_4 &= \frac{1}{2}(ja_1 - a_2) \\ b_5 &= 0 \\ b_6 &= 0 \end{aligned} \tag{4.4}$$

Since

$$[b] = [S][a] \tag{4.5}$$

The relationship between incident wave and reflected wave for the first configuration shown

in Figure 4.1 (a) can be expressed as follows:

$$\begin{bmatrix} b_1 \\ b_2 \\ b_3 \\ b_4 \\ b_5 \\ b_6 \end{bmatrix} = \frac{1}{2} \begin{bmatrix} 0 & 0 & 0 & 0 & j & j \\ 0 & 0 & 0 & 0 & -1 & j \\ 0 & 0 & 0 & 0 & -1 & 1 \\ 0 & 0 & 0 & 0 & j & -1 \\ j & -1 & -1 & j & 0 & 0 \\ j & j & 1 & -1 & 0 & 0 \end{bmatrix} \begin{bmatrix} a_1 \\ a_2 \\ a_3 \\ a_4 \\ a_5 \\ a_6 \end{bmatrix} \tag{4.6}$$

For the other two configurations shown in Figure 4.1 (b) and Figure 4.1 (c), with the same procedure we can relate the incident wave to reflected wave in the similar form of (4.6). Therefore, the S-parameters of each configuration shown in Figure 4.1 are obtained as follows

$$S_a = \frac{1}{2} \cdot \begin{pmatrix} 0 & 0 & 0 & 0 & j & j \\ 0 & 0 & 0 & 0 & -1 & j \\ 0 & 0 & 0 & 0 & -1 & 1 \\ 0 & 0 & 0 & 0 & j & -1 \\ j & -1 & -1 & j & 0 & 0 \\ j & j & 1 & -1 & 0 & 0 \end{pmatrix} \tag{4.7a}$$

$$S_b = \frac{1}{2} \cdot \begin{pmatrix} 0 & 0 & 0 & 0 & 1 & j \\ 0 & 0 & 0 & 0 & -j & j \\ 0 & 0 & 0 & 0 & j & 1 \\ 0 & 0 & 0 & 0 & -1 & -1 \\ 1 & -j & j & -1 & 0 & 0 \\ j & j & 1 & -1 & 0 & 0 \end{pmatrix} \tag{4.7b}$$

$$S_c = \frac{1}{2} \cdot \begin{pmatrix} 0 & 0 & 0 & 0 & j & -1 \\ 0 & 0 & 0 & 0 & -j & j \\ 0 & 0 & 0 & 0 & -1 & j \\ 0 & 0 & 0 & 0 & -1 & -1 \\ j & -j & -1 & -1 & 0 & 0 \\ -1 & j & j & -1 & 0 & 0 \end{pmatrix} \tag{4.7c}$$

The phases from two input ports to four output ports are critical in order to determine the demodulation results of the six-port junction. The phases can be obtained from the S parameter matrix. For example, for the first type, the phase differences between adjacent

output ports are shown as follows:

$$\begin{aligned} \angle S_{32} - \angle S_{31} &= 180^\circ \\ \angle S_{42} - \angle S_{41} &= 0^\circ \\ \angle S_{52} - \angle S_{51} &= 90^\circ \\ \angle S_{62} - \angle S_{61} &= -90^\circ \end{aligned} \tag{4.8}$$

The three previous S parameter matrices are generated for the ideal cases that all the input ports and output ports are connected to perfect matching loads. However, in the application of a six-port receiver, four output ports are connected to other circuits such as power detectors, which sometimes have a limited matching condition. In these cases, a matching network is necessary to reduce undesired reflections.

4.3 The Operational Principle of Six-Port Interferometric circuit

Regardless of which view of the six-port receiver is chosen as the wireless sensing or communications setup, the basic principle is the same based on the function of interferometer. We will evaluate the S-parameters of the Six-Port starting from the general relation which gives the vector of the reflected waves b, to the vector of incident waves a:

$$[b] = [S] \cdot [a] \tag{4.9}$$

By supposing that hybrid couplers and the power divider are lossless, based on the analysis in the last section, we can calculate the S parameters of the Six-Port and obtain:

$$[S] = \frac{1}{2} \cdot \begin{pmatrix} 0 & 0 & 0 & 0 & j & j \\ 0 & 0 & 0 & 0 & -1 & j \\ 0 & 0 & 0 & 0 & -1 & 1 \\ 0 & 0 & 0 & 0 & j & -1 \\ j & -1 & -1 & j & 0 & 0 \\ j & j & 1 & -1 & 0 & 0 \end{pmatrix} \tag{4.10}$$

The Six-Port presented in Figure 4.1 (a) is linear and we can deduce the expressions from the forms of the four incident waves b_1, b_2, b_3, b_4, according to the two incidental waves a_5 and a_6.

$$b_1 = \frac{1}{2}(ja_5 + a_6) \tag{4.11a}$$

$$b_2 = \frac{1}{2}(-a_5 + ja_6) \tag{4.11b}$$

$$b_3 = \frac{1}{2}(-a_5 + a_6) \tag{4.11c}$$

$$b_4 = \frac{1}{2}(ja_5 - a_6) \tag{4.11d}$$

The two input signals are described by:

$$a_5 = |a_5| \cdot e^{j\phi_5} \tag{4.12a}$$

$$a_6 = |a_6| \cdot e^{j\phi_5} \tag{4.12b}$$

The angles represent the state of phase of the signals at the ports of the Six-Port. Ports LO and RF are insulated, the input signals are propagated only at the ports of the six-port where they are superimposed according to shifting relations of phase. Let us suppose two input signals of the same frequency, of the same amplitude $|a_5| = |a_6| = A$, and suppose that each port is adapted, the equations of the waves (4.18) at the four ports become:

$$b_1 = \frac{A}{2} \cdot (exp(j(\phi_5 - \phi_6) + 1)) \tag{4.13a}$$

$$b_2 = \frac{A}{2} \cdot (exp(j(\phi_5 - \phi_6 + \frac{\pi}{2}) + 1)) \tag{4.13b}$$

$$b_3 = \frac{A}{2} \cdot (exp(j(\phi_5 - \phi_6 + \pi) + 1)) \tag{4.13c}$$

$$b_4 = \frac{A}{2} \cdot (exp(j(\phi_5 - \phi_6 - \frac{\pi}{2}) + 1)) \tag{4.13d}$$

From (4.13), we can see that the processing is performed by superposing two input signals with four different relative phases. If the power of the input signals is similar, constructive or destructive interactions occur, respectively, depending on the phase difference and amplitude produced. For the in-phase superposition, the output amplitude will be greater; for the opposite cases, attenuation will be observed. If only one overlay is performed, the results will be ambiguous. By moving the relative phase to four different angles, other equations will be obtained to resolve the ambiguity. For a six-port architecture, the total phase of a full wave period is divided into four parts, which are offset by $\pi/2$, respectively. Therefore, the relative phase difference between the two input signals is $0, \pi/2$, and $3\pi/2$. At microwave frequencies, these phase shifts are usually achieved by couplers [86].

4.4 Demodulation principle of Six-port Receiver

4.4.1 Multi-port technique

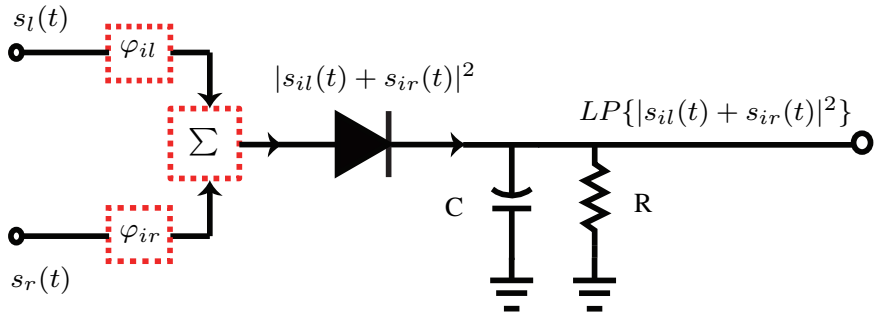

Figure 4.4 Signal characteristics of multi-port technique

In the last section, we know the processing of six-port interferometer is performed by superposing two input signals with four different relative phases. Introducing arbitrary phase shifts in each input path, the phase difference between input signal and output signal on i_{th} independent path is ϕ_{il} and ϕ_{ir}, as shown in Figure 4.4. Assuming two input signals are described by

$$\begin{aligned} s_l(t) =& A_{LO}\cos(\omega_{LO}t+\phi_{LO}) && \text{(4.14a)}\\ s_r(t) =& Re\{|x_B(t)|\cdot e^{j\phi_B t}\cdot A_{RF}\cdot e^{j(\omega_{RF}t+\phi_{RF})}\} \\ =& A_{RF}[x_I(t)\cos(\omega_{RF}t+\phi_{RF})-x_Q(t)\sin(\omega_{RF}t+\phi_{RF})] && \text{(4.14b)}\end{aligned}$$

where $x_I(t)=\cos\phi_B(t)$, $x_Q(t)=\sin\phi_B(t)$ are in-phase component and quadrature component of received modulated signal.

Considering the transmission coefficient a_{il} of each independent path from input to output, the output signal response at i_{th} output port after getting through multi-port network can be expressed as

$$\begin{aligned} s_i(t) =& s_{il}(t)+s_{ir}(t) \\ =& |a_{il}|\cdot e^{j\phi_{i1}}\cdot s_l(t)+|a_{ir}|\cdot e^{j\phi_{i2}}\cdot s_r(t) && \text{(4.15)}\end{aligned}$$

With $s_i(t)$ getting into the diode as shown in Figure 4.4, and, after lowpass filter, the output

signal can be calculated as

$$\begin{pmatrix} V_{o1} \\ V_{o2} \\ \vdots \\ V_{on} \end{pmatrix} = \begin{pmatrix} 0.5|a_{1l}|^2 A_{LO} & 0.5|a_{1r}|^2 A_{RF} & M_1 \cos\Delta\Theta_1 & M_1 \sin\Delta\Theta_1 \\ 0.5|a_{2l}|^2 A_{LO} & 0.5|a_{2r}|^2 A_{RF} & M_2 \cos\Delta\Theta_2 & M_2 \sin\Delta\Theta_2 \\ \vdots & \vdots & \vdots & \vdots \\ 0.5|a_{\mathrm{nl}}|^2 A_{RF} & 0.5|a_{\mathrm{nr}}|^2 A_{RF} & M_{\mathrm{n}} \cos\Delta\Theta_{\mathrm{n}} & M_{\mathrm{n}} \sin\Delta\Theta_{\mathrm{n}} \end{pmatrix} \cdot \begin{pmatrix} 1 \\ B \\ x_I \\ x_Q \end{pmatrix} \tag{4.16}$$

where,

$$\Delta\Theta_i = (\omega_{LO} - \omega_{RF})t + \phi_{LO} - \phi_{RF} + \phi_{il} - \phi_{ir},$$

$$M_i = |a_{il}|A_{LO}|a_{ir}|A_{RF},$$

and

$$B = x_I^2(t) + x_Q^2(t)$$

By introducing a complex calibration coefficient c_i, a general multi-port receiver equation is formulated

$$x_I(t) - x_Q(t) = \sum_{i=1}^{n} c_i \cdot V_{oi}(t) \tag{4.17}$$

4.4.2 Six-port receiver

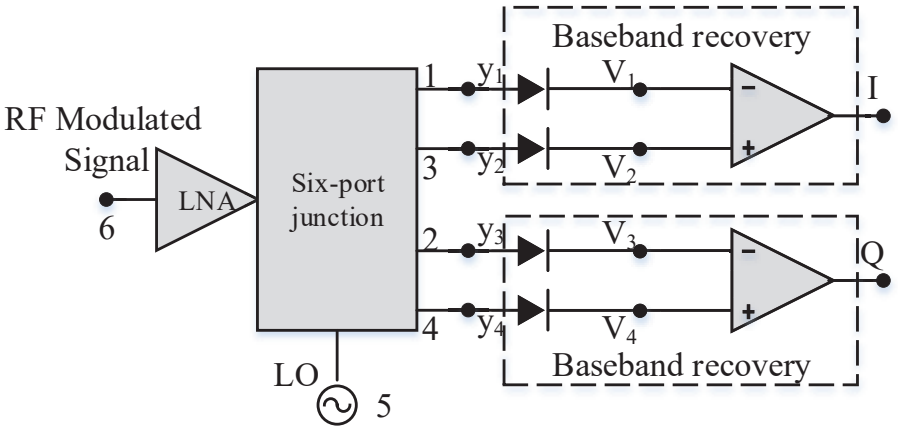

Figure 4.5 Six-Port QPSK demodulation

If we choose

$$\Delta\phi_i = \begin{bmatrix} 0 & \frac{\pi}{2} & \pi & -\frac{\pi}{2} \end{bmatrix}, \qquad and\ \Delta\omega = 0,$$

They can lead to $c_i = \begin{bmatrix} 0 & \frac{\pi}{2} & \pi & -\frac{\pi}{2} \end{bmatrix}^T$.

Therefore, (4.16) can be simplified as

$$\begin{pmatrix} V_1 \\ V_2 \\ V_3 \\ V_4 \end{pmatrix} = \begin{pmatrix} \frac{A_{LO}^2}{8} & \frac{A_{RF}^2}{8} & \frac{\cos(\phi_B(t)-\phi_{LR})}{4} \\ \frac{A_{LO}^2}{8} & \frac{A_{RF}^2}{8} & -\frac{\sin(\phi_B(t)-\phi_{LR})}{4} \\ \frac{A_{LO}^2}{8} & \frac{A_{RF}^2}{8} & -\frac{\cos(\phi_B(t)-\phi_{LR})}{4} \\ \frac{A_{LO}^2}{8} & \frac{A_{RF}^2}{8} & \frac{\sin(\phi_B(t)-\phi_{LR})}{4} \end{pmatrix} \cdot \begin{pmatrix} 1 \\ |x_B|^2 \\ A_{LO}A_{RF}|x_B| \end{pmatrix} \tag{4.18}$$

Output voltage of diode at one of four independent path can be measured, and the LO power is assumed to be known. Therefore, only $|x_B|$ and $\phi_B(t)$ are unknown while four equations are available and one of the equations is linearly dependent on the others. It is seen that the data of I channel can be recovered by taking the difference of $V_3 - V_1$, and the detected Q channel by taking the difference of $V_4 - V_2$. Therefore

$$x_I(t) = |x_B(t)| \cdot \cos\phi_B(t) = \frac{2(V_1 - V_3)}{A_{LO}A_{RF}} \cdot \cos\phi_{LR} - \frac{2(V_4 - V_2)}{A_{LO}A_{RF}} \cdot \sin\phi_{LR} \tag{4.19a}$$

$$x_Q(t) = |x_B(t)| \cdot \sin\phi_B(t) = \frac{2(V_1 - V_3)}{A_{LO}A_{RF}} \cdot \sin\phi_{LR} + \frac{2(V_4 - V_2)}{A_{LO}A_{RF}} \cdot \cos\phi_{LR} \tag{4.19b}$$

4.5 Six-port Circuit Design

The entire six-port circuit design is presented in this section. It is designed based on the previous analysis and design of power divider and hybrid coupler. By using commercial software ADS2017, the six-port circuit is designed and optimized over the 2.35-2.55 GHz frequency range.

Since the designed six-port junction will be used in a system for energy harvesting applications, a simple low-loss structure is needed. The second type of six-port junction in Figure 4.1 is a good candidate since it is just made of hybrid couplers and phase shifter with no need of power dividers. However, the six-port junctions made of power divider and couplers can provide more bandwidth (the use of phase shifter generally limits the bandwidth). Then, a six-port circuit is designed at 2.45 GHz using microstrip technology based on configuration shown in Figure 4.1 (b). The designed circuit is fabricated on a 20-mil-thick ceramic substrate with relative permittivity of $\varepsilon_r = 2.94$. The layout and fabricated prototype of the circuit with the size of $140mm \times 140mm$ are shown in Figure 4.6 and Figure 4.7, respectively. The six-port junction consists of four 90° hybrid couplers connected together using microstrip

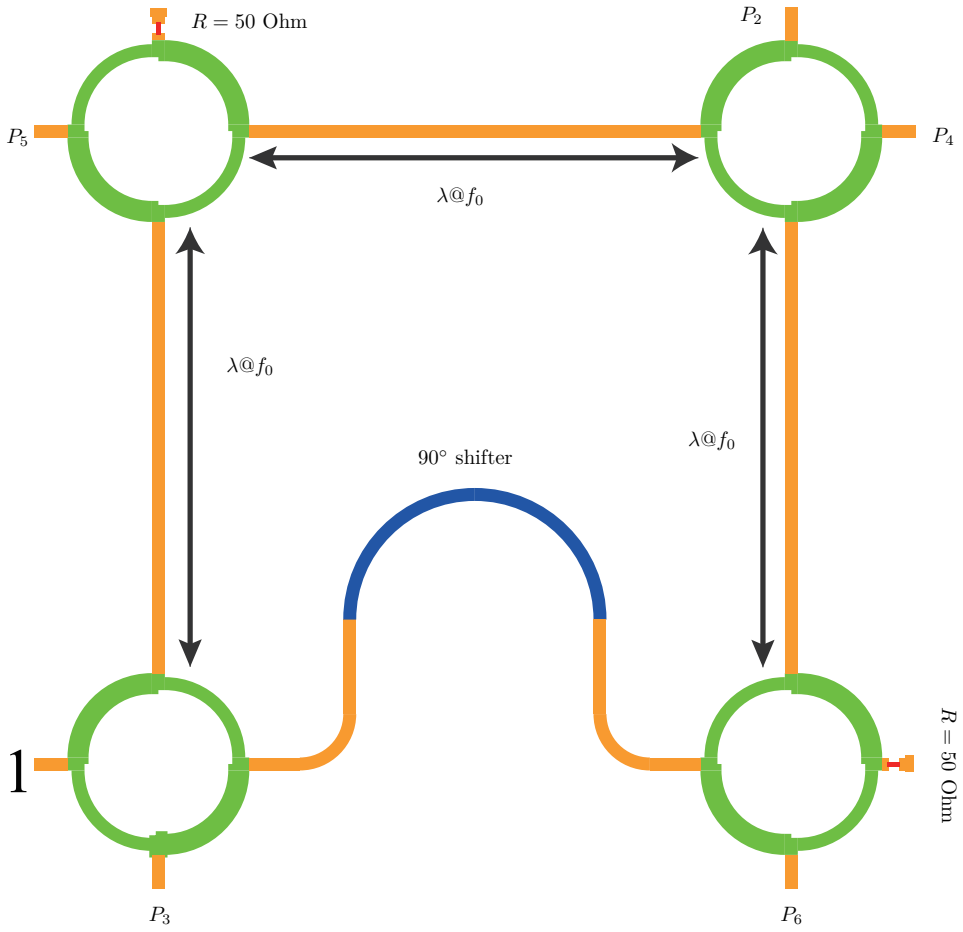

Figure 4.6 The designed six-port junction.

line of characteristic impedance $Z_\circ = 50\ \Omega$. Two 50 Ω loads (made by thin film technology) are used at the output of the unused ports to prevent any reflections. The required 90° phase shift is provided using an extra three-quarter-wave transmission line. The circuit is designed and optimized using momentum simulator to operate at 2.45 GHz [5, 87].

The S-parameters are measured using a two-port VNA. With the two-port measurement setup in Figure 4.7, the S-parameters of two ports of the six-port are obtained at the same time while the four other ports matched to 50 Ω. Since in a six-port junction, the number of ports to be measured is more than that of VNA ports, multiple sets of six-port parameters are measured in order to have the complete results of measured S-parameters. In the designed six-port, port 5 (P5) and port 6 (P6) are input ports injected by the LO power or RF signal. The other four ports (P1 to P4) are considered as output ports. Measured results are in good agreement with simulated ones. As shown in Figure 4.8, excellent return losses and

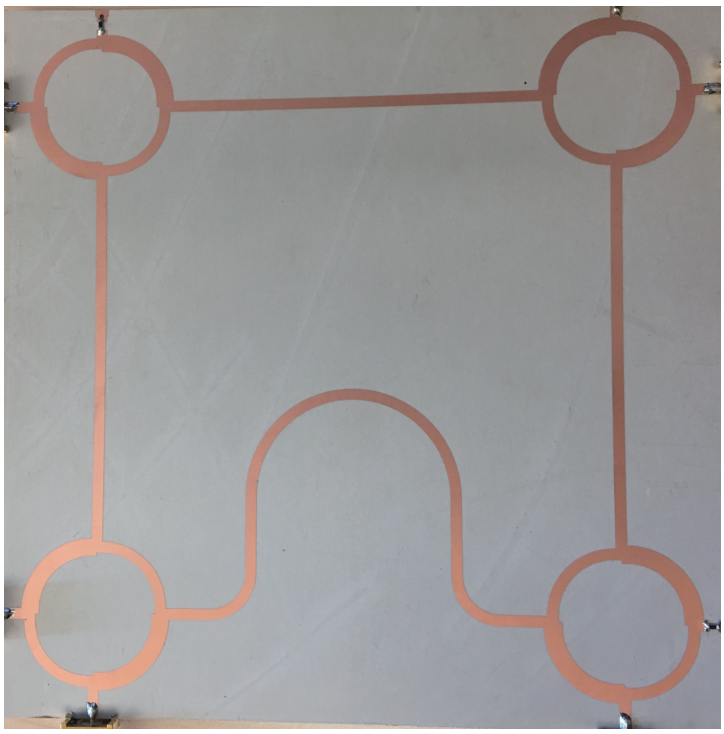

(a)

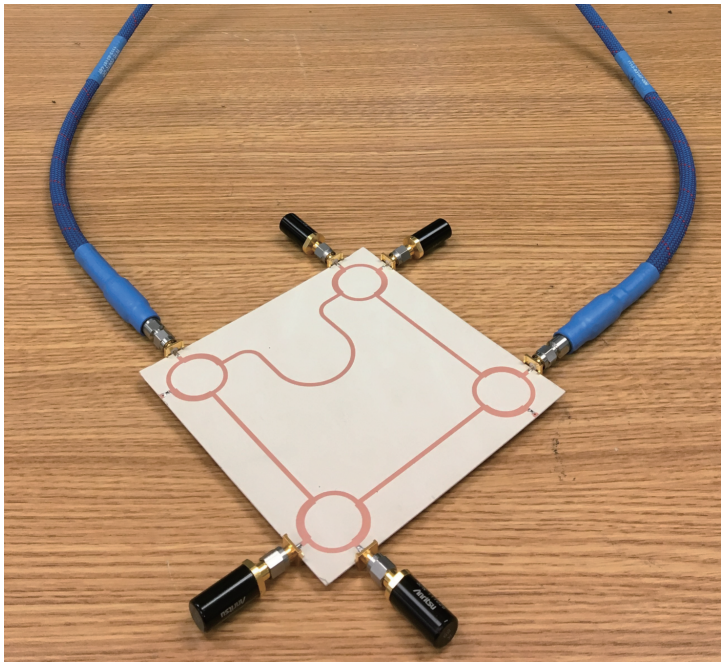

(b)

Figure 4.7 (a) The fabricated six-port prototype, (b) Measurement setup for six-port prototype.

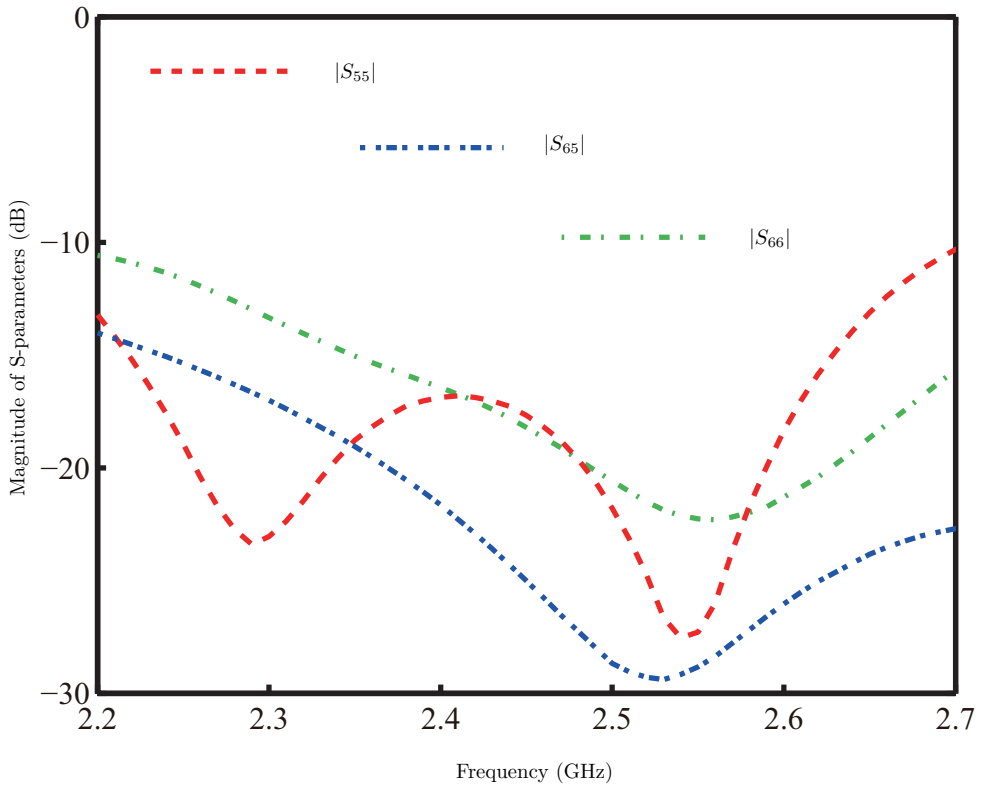

Figure 4.8 The isolation and matching condition of two input ports.

isolations between RF and LO inputs are obtained at the 2.45 GHz operating frequency. Figure 4.9 presents the matching condition of four output ports and transmission from RF port to four outputs while Figure 4.10 presents the isolation condition of four output ports and transmission from LO port to four outputs. Compared to the ideal six-port model, the measured transmission of RF and LO signals has an additional loss of 0.5 dB (-6.5 dB at 2.45 GHz). Figure 4.11 shows the phase of transmission S-parameters between the input signals (RF and LO)and outputs versus frequency. As it can be seen, the measured 90° phase shift is obtained among the output ports at 2.45 GHz.

4.6 Rectifying Circuit Design

The rectenna, an integrated body combining electromagnet-ic rectifier and antenna, is a key element for wireless power transmission and harvesting [95, 96]. The conversion efficiency of a rectifying circuit fundamentally determines the overall performance of the rectenna [19, 97]. Various design strategies have been employed to achieve a high or better conversion efficiency [98,99]. The maximum measured efficiency can be realized over 70% at an optimum

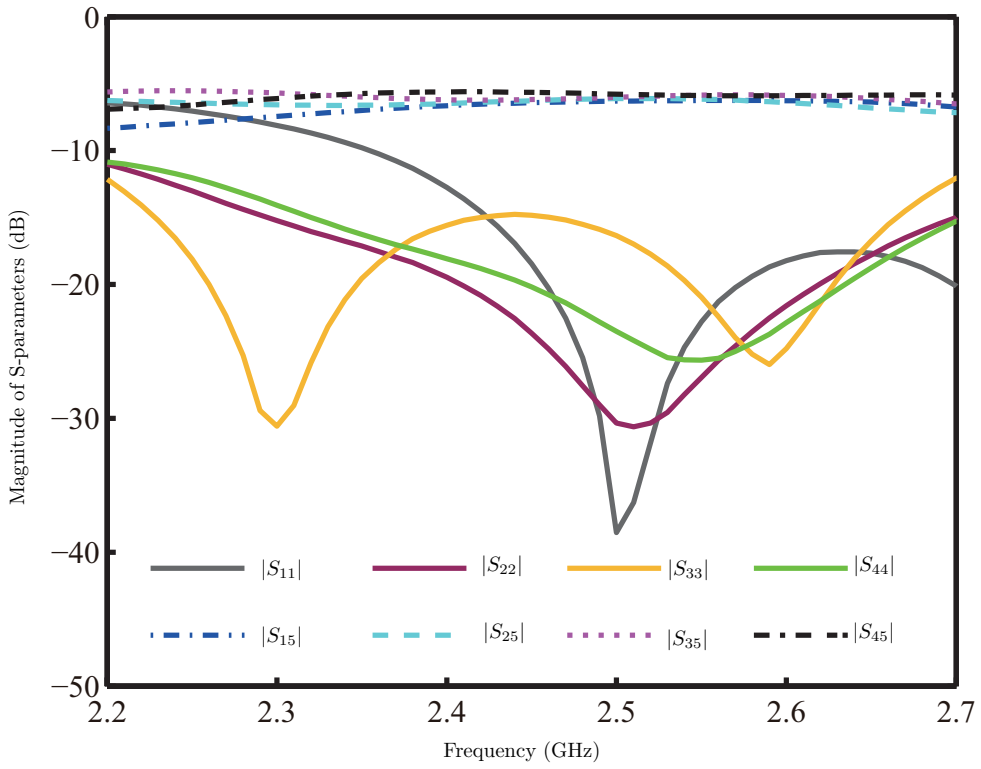

Figure 4.9 The matching condition of four output ports and transmission from RF port to outputs.

input power level which is usually larger than 0 dBm [30, 51, 55, 100].

Since ambient RF energy resources including man-made wireless power base-stations are usually measured at low power levels, typically from −10 dBm down to −30 dBm or even lower, rectifiers with a high conversion efficiency operating at such a low input power are greatly demanded. Several design techniques have been reported for low input power harvesting scenarios [101–103]. The classical filtering matching methods are employed in the input port of rectifying circuit. The maximum conversion efficiency at −20 dBm input power reported so far was about −28% [102, 103]. It employs a much complicated structure, and achieves this high efficiency using a two-tone input signal.

In this work, we propose a novel IRR scheme which includes a very simple rectifier capable of realizing a relatively high efficiency at low input power level with the ability of decoding data information. The measured conversion efficiency reaches 30% at −20 dBm input power. The maximum measured efficiency is higher than 60% around −5 dBm input power. Such a rectifier is very useful for various applications where the input power is below −10 dBm.

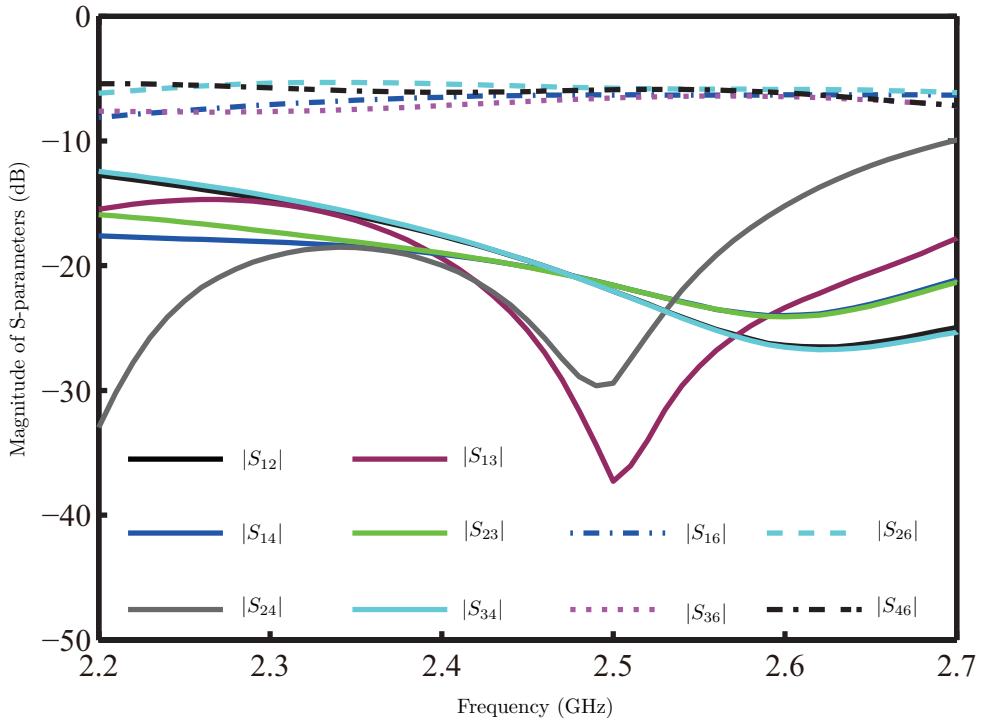

Figure 4.10 The isolation condition of four output ports and transmission from LO port to outputs.

4.6.1 Design principle of proposed rectifier

For a rectifier operating at low power level, the key to achieve a high efficiency lies in its simplicity in connection with low loss and better integration. One should employ a number of parts or building blocks as small as possible to avoid parasitic losses as well as extra components. The proposed rectifying circuit is shown in Fig. 4.12 (a), where a Schottky diode is connected with an inductor, a capacitor and a resistive load. The capacitor combined with the resistive load acts as a low-pass filter which reflects back the RF signal and higher-order harmonics generated by the diode. The Schottky diode in series connection, different from the dominant parallel connections in [95, 96], exhibits a better performance at the low power level. In our design, we choose zero-bias diode, namely Schottky diode SMS7630 from Skyworks Corporation, so there is no bias circuit in proposed rectifier circuit.

The inductor after the diode is the key in the whole circuit. It acts as a matching circuit to allow a proper impedance for the input port. As mentioned in Chapter 2, In a low input power level, energy harvesting efficiency at a low input power level becomes lower partially due to high matching network loss. Simply placing inductors in series with the diode would help reduce the VSWR and further reduce the transmission line loss. Fig. 4.13 and Fig. 4.14 show

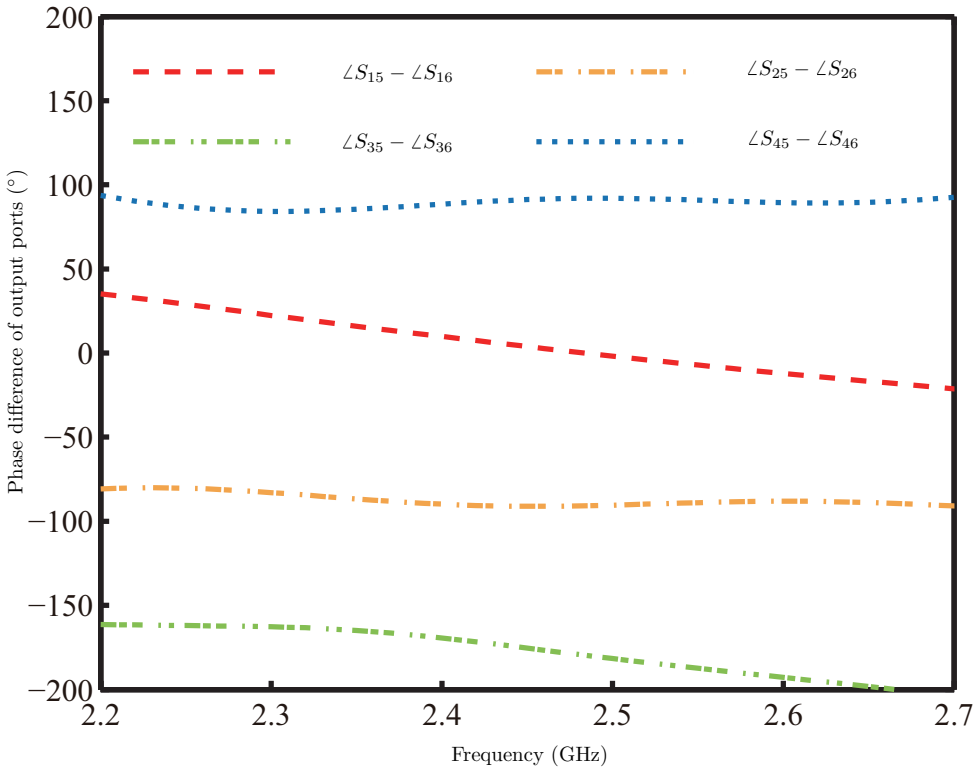

Figure 4.11 Phase difference of the input signals at output ports.

input impedance and S-parameters of the proposed rectifying circuit at different inductance values, respectively. The inductor in the circuit also controls the boundary condition on the right side of the diode, so as to change the conversion efficiency curve.

Fig. 4.12 (b) shows a typical power conversion efficiency of an example working at 2.45 GHz as a function of different inductance value. The power conversion efficiency is calculated by $\eta = V_{\text{out}}^{\text{DC}^2}/(P_{\text{in}}R)$. Note that the peak of conversion efficiency curves shifts to the lower end of the input power as the inductance decreases. It turns out that a relatively high efficiency at a low power level could be achieved by properly tuning the inductance. Note that the efficiency at -20 dBm reaches 37% when the inductance is 33 nH. The maximum efficiency is around 55% occurring at -10 dBm when the inductance is 42 nH.

4.6.2 Microstrip Implementation and Results

Fig. 4.15 (a) shows a microstrip implementation of the proposed rectifying circuit as described in Fig. 4.12. The inductor is implemented using a simple thin transmission line of high impedance, while the capacitor is replaced by two quarter-wavelength open stubs to block the dominant and second-order harmonics.

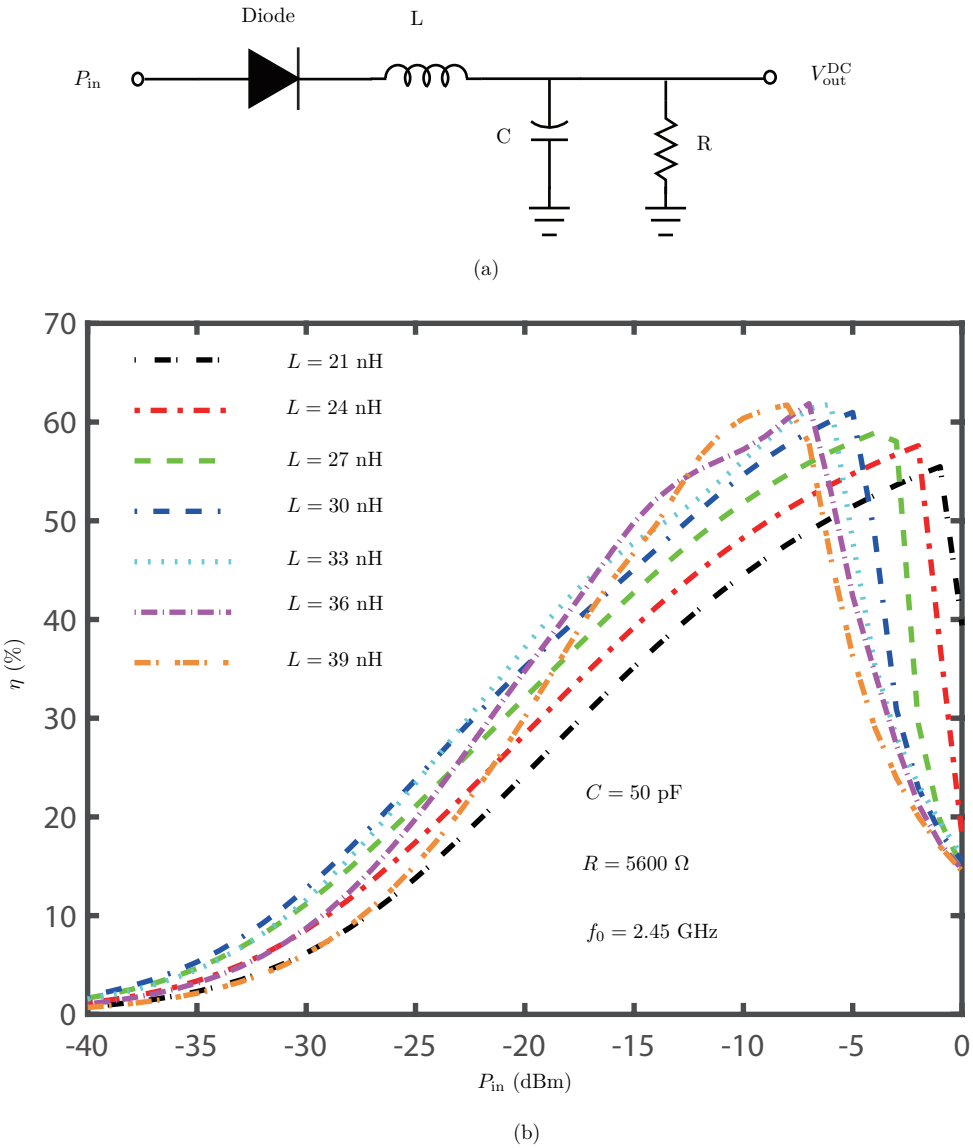

Figure 4.12 (a) The proposed rectifying circuit, (b) RF-DC power conversion efficiency at different inductance values.

The rectifying circuit works at $f_0 = 2.45$ GHz. The Schottky diode SMS7630 from Skyworks Corporation is used in this work. Key SPICE and packaging parameters of SMS7630 are listed in Table 4.1. The circuit parameters are optimized by Bode-Fano criterion [80]to achieve the maximum efficiency at -20 dBm input power level. Fig 4.15 (b) and (c) show the efficiency and reflection responses for both lumped-element and microstrip circuits. Note from Fig. 4.15 (b) that the efficiency achieved by microstrip rectifier is almost close to the counterpart based on the lumped-element circuit, which verifies that the proposed microstrip implementation is feasible.

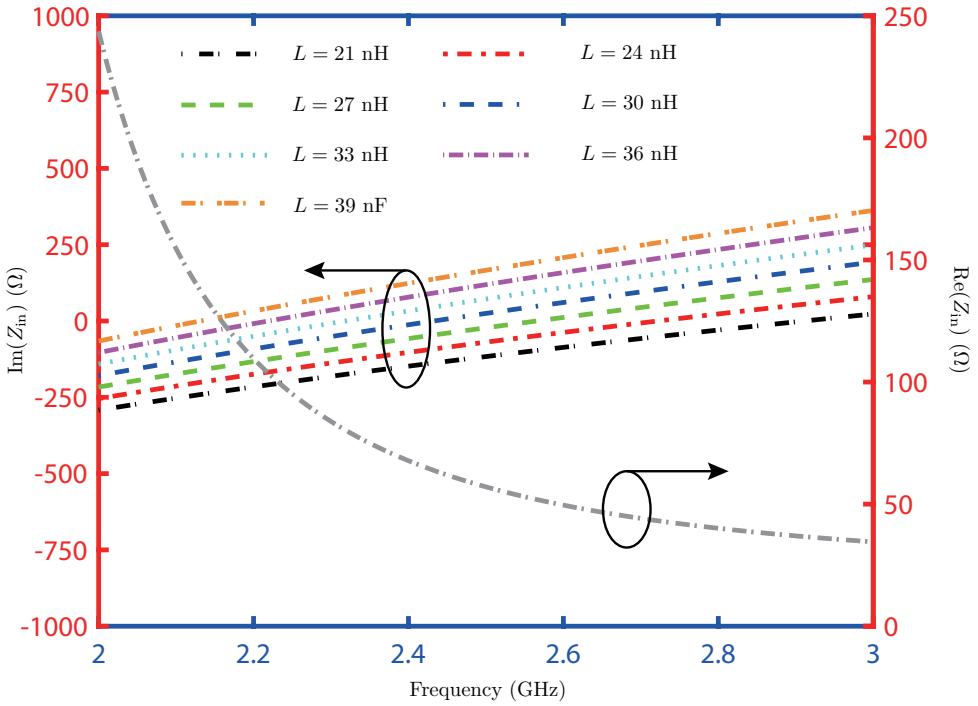

Figure 4.13 Input impedance of the proposed rectifying circuit at different inductance values.

Table 4.1 Key SPICE and Packaging Parameters.

Parameters	Units	SMS7630
I_s	A	5e-6
n	-	1.05
R_s	ω	20
C_{j0}	pF	0.14
L_p	nH	0.7
C_p	pF	0.16

Fig. 4.16 (a) shows the fabricated prototype of the rectifier in Fig. 4.15 (a). The substrate is 60-mil-thick Rogers RO4360 (with dielectric constant 6.15 and loss tangent 0.0038). The measured conversion efficiencies and DC output voltages at 2.43, 2.45, and 2.47 GHz are plotted in Fig. 4.16 (b), respectively. Note that the conversion efficiency is not very sensitive to the frequency shift. The conversion efficiency at -20 dBm input power reaches 30% at 2.45 GHz. The maximum conversion efficiency goes up to 60% occurring at -5 dBm input power. The proposed rectifying circuit has a relatively high efficiency at the low input power below 0 dBm, which is of significant interest for wireless energy harvesting applications.

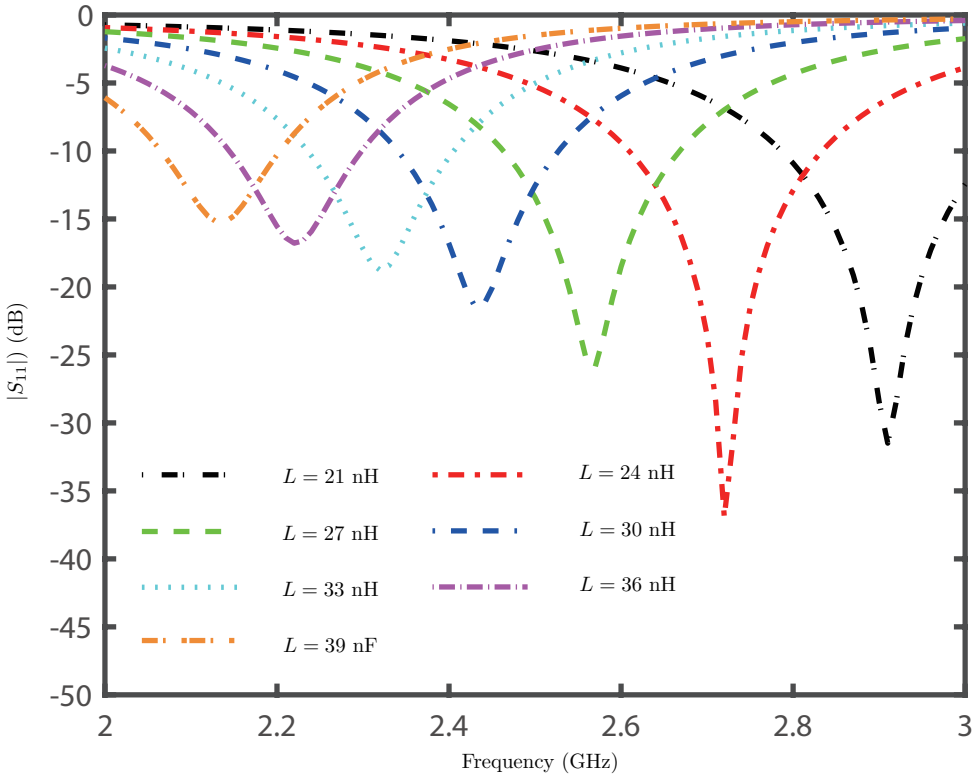

Figure 4.14 S-parameters of the proposed rectifying circuit at different inductance values.

4.7 Conclusion

This chapter has described the design of six-port junction and rectifying circuit. Firstly, the six-port circuit theory is derived and explained. The review of different configurations of six-port junction and extraction of the related S-parameters of each configuration are presented. Also, the design and fabrication process of a six-port junction operating at 2.45 GHz are explained and the measurement results are given and explained. In addition, a high-efficiency rectifier structure that operates at low input energy is designed and connected to a six-port junction so to implement a receiver. The operating principle of six-port receiver is provided and the baseband signal is recovered.

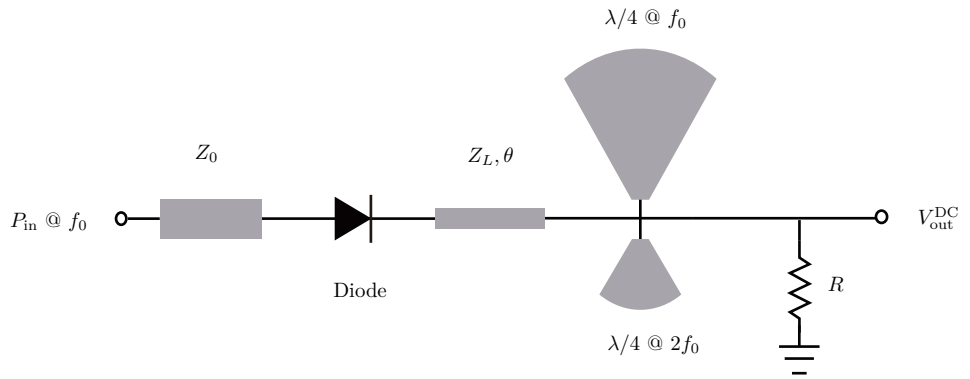

(a)

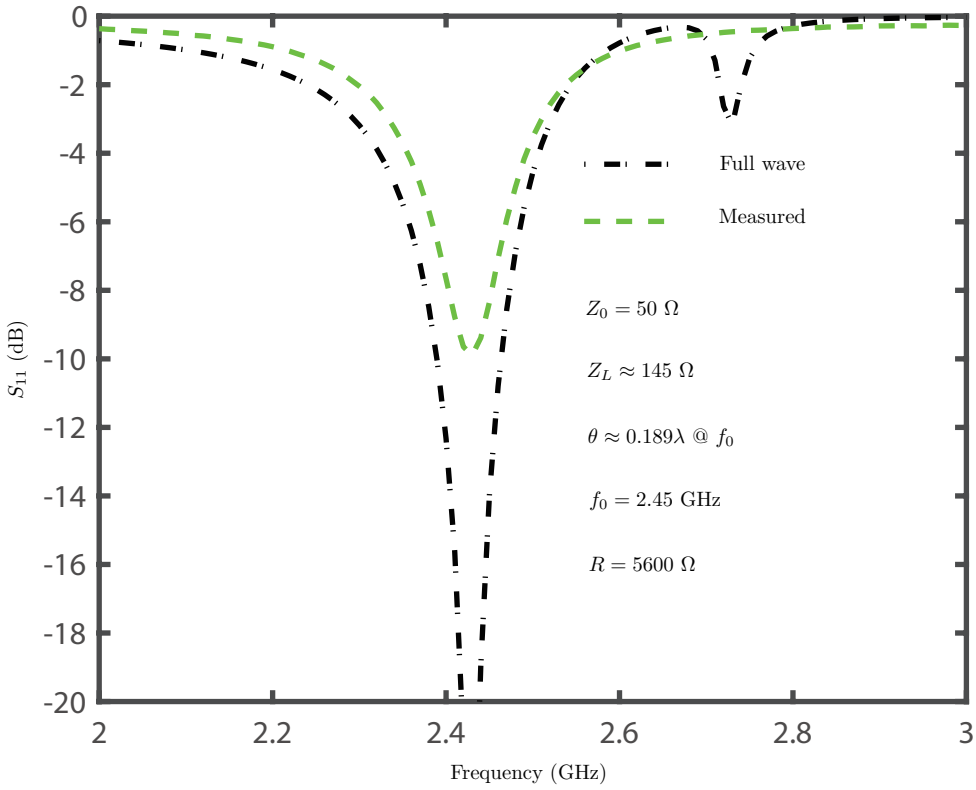

(b)

Figure 4.15 (a) Microstrip implementation of the rectifying circuit in Fig. 4.12; (b) Comparison of the corresponding reflection coefficients.

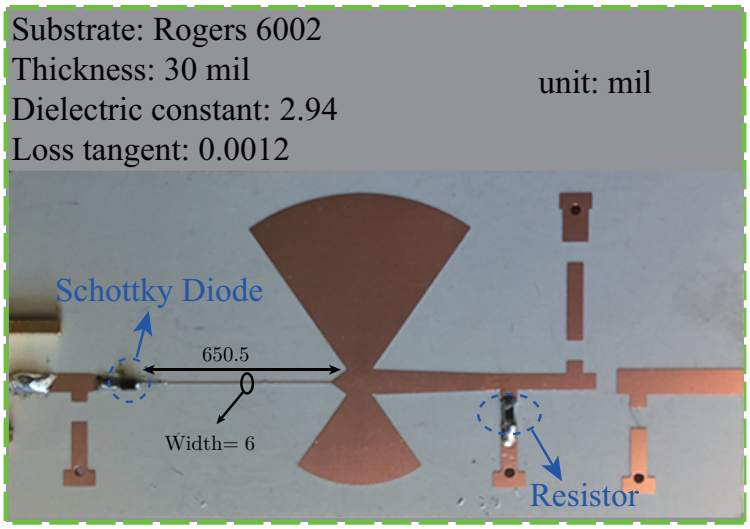

(a)

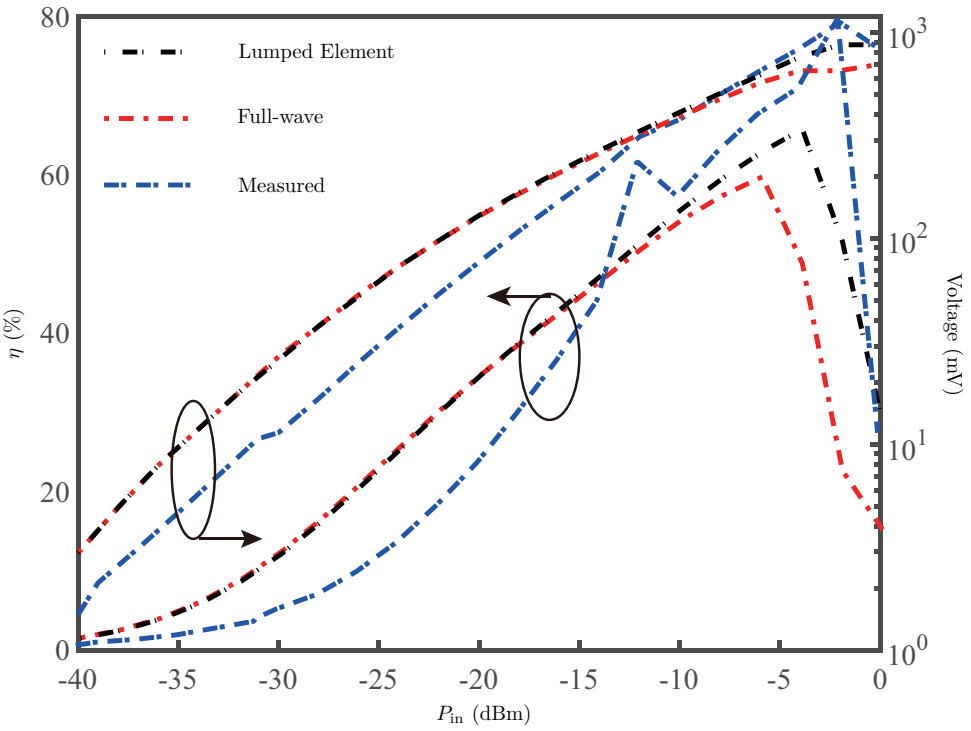

(b)

Figure 4.16 (a) Fabricated prototype of the rectifier in Fig. 4.15(a); (b) Measured efficiency and voltage for the fabricated prototype.

CHAPTER 5 SIMULTANEOUS DATA COMMUNICATION AND ENERGY HARVESTING

Microwave power transmission technologies have been extensively studied and developed in theory and applications such as WEH and SSPS. As research is in progress, wireless power transmission is expected to become a viable alternative that can generate clean energy. At the same time, with the advent of 5G wireless communication, lower power consumption and lower voltage wireless sensors have become a trendy development, and many researchers have been exploring the feasibility of powering these devices by collecting ambiant electromagnetic energy. On one hand, due to the rapid development of wireless communication systems, data transmission is ubiquitous. On the other hand, low-power wireless communication systems provide possibilities for implementing self-powered systems. Therefore, platforms supporting synchronous energy harvesting and data communication are expected to be used in the next generation of self-powered communication systems.

5.1 Simultaneous Wireless Information and Power Transmission

The concept of SWIPT, the fusion of wireless power transmission and wireless communication originated from earlier work, has become appealing than ever due to the emerging needs of 5G and the Internet of Things for the effective use of wireless networks. Transmitting signals to power network sensors (or other devices) and transmitting information can be accomplished because wireless signals can transmit energy and information simultaneously [104–109], The power and information flows from transmitter to the receiving terminals in the SWIPT system are shown in Figure 5.1.

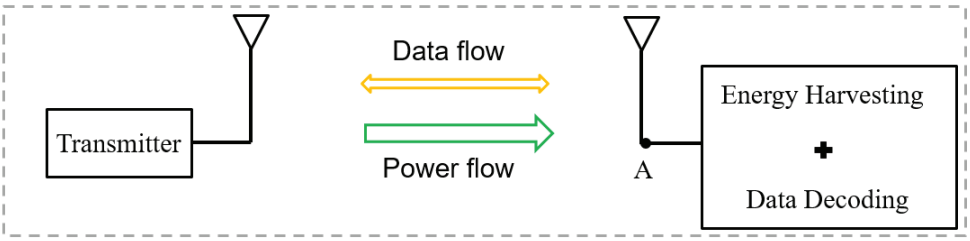

Figure 5.1 General schematic of a SWIPT system.

At present, a rectifier antenna circuit, as a core for a common wireless energy harvesting system, cannot demodulate the received modulation signal, and also the output signal of the

rectifier cannot be directly used for data detection but used for energy storage. In order to achieve the function of energy harvesting and data communication at the same time, most of methods are to divide the received RF signal into two streams, which can be used for data detection and energy collection, respectively.

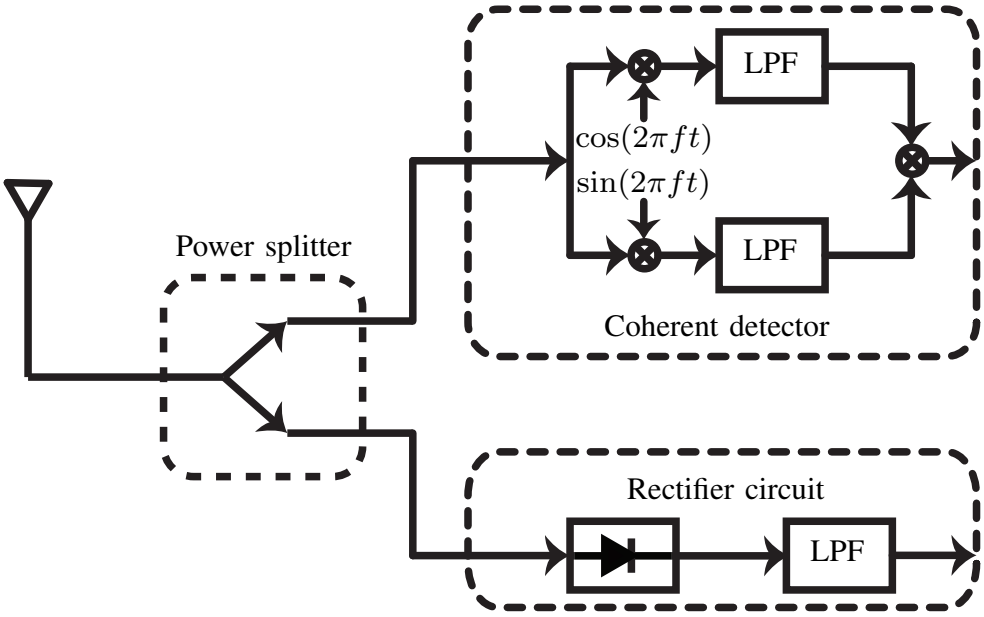

Figure 5.2 The straightforward block diagram with received signal divided.

Figure 5.2 shows the straightforward block diagram with received signal divided. However, such a receiver requires additional power consumption in the downconverter stage (ie, DC power to the mixer and local oscillator), while less power goes into the rectifier because of the splitter.

Therefore, the second scenario proposed is to pass the complete received signal through a non-linear module to receive information and power, as shown in Figure 5.3. As mentioned in the introduction, simple structure, low power consumption, compact, low cost and broadband transceivers are essential for the development of wireless communication systems. In order to obtain these good specifications and eliminate the rectification noise in the second method, we can use multi-port technology to convert the received RF power into a DC plus baseband signal. Moreover, it is worth noting that because multiport technology has been proven to provide simpler circuits compared to heterodyne transceivers [92], it has attracted considerable attention when designing transceivers. Therefore, in the subsequent six-port technology, its application and proposed simultaneous energy harvesting and data communication will be discussed in detail.

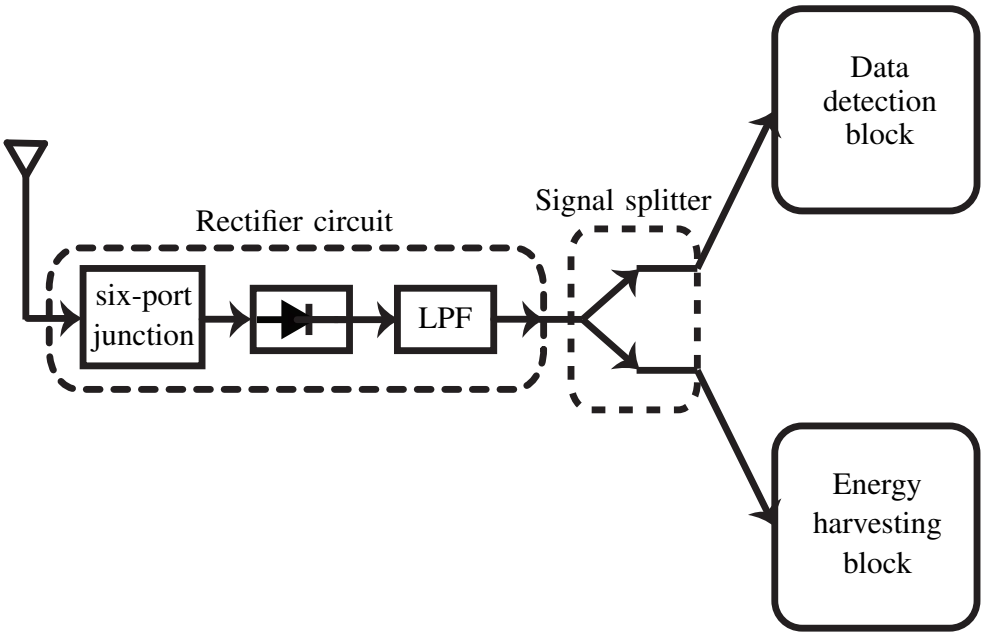

Figure 5.3 The modified block diagram with rectifier integrated into receiver.

5.2 Simultaneous Wireless Energy Harvesting and Data Communication

The main purpose of this research work is to design a six-port receiver with simultaneous wireless energy harvesting and data communication. Therefore, we need a new detector circuit of the six-port receiver to improve its RF-DC conversion efficiency and achieve its detection and harvesting capabilities at the same time. Based on the integrated rectifier and detector, the new receiver architecture is proposed.

5.2.1 Proposed Receiver Architecture

As analyzed in Chapter 4, the modulated RF and LO signals of six-port receiver are described in the complex domain as follows,

$$s_l(t) = A_{LO} \cdot e^{j(\omega t + \phi_{LO})} \tag{5.1a}$$

$$\begin{aligned} s_r(t) =& Re\{|x_B(t)| \cdot e^{j\phi_B t} \cdot A_{RF} \cdot e^{j(\omega t + \phi_{RF})}\} \\ =& A_{RF}[x_I(t)\cos(\omega_{RF} t + \phi_{RF}) - x_Q(t)\sin(\omega_{RF} t + \phi_{RF})] \end{aligned} \tag{5.1b}$$

where ω denotes angular frequency, A_{LO} and A_{RF} represent the amplitude of the RF modulated signal and local signal shown in Figure 5.4, respectively. $x_I(t) = |x_B(t)| \cdot \cos(\phi_B(t))$ and $x_Q(t) = |x_B(t)| \cdot \sin(\phi_B(t))$ are transmitted baseband I and Q data.

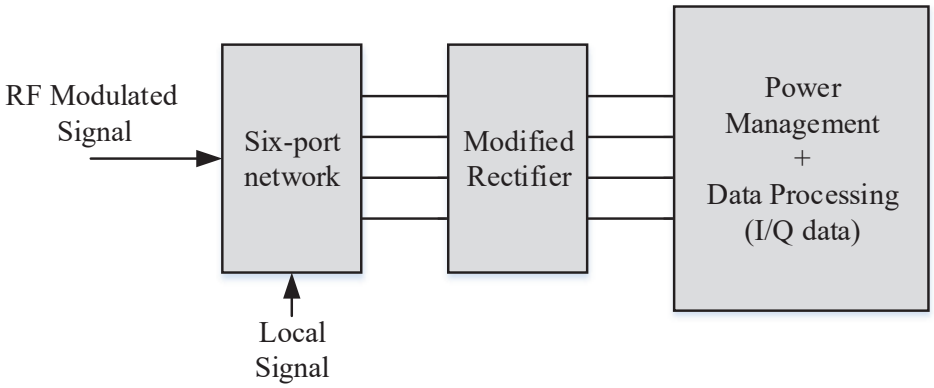

Figure 5.4 System configuration with the capability of power harvester and data communication.

And then, according to the results obtained in Chapter 4, output voltage of diode at one of four independent path can be expressed as

$$V_{oi}(t) = K \cdot \left[\frac{A_{LO}^2}{8} + \frac{A_{RF}^2}{8}|x_B(t)|^2 + \frac{A_{RF}A_{LO}}{4}|x_B(t)| \cdot \cos(\phi_B(t) - \Delta\phi_{LR} + \Delta\phi_i) \right] \quad (5.2)$$

where K is the constant value associated to parameters of selected diode, $\phi_B(t)$ is the phase of baseband signal and $\Delta\phi_{LR} = \phi_{LO} - \phi_{RF}$ is the phase difference between the modulated RF signal and LO signal, this phase difference is constant value once the system is set up and calibrated. $\Delta\phi_i$ is the path phase difference with the signal getting through interferometer. For the six-port network, the path phase difference between input port and output port for two input signal is constant value, namely, $\Delta\phi_i = \left[\begin{array}{cccc} 0, & \frac{\pi}{2}, & \pi, & \frac{3\pi}{2} \end{array} \right]$

In order to process the baseband signal after power detectors, we are concerned with (5.2) which describes the output voltage of diode. In general, from the point of frequency ω of the input RF and LO signals, the whole output voltage $V_{oi}(t)$ is DC signal with zero frequency. This entire output power can be stored and used to drive electrical device in an energy harvesting system. On the other hand, from the point of information transmission, the output voltage be considered with three components, the desired modulated information ($\frac{A_{RF}A_{LO}}{4}|x_B(t)| \cdot \cos(\phi_B(t) - \Delta\phi_{LR} + \Delta\phi_i)$), the self-mixing component of the LO signal ($\frac{A_{LO}^2}{8}$) and the product of the self-mixing component of the RF signal and the power of baseband signal ($\frac{A_{RF}^2}{8}|x_B(t)|^2$)

As explained in Chapter 4, in the conventional six-port receiver to recover the I and Q channels, the DC offset from LO as well as RF signal should be cancelled out, which leads to the waste of the rectified power. However, since we are interested to harvest the power of the

rectified signal, so we need to harvesting the energy dropped out in the conventional six-port receiver. This can be done by using a different structure of the power detector/rectifier at the output ports of the six-port junction to have energy harvesting and signal detection at the same time. The structure of the proposed six-port receiver is shown in Figure 5.4.

5.2.2 Integral Detector and Rectifier

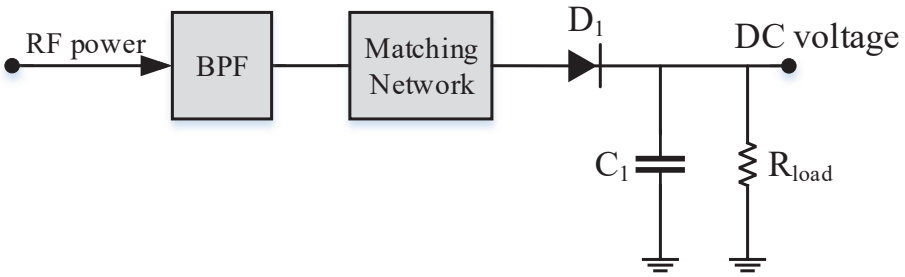

Figure 5.5 A typical structure of a detector circuit.

As an energy harvesting, RF-to-DC conversion efficiency of the rectifying circuit is another important issue which has to be considered. A typical structure of detector circuit used in a conventional six-port receiver is shown in Figure 5.5. It includes a matching circuit to match the input impedance of the Schottky diode to the six-port outputs (in our case it is matched to 50 Ω), the Schottky diode, a DC-pass filter and a resistive load. The diode that is normally employed in the detector circuit is not a good candidate for efficient RF-to-DC rectification since it has a high series resistance which causes more loss inside the diode. Therefore, we select SMS7630 to improve the RF-to-DC conversion efficiency and keep the square law to detect received signal. The detail of our proposed integrated rectifier and detector circuit has been presented in Chapter 3.

After obtaining a high efficiency rectification, we need to extract the modulated information component of DC outputs from diodes and also to harvest all remaining DC power. To achieve this purpose, we proposed two programs: adaptive voltage divider and coupling extraction of information. component

Adaptive voltage divider

Adaptive voltage divider is a straightforward method where the rectifying DC outputs power is directly divided into two streams at some rate. one stream is further proceeded to resume the baseband signal while the other stream is collected and stored to function as power source.

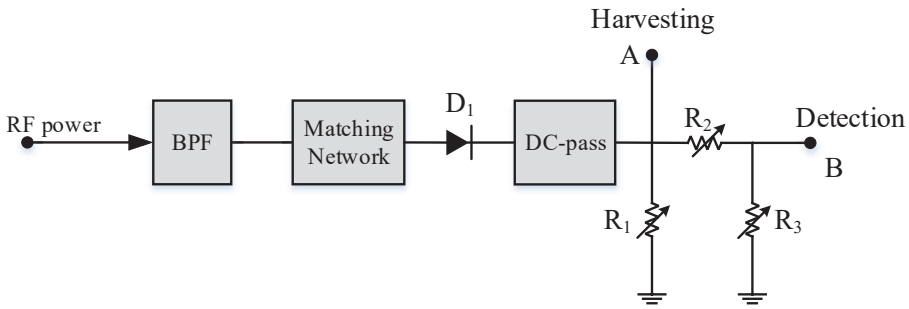

Figure 5.6 A kind of configuration of the modified detector used for simultaneous wireless energy harvesting and data communication.

An adaptive voltage divider network [5] generally consists of several variable resistors which have been designed and placed at the output of a rectifying diode circuit shown in Figure 5.5. The structure of the modified detector is shown in Figure 5.6. As it is seen in Figure 5.6, the output voltage at point A can go for harvesting while the output voltage at point B can be transmitted to differential amplifiers to perform the I and Q detection process. Here, R1, R2 and R3 are the variable resistors which determine how many percent of the rectified wave can be dedicated to the harvesting and detection process.

However, such a detector with detection and energy harvesting functions need meet two main criteria, which is also the main disadvantage: the adaptive voltage divider consists of three resistors, which consume some rectified power. The structure itself destroys the efficiency of the energy harvesting system; compared with the conventional six-port receiver, the threshold level (used to detect the transmitted data from the obtained I and Q signals) must be adjusted to obtain the best detection performance.

Coupling extraction of information component

In order to overcome the drawbacks of adaptive voltage divider proposed above, we revisit the output voltage response of diode in six-port receiver. In (5.2), the modulated information desired is contained in the third component

$$V_{oi}^{AC}(t) = \frac{A_{RF}A_{LO}}{4}|x_B(t)| \cdot \cos(\phi_B(t) - \Delta\phi_{LR} + \Delta\phi_i) \tag{5.3}$$

where 'AC' denotes this component varies as time increasing while the value is constant during one symbol time. Also note that if the modulation mode is MPSK, $|x_B(t)|$ is a constant value with time increasing and can be normalized to one. In this case, the output waveform of diode in six-port receiver is a square wave with the center value deviating from

zero up to $\frac{A_{LO}^2}{8} + \frac{A_{RF}^2}{8}$. If the modulation mode is MQAM, $|x_B(t)|$ will vary periodically with time increasing and periodic property is determined by the time length of one symbol of transmitting modulation signal. In this case, the output waveform of diode in six-port receiver is also a square wave, but the center value deviating from zero will also vary as time increases.

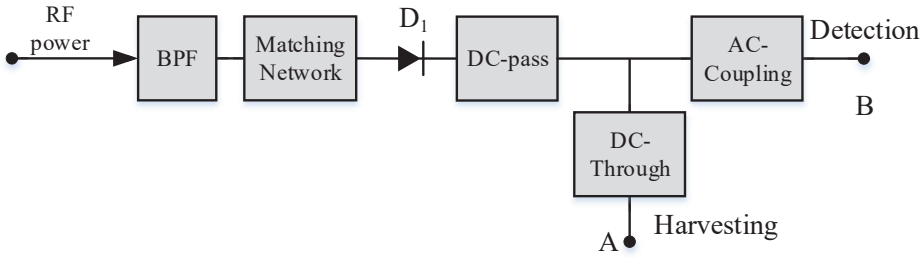

Figure 5.7 Configuration of integral detector and rectifier used for simultaneous wireless energy harvesting and data communication.

Based on the analysis mentioned above, we can conclude two points. On one hand, the output DC voltage consists of two parts, one of which is constant over time and the other of which is square wave changing over time; On the other hand, the received modulation information only exists in signal components which change over time.

In order to get the modulated information, we can employ AC coupling circuit to extract the signal component changing over time while the real DC power is harvested to support device. the proposed integral detector and rectifier is shown in Figure 5.7. The proposed program can fully obtain received information shown as in (5.3) while all of DC power is harvested. Compared to adaptive voltage divider shown in Figure 5.6, the program of coupling extraction of information component is more suitable foe our proposed receiver architecture. The fabricated prototype and performance of our proposed integrated rectifier and detector are shown in Chapter 4.

5.2.3 Systematic Simulation for Receiver Architecture of Simultaneous Wireless Power Transmission and Data Communication

AS mentioned earlier, we will employ six-port junction and integrated rectifier and detector to build receiver architecture with the capability of wireless power transmission and communication. In Chapter 4, we introduced the detail of designing the six-port junction and integrated rectifier and detector. In order to design a six-port receiver using ADS simulation at system level, the six-port junction and the rectifier-detector circuits are first designed

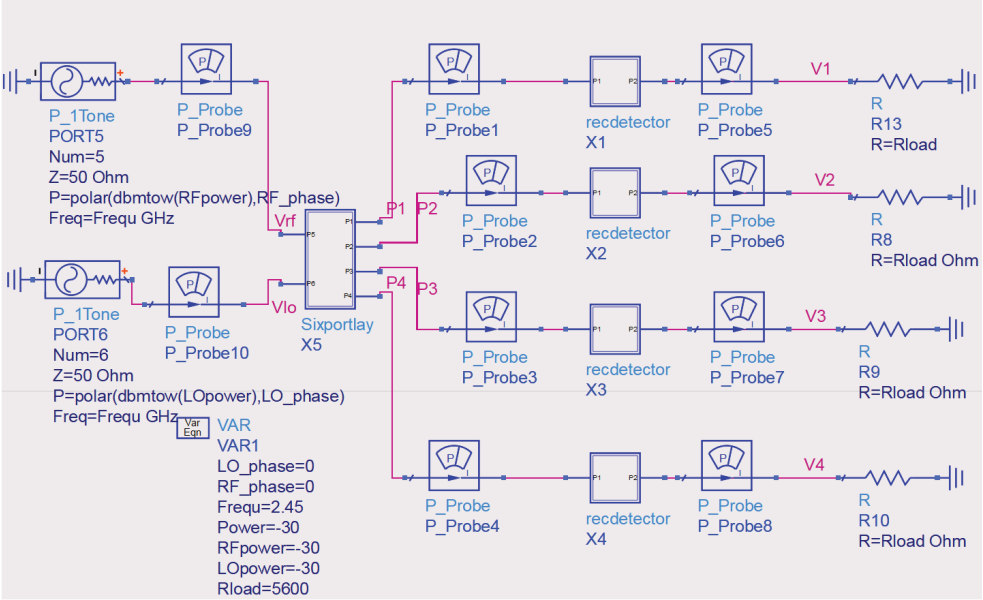

Figure 5.8 ADS simulation of a conventional six-port detector.

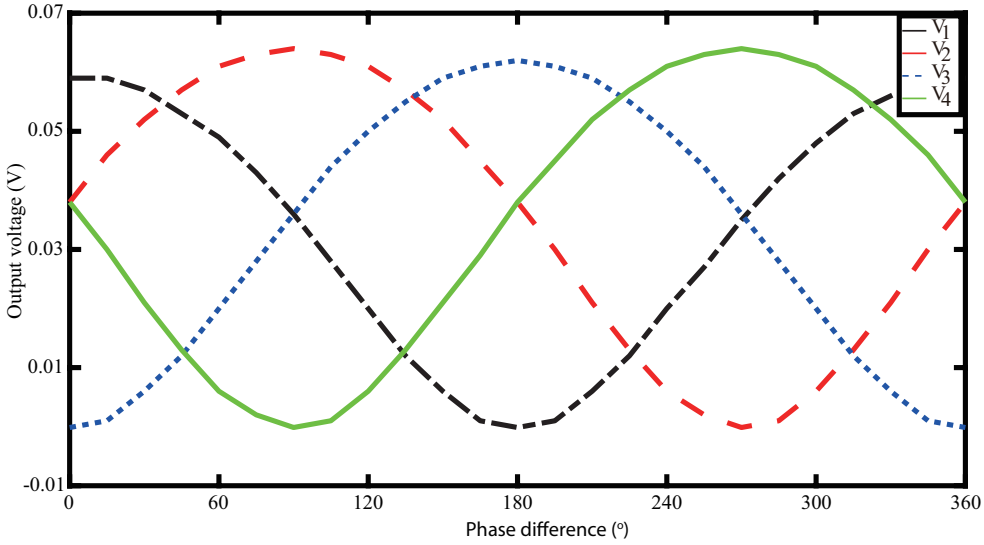

Figure 5.9 Simulated results of DC voltage versus phase difference between the two input ports of a conventional six-port.

and tested individually by ADS to make sure that the required isolation and the matching condition are met. In order to have accurate results, simulations of the six-port and rectifiers are carried out on both schematic with HB simulator and layout levels with Momentum simulator. Then, the circuit cosimulation is run to guarantee the performance of the designed modules. Before analyzing the performance of the designed receivers systematically,

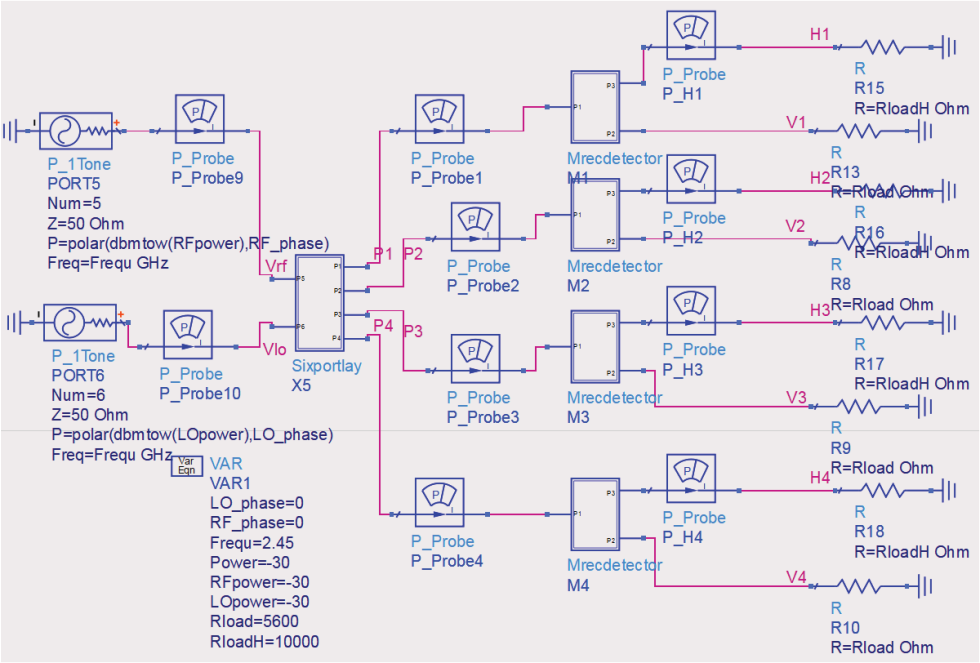

Figure 5.10 ADS simulation of six-port with the function of harvesting and data communication.

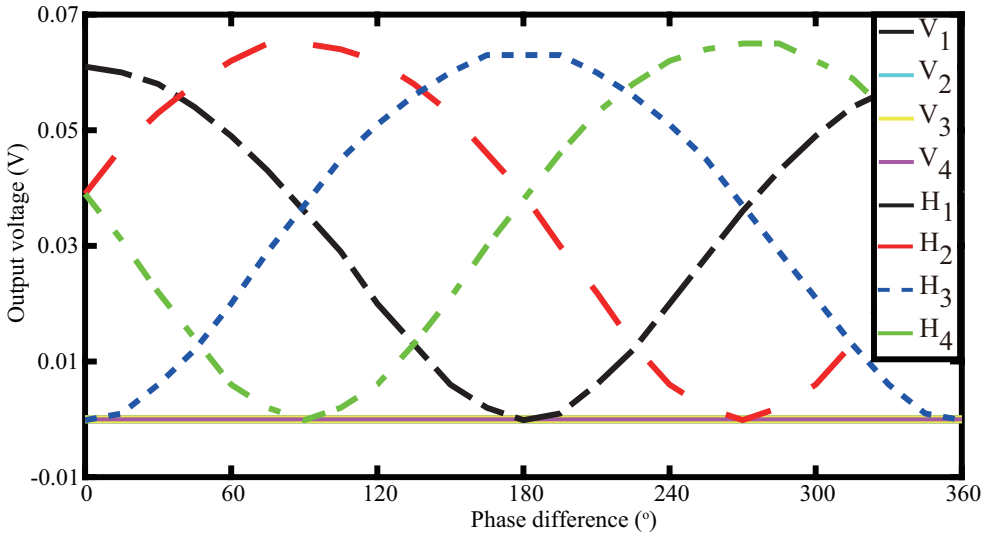

Figure 5.11 Simulated results of DC voltage versus phase difference between the two input ports of six-port with the function of harvesting and detection.

we should check the output of the rectifiers as well as the detectors which are connected to the six-port junction in the circuit simulation. The four DC outputs after rectifier-detector circuit, namely from P1 to P4 in Figure 5.8 and Figure 5.10, will be verified to meet the requirement of 90° phase shifts. In order to do so, the HB simulator is run at the operating

frequency of 2.45 GHz while the phase difference between two RF input signals (RF and LO in practical case) is swept from 0° to 360°. Figure 5.9 and Figure 5.11 show the results of the output detected voltages versus the phase difference for both circuits. Note that because HB simulator is the kind of frequency simulation, For the coupling extraction IRR, all of output voltage of IRR goes to the harvesting point. Therefore, the voltage in the detection point is zero as shown in Figure ??.

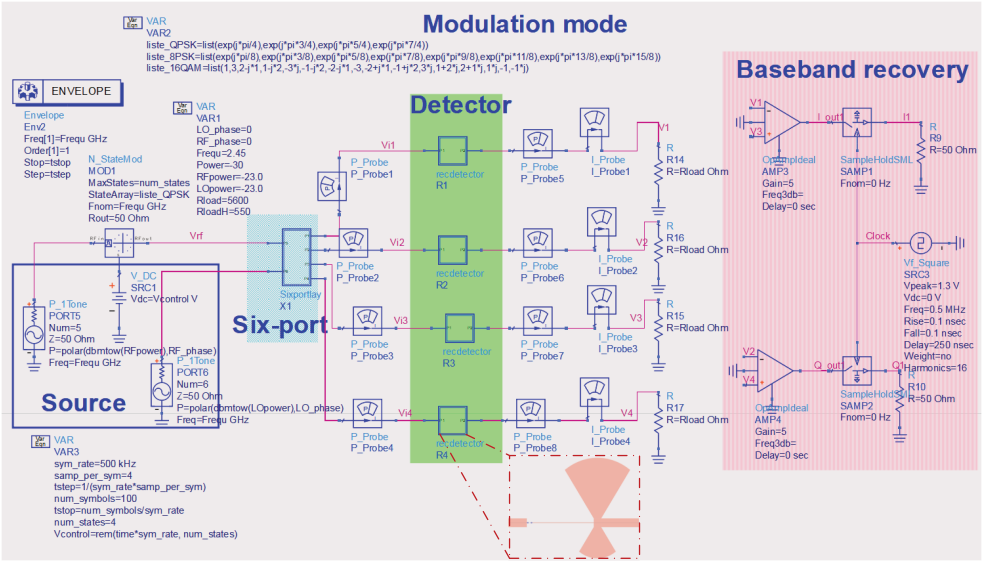

Figure 5.12 ADS simulation of a conventional six-port receiver.

when we use the adaptive voltage divider, the proposed six-port receiver has a rectifier-detector with the special design that provides the capability of harvesting and communication at the same time. The DC voltage at the output of this rectifier-detector is split by a specific ratio in such a way that some part of DC power (V1 to V4 in Figure 5.10) goes to the differential amplifiers to perform the I and Q detection process, while the rest (H1 to H4 in Figure 5.10) is sent to the harvesting unit to be stored. By comparing results shown in Figure 5.9 and Figure 5.11, it can be concluded that the level of DC voltage obtained from the proposed six-port is smaller than that achieved from the conventional model; but still the proposed configuration grants the correct phase difference which can guarantee the precision of I and Q detection.

Consequently, in order to demonstrate the demodulation capability of the two receivers, the conventional model and the other with the capability of harvesting and data communication, both receivers are simulated using the ADS envelope simulator for different types of modulation schemes (QPSK, 8PSK and 16PSK). The ADS schematics of both six-port receivers are shown in Figure 5.12 and Figure 5.13. Parameters of envelop simulation setup for QPSK

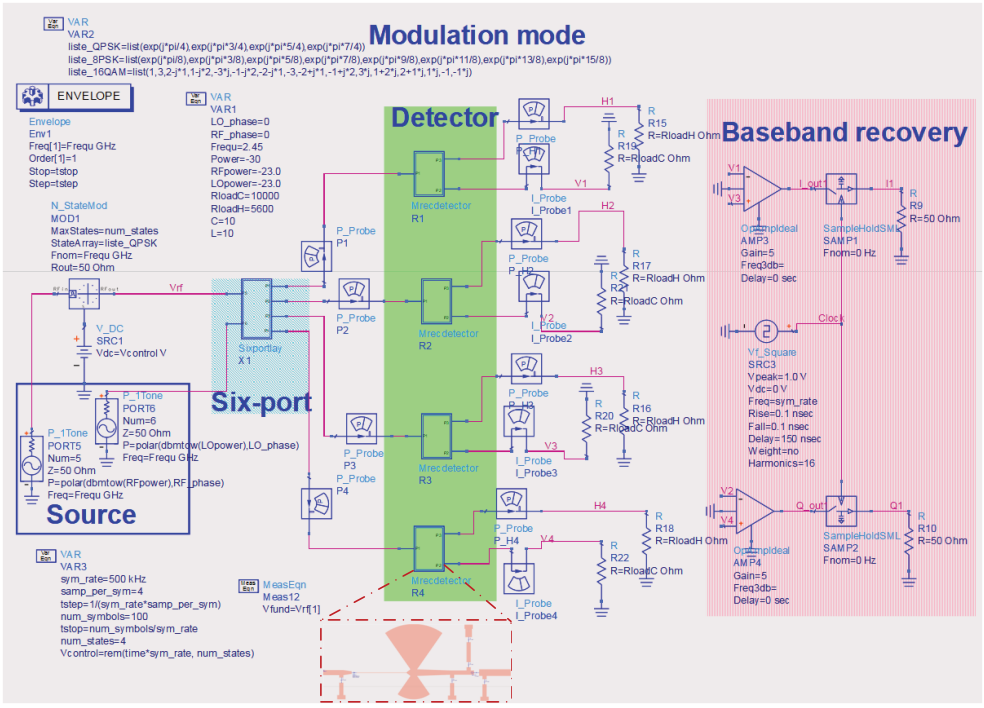

Figure 5.13 ADS simulation of the six-port receiver with the capability of simultaneous wireless power transmission and data communication .

Table 5.1 Parameters of envelop simulation setup for conventional receiver and proposed receiver.

Parameters	Units	Simulation setup
Operating frequency	GHz	2.45
Symbol rate	KHz	500
Sample rate	KHz	2000
RF power	dBm	-23
LO power	dBm	-23
RMS value of modulator	-	1
Tstop	us	200
Tstep	us	0.5
Clock frequency	KHz	500
Modulation mode	-	QPSK

modulation mode are listed in Table 5.1. As seen in Table 5.1, for both receivers, the envelop simulation is performed during 200 us with time step of 0.5 us and the operating frequency is set at 2.45 GHz. In order to verify the performance of the proposed receiver, the input power is set to -23dBm Moreover, to obtain a clearly demodulated constellation points, two sample-and-hold(SHCs) are considered at the output of differential amplifiers. The output

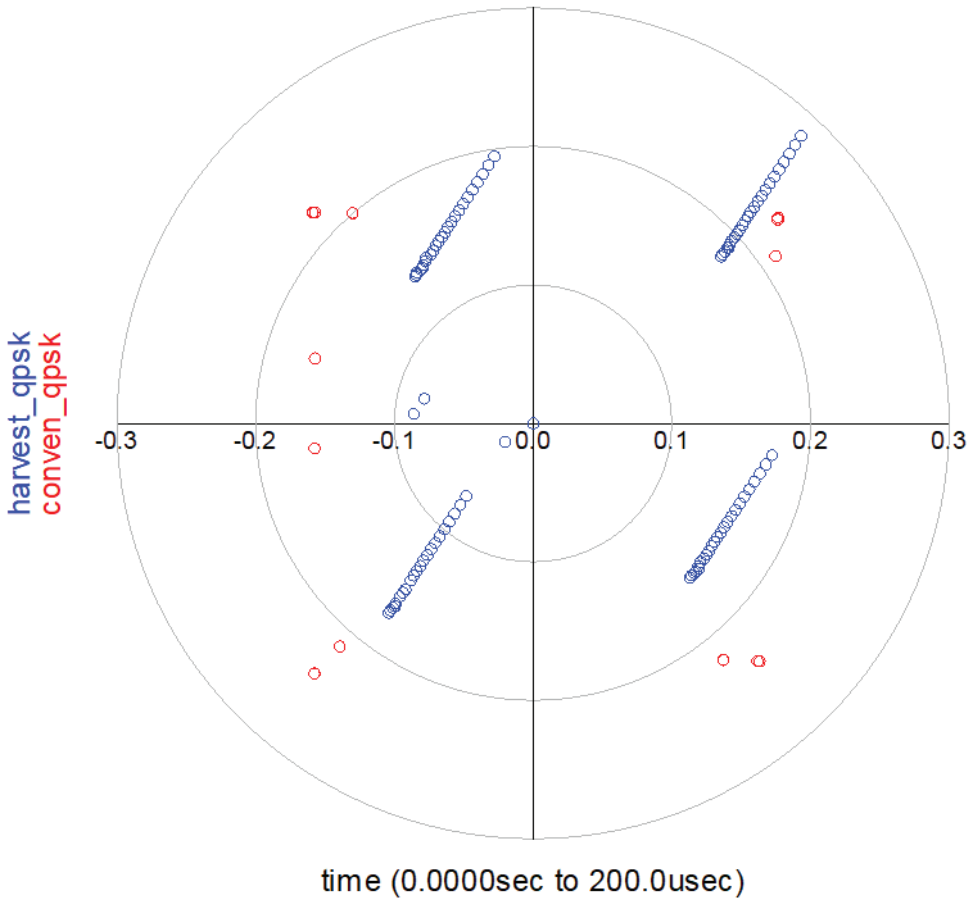

Figure 5.14 Constellation of the demodulated QPSK signal.

signals change only once at each time clock.

Therefore, the constellation is realized by discrete points. Figure 5.14, Figure 5.15 and Figure 5.16 show the related demodulated constellation diagram for each QPSK, 8PSK and 16PSK modulation. Additionally, Figure 5.14 gives the demodulated constellation diagram of 16QAM. As it is seen, all the clusters of demodulated constellations are well positioned and individualized. Notes that the clusters get through a progressive formation. The reason is that for our proposed receiver, it takes time to smoothly extract the information component from the output DC voltage by coupling method. In actual system operation, this time is very short compared to the time of the entire system and can be ignored.

For the case of receiver performing simultaneously wireless power transmission and data communication, the constellation points are closer together compared to the conventional receiver, but still the Euclidean distance is granted and the detection can be performed precisely. Since it was explained before, in the simultaneous wireless power transmission and

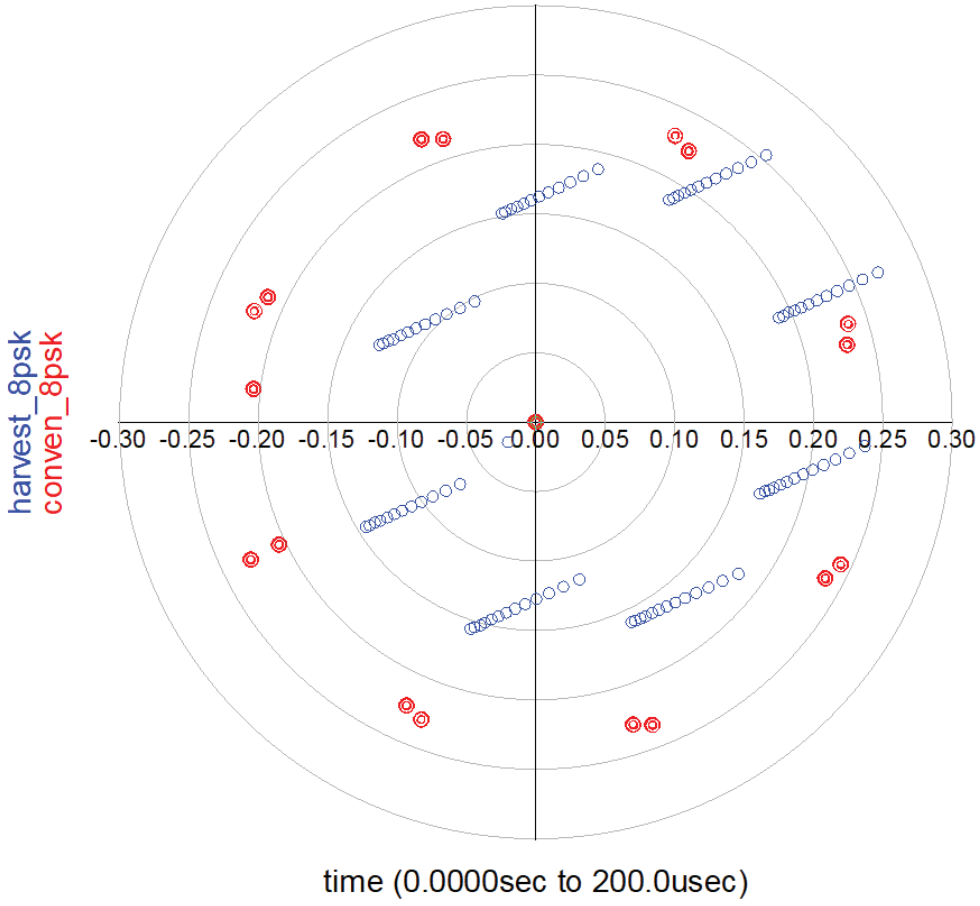

Figure 5.15 Constellation of the demodulated 8PSK signal.

data communication, the extracted DC power from V1 to V4 in Figure 5.13 are dedicated to the detection process and transferred to the differential amplifiers while the generated DC powers collected at points from H1 to H4 in Figure 5.13 are considered as the harvested powers.

For the case of QPSK modulated signal, voltage level of harvesting power is compared to that of detecting signal in the time domain, as shown in Figures 5.18 - 5.21. As shown in the curves, both signals at detection point and harvesting point experience a gradual progression. Eventually, the detecting voltage fluctuate up and down with the central value of zero voltage. According to the obtained results, it can be concluded that the designed six-port receiver can realize the energy harvesting and data communication at the same time.

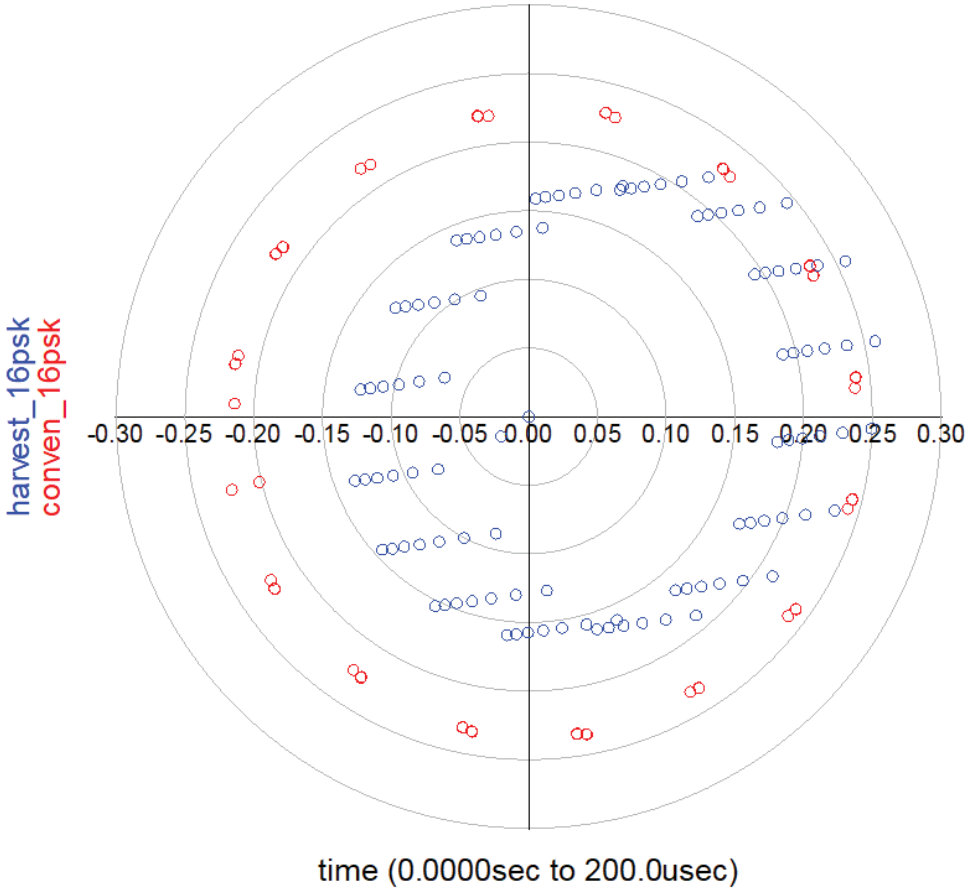

Figure 5.16 Constellation of the demodulated 16PSK signal.

5.3 Performance Analysis

5.3.1 BER performance analysis

In order to study the effect of the proposed simultaneous energy harvesting and data communication structure on the performance of the communication part, the BER of the conventional six-port and the proposed structure is compared in Figure 5.22. It is depicted that the BER of the system is not affected by employing integrated rectifier and detector, due to the fact that coupling extraction of information component has obtained entire signal energy carrying information and the signal to noise ratio remains constant.

5.3.2 Efficiency of energy harvesting

As mentioned earlier, the total efficiency of one energy harvesting is determined by antenna efficiency, matching network efficiency, parasitic efficiency, RF-DC conversion efficiency and

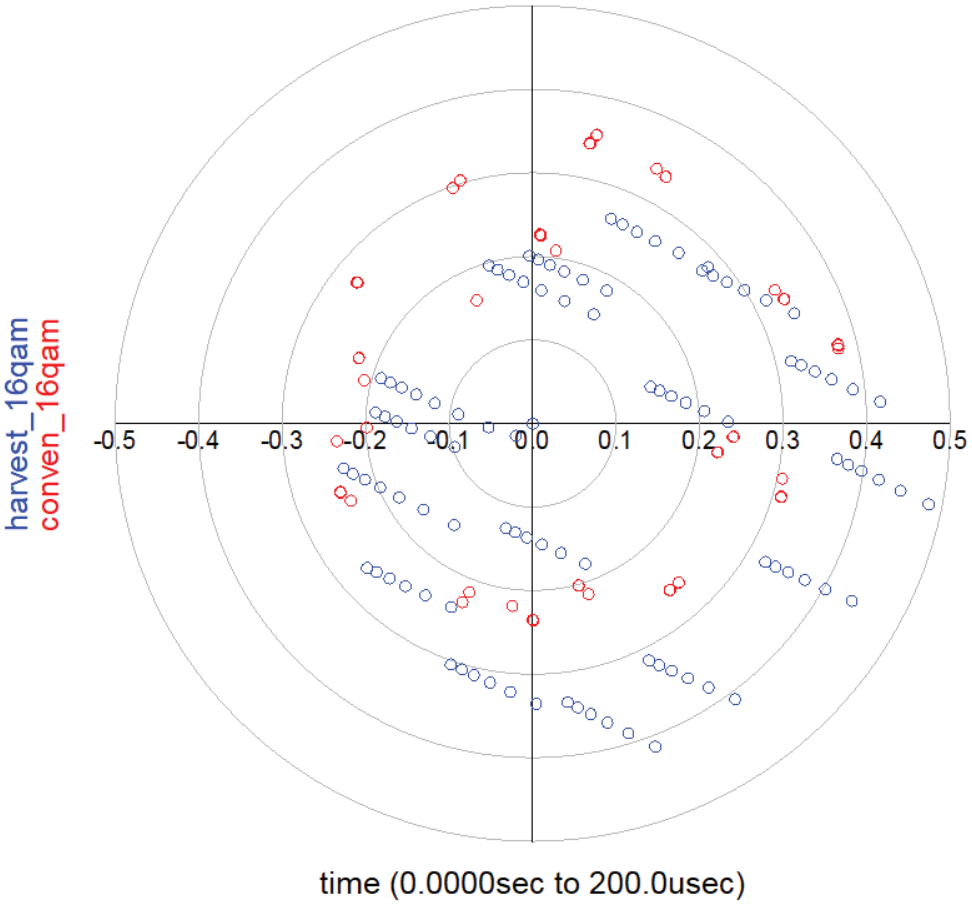

Figure 5.17 Constellation of the demodulated 16QAM signal.

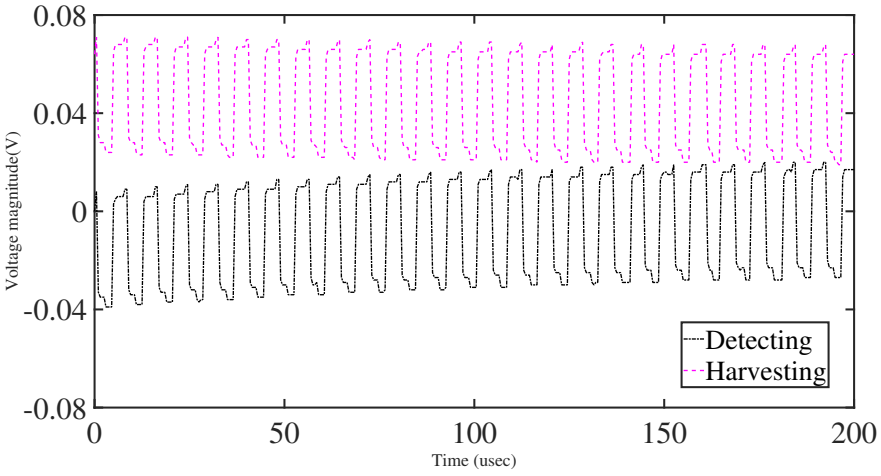

Figure 5.18 Collected DC voltage of V1 and H1 shown in Figure 5.13.

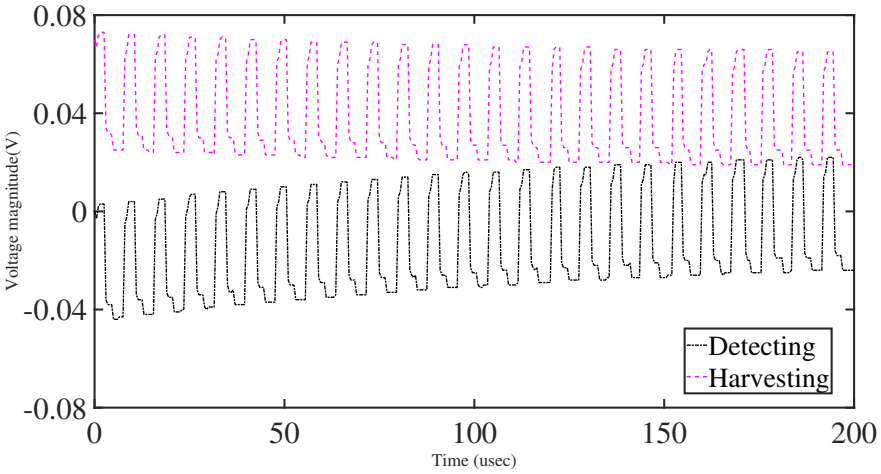

Figure 5.19 Collected DC voltage of V2 and H2 shown in Figure 5.13.

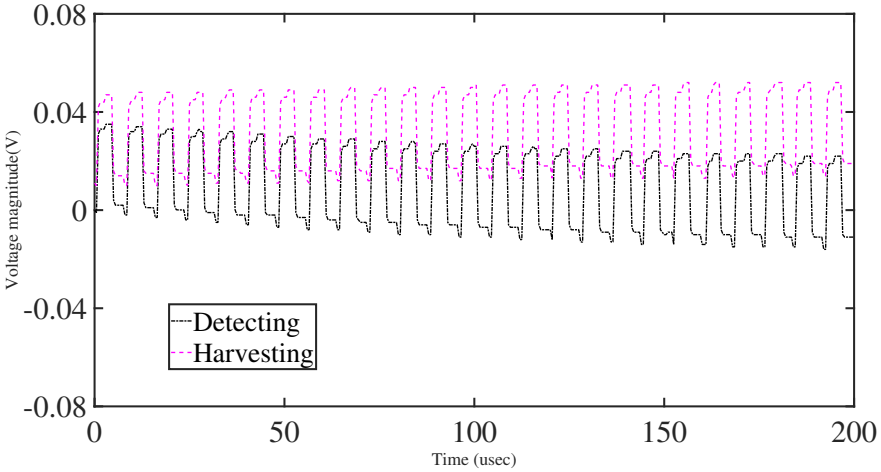

Figure 5.20 Collected DC voltage of V3 and H3 shown in Figure 5.13.

source-to-load efficiency. Here, we are focused on RF-DC conversion efficiency.For four diodes of six-port receiver, the total conversion efficiency at time t can be expressed as

$$\eta(t) = \frac{\sum_{i=1}^{4} P_{DCi}}{\sum_{i=1}^{4} P_{infi}} \tag{5.4}$$

and average RF-DC conversion efficiency in any signal transmission period can be calculated by

$$\overline{PCE} = \frac{\sum_{t=1}^{n} \eta_t}{n} \tag{5.5}$$

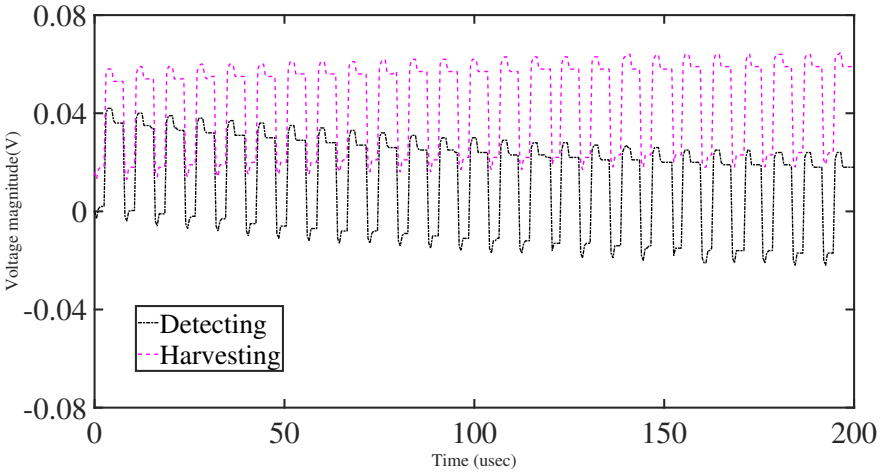

Figure 5.21 Collected DC voltage of V4 and H4 shown in Figure 5.13.

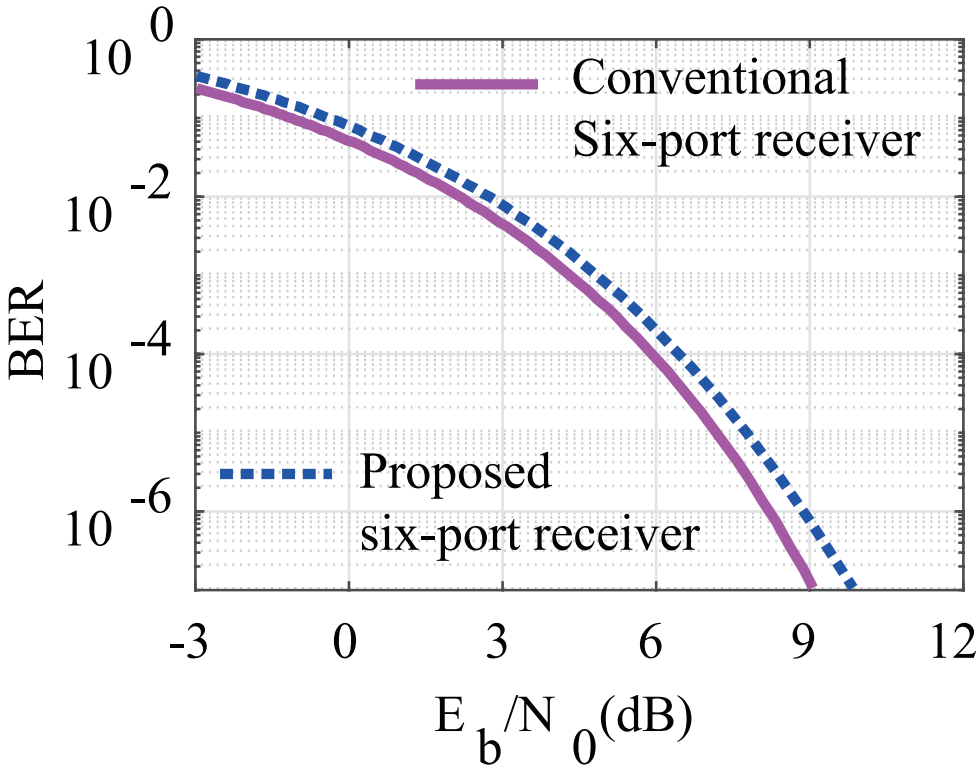

Figure 5.22 BER Performance of ADS simulation for conventional six port receiver and proposed receiver QPSK modulation.

where $n = M * R_{sps}$ is the number of receiving signal in one period. M is the number of states of signal for different modulation mode and R_{sps} is sampling rate of symbol.

By employing (5.4) and (5.5), we can get the average RF-DC conversion efficiency of conventional six-port receiver and proposed six-port receiver. At the input power of -23dBm for LO signal and RF signal, the average RF-DC conversion efficiency for both receiver is calculated for 24.789% and 19.730%, respectively. For conventional six-port receiver, the total output power after detector is proceeded to recover baseband signal, so we cannot harvest DC power. In the proposed receiver architecture, average energy harvesting efficiency is 19.730% at the input power of -23dBm for LO signal and RF signal.

5.4 Conclusion

This chapter has presented and implemented an idea of simultaneous wireless energy harvesting and data communication system. The proposed system is based on multi-port interferometer technology. Firstly, it has briefly reviewed the different configurations of wireless receivers and explained the reasons for choosing multi-port technology to design such systems. Based on the designed six-port network and the proposed rectifier circuit in Chapter 4, the design process of a special detector module with high RF-DC conversion efficiency is introduced. Next, the designed integrated rectifier and detector is connected to the six-port output to implement the receiver. Finally, the ADS simulation of a six-port receiver with power collection and data detection functions is introduced, and its performance in constellation diagram and BER is compared with traditional receivers. The simulation starts with the ideal component model provided in ADS and ends with a more realistic model obtained in EM simulation and measurement.

CHAPTER 6 CONCLUSION

6.1 Summary of Works

This dissertation presented the analysis, design and implementation of multi-port interferometer technology for simultaneous wireless energy harvesting and data communication. Combining with the diode rectifier circuit and wireless receiver technology, a research framework for this subject has been established. Therefore, to realize the proposed framework in this research, the following steps are summarized and accomplished:

- Starting from the characteristics of nonlinear devices, the application of nonlinear characteristics of devices in energy conversion and information transmission is presented and disscussed.
- Using the nonlinear characteristics of the diode, the energy conversion rectifier and the information demodulation detector are unified, and the feasibility of using a diode to achieve simultaneous energy harvesting and information transmission is theoretically analyzed and derived.
- The various configurations of the six-port network are studied and their parameters related to microwave technology are derived. Then, A six-port network composed of four hybrid couplers is designed to act as interferometer to decode the received modulation signal.
- Different architectures of wireless receivers are studied. Considering the requirement of wireless communication systems, such as compact size, low power consumption and low cost, multi-port (six-port) interferometer technology is considered to be a suitable method for developing receivers for simultaneous energy harvesting and data communication.
- A high-efficiency rectifier structure that operates at low input energy is designed and connected to a six-port junction to implement a six-port receiver.
- A coupling extraction circuit is proposed and designed to extract the data information component of the rectifier output DC signal in the time domain. This scheme can completely extract the information component, thus improving the energy harvesting efficiency of the proposed system and ensuring the performance of the wireless receiver.

- A series of ADS envelope simulations are carried out on the designed six-port receiver, which has the functions of energy harvesting and data communication at the same time. The performance of the designed receiver in terms of constellation points and BER is compared with the conventional six-port receiver.
- The energy harvesting efficiency of the proposed system was analyzed and calculated.

6.2 Future Research

As time is running out at this moment, there are many unfinished works that need to be continued. The research contributions presented in this thesis may be extended in the following ways:

- First, it is recommended to integrate the antenna, LNA, and power amplifier into the entire proposed wireless receiver and energy harvesting system to perform BER measurement and energy harvesting performance testing of the receiver.
- This work focuses on QPSK modulation and demodulation. But the potential of the six-port technology is huge. Other modulation schemes, such as high-order QAM and MPSK, can be implemented on the six-port receiver.
- Due to the fact that the sensitivity of data communication receivers is generally much higher than the sensitivity of RF energy harvesters, there is a need to improve the system of simultaneous power collection and data communication in terms of sensitivity.
- Because receivers that conduct energy harvesting and data communication simultaneously have strict operating power constraints. Therefore, existing modulation and coding schemes and algorithms for such receivers need to be adopted to increase energy harvesting efficiency and lower power consumption.
- At higher millimeter wave frequencies (such as V-band and W-band), a large number of frequency resources can be used, and the atmospheric attenuation of radio waves is also very low, therefore, the proposed simultaneous wireless power transmission and data communication system can be expanded to these bands.

REFERENCES

[1] W. C. Brown, "The history of power transmission by radio waves," *IEEE Transactions on microwave theory and techniques*, vol. 32, no. 9, pp. 1230–1242, 1984.

[2] J. O'Neill, *Prodigal genius: the life of Nikola Tesla*. Book Tree, 2007.

[3] G. Goubau and F. Schwering, "On the guided propagation of electromagnetic wave beams," *IRE Transactions on Antennas and Propagation*, vol. 9, no. 3, pp. 248–256, 1961.

[4] W. C. Brown *et al.*, "Microwave to dc converter," Mar. 25 1969, uS Patent 3,434,678.

[5] S. Ladan, "Simultaneous wireless power transmission and data communication," Ph.D. dissertation, 'E cole Polytechnique de Montr é al, 2014.

[6] B. Razavi, "Design considerations for direct-conversion receivers," *IEEE Transactions on Circuits and Systems II: Analog and Digital Signal Processing*, vol. 44, no. 6, pp. 428–435, 1997.

[7] M. Fu, C. Ma, and X. Zhu, "A cascaded boost–buck converter for high-efficiency wireless power transfer systems," *IEEE Transactions on industrial informatics*, vol. 10, no. 3, pp. 1972–1980, 2013.

[8] Z. Popovic, "Cut the cord: Low-power far-field wireless powering," *IEEE Microwave Magazine*, vol. 14, no. 2, pp. 55–62, 2013.

[9] M. D. Rohde, "Universal inductive battery charger system," Sep. 28 1999, uS Patent 5,959,433.

[10] T. Taguchi, "Vehicle charging system, vehicle charging device and electric vehicle," Jan. 17 2012, uS Patent 8,098,044.

[11] N. Shinohara and H. Matsumoto, "Experimental study of large rectenna array for microwave energy transmission," *IEEE Transactions on Microwave Theory and Techniques*, vol. 46, no. 3, pp. 261–268, 1998.

[12] L. W. Epp *et al.*, "A compact dual-polarized 8.51-ghz rectenna for high-voltage (50 v) actuator applications," *IEEE Transactions on Microwave Theory and Techniques*, vol. 48, no. 1, pp. 111–120, 2000.

[13] W. C. Brown, "The technology and application of free-space power transmission by microwave beam," *Proceedings of the IEEE*, vol. 62, no. 1, pp. 11–25, 1974.

[14] J. O. McSpadden and J. C. Mankins, "Space solar power programs and microwave wireless power transmission technology," *IEEE microwave magazine*, vol. 3, no. 4, pp. 46–57, 2002.

[15] B. Strassner and K. Chang, "Microwave power transmission: Historical milestones and system components," *Proceedings of the IEEE*, vol. 101, no. 6, pp. 1379–1396, 2013.

[16] Y.-H. Suh and K. Chang, "A high-efficiency dual-frequency rectenna for 2.45-and 5.8-ghz wireless power transmission," *IEEE Transactions on Microwave Theory and Techniques*, vol. 50, no. 7, pp. 1784–1789, 2002.

[17] S. Hemour *et al.*, "Towards low-power high-efficiency rf and microwave energy harvesting," *IEEE transactions on microwave theory and techniques*, vol. 62, no. 4, pp. 965–976, 2014.

[18] N. Shinohara, *Recent wireless power transfer technologies via radio waves*. River Publishers, 2018.

[19] C. Song *et al.*, "A high-efficiency broadband rectenna for ambient wireless energy harvesting," *IEEE Transactions on Antennas and Propagation*, vol. 63, no. 8, pp. 3486–3495, 2015.

[20] A. Mavaddat, S. H. M. Armaki, and A. R. Erfanian, "Millimeter-wave energy harvesting using 4×4 microstrip patch antenna array," *IEEE Antennas and wireless propagation letters*, vol. 14, pp. 515–518, 2014.

[21] H. Miyagoshi *et al.*, "High-impedance wideband folded dipole antenna for energy harvesting applications," in *2014 International Symposium on Antennas and Propagation Conference Proceedings*. IEEE, 2014, pp. 601–602.

[22] M. Arrawatia, M. S. Baghini, and G. Kumar, "Broadband rf energy harvesting system covering cdma, gsm900, gsm1800, 3g bands with inherent impedance matching," in *2016 IEEE MTT-S International Microwave Symposium (IMS)*. IEEE, 2016, pp. 1–3.

[23] ——, "Broadband bent triangular omnidirectional antenna for rf energy harvesting," *IEEE Antennas and Wireless Propagation Letters*, vol. 15, pp. 36–39, 2015.

[24] D. Wang, X. A. Nghiem, and R. Negra, "Design of a 57% bandwidth microwave rectifier for powering application," in *2014 IEEE Wireless Power Transfer Conference*. IEEE, 2014, pp. 68–71.

[25] C. H. Petzl Lorenz, "M 'e physical mechanisms and theoretical foundations of the reuse of ambient microwave energy for devices wireless 'a low consumption," Ph.D. dissertation, 'E cole Polytechnique de Montr é al, 2015.

[26] T. Guo, Q. Zhang, and K. Wu, "A simple high-efficiency rectifier for low power harvesting," in *2018 IEEE Wireless Power Transfer Conference (WPTC)*. IEEE, 2018, pp. 1–3.

[27] D. Wang, M.-D. Wei, and R. Negra, "Design of a broadband microwave rectifier from 40 mhz to 4740 mhz using high impedance inductor," in *2014 Asia-Pacific Microwave Conference*. IEEE, 2014, pp. 1010–1012.

[28] A. Collado and A. Georgiadis, "24 ghz substrate integrated waveguide (siw) rectenna for energy harvesting and wireless power transmission," in *2013 IEEE MTT-S International Microwave Symposium Digest (MTT)*. IEEE, 2013, pp. 1–3.

[29] Z. Liu, Z. Zhong, and Y.-X. Guo, "Enhanced dual-band ambient rf energy harvesting with ultra-wide power range," *IEEE microwave and wireless components letters*, vol. 25, no. 9, pp. 630–632, 2015.

[30] T. W. Barton, J. M. Gordonson, and D. J. Perreault, "Transmission line resistance compression networks and applications to wireless power transfer," *IEEE Journal of Emerging and Selected Topics in Power Electronics*, vol. 3, no. 1, pp. 252–260, 2014.

[31] S. H. Abdelhalem, P. S. Gudem, and L. E. Larson, "An rf–dc converter with wide-dynamic-range input matching for power recovery applications," *IEEE Transactions on Circuits and Systems II: Express Briefs*, vol. 60, no. 6, pp. 336–340, 2013.

[32] C. H. P. Lorenz *et al.*, "Breaking the efficiency barrier for ambient microwave power harvesting with heterojunction backward tunnel diodes," *IEEE Transactions on Microwave Theory and Techniques*, vol. 63, no. 12, pp. 4544–4555, 2015.

[33] A. Sharma *et al.*, "A carbon nanotube optical rectenna," *Nature nanotechnology*, vol. 10, no. 12, pp. 1027–1032, 2015.

[34] X. Gu, S. Hemour, and K. Wu, "Enabling far-field ambient energy harvesting through multi-physical sources," in *2018 Asia-Pacific Microwave Conference (APMC)*. IEEE, 2018, pp. 204–206.

[35] X. Gu *et al.*, "Hybridization of integrated microwave and mechanical power harvester," *IEEE Access*, vol. 6, pp. 13 921–13 930, 2018.

[36] C. H. Lorenz *et al.*, "Hybrid power harvesting for increased power conversion efficiency," *IEEE Microwave and Wireless Components Letters*, vol. 25, no. 10, pp. 687–689, 2015.

[37] X. Gu *et al.*, "Integrated cooperative ambient power harvester collecting ubiquitous radio frequency and kinetic energy," *IEEE Transactions on Microwave Theory and Techniques*, vol. 66, no. 9, pp. 4178–4190, 2018.

[38] X. Gu, S. Hemour, and K. Wu, "Integrated cooperative radiofrequency (rf) and kinetic energy harvester," in *2017 IEEE Wireless Power Transfer Conference (WPTC)*. IEEE, 2017, pp. 1–3.

[39] ——, "Cooperative radiofrequency (rf) and piezoelectric energy harvesting for global efficiency enhancement," in *Proc. 32nd URSI GASS*, 2017, p. 1.

[40] F. Giuppi *et al.*, "Challenges in energy harvesting techniques for autonomous self-powered wireless sensors," in *2013 European Microwave Conference*. IEEE, 2013, pp. 854–857.

[41] L. Guo *et al.*, "Collaboratively harvesting ambient radiofrequency and thermal energy," *IEEE Transactions on Industrial Electronics*, vol. 67, no. 5, pp. 3736–3746, 2019.

[42] X. Gu, S. Hemour, and K. Wu, "Low thermally activated schottky barrier rectifier: A new class of energy harvester," in *2019 IEEE International Conference on RFID Technology and Applications (RFID-TA)*. IEEE, 2019, pp. 76–79.

[43] X. Gu *et al.*, "Accurate analytical model for hybrid ambient thermal and rf energy harvester," in *2018 IEEE/MTT-S International Microwave Symposium-IMS*. IEEE, 2018, pp. 1122–1125.

[44] ——, "Diplexer-based fully passive harmonic transponder for sub-6-ghz 5g-compatible iot applications," *IEEE Transactions on Microwave Theory and Techniques*, vol. 67, no. 5, pp. 1675–1687, 2018.

[45] X. Gu, S. Hemour, and K. Wu, "Improving conversion loss performance of fully passive harmonic transponder at low temperature," in *2019 IEEE Wireless Power Transfer Conference (WPTC)*. IEEE, 2019, pp. 395–398.

[46] X. Gu *et al.*, "Analysis and exploitation of diplexer-based fully passive harmonic transponder for 5g applications," in *2018 IEEE MTT-S International Microwave Workshop Series on 5G Hardware and System Technologies (IMWS-5G)*. IEEE, 2018, pp. 1–3.

[47] A. Collado and A. Georgiadis, "Optimal waveforms for efficient wireless power transmission," *IEEE Microwave and Wireless Components Letters*, vol. 24, no. 5, pp. 354–356, 2014.

[48] A. J. S. Boaventura *et al.*, "Spatial power combining of multi-sine signals for wireless power transmission applications," *IEEE Transactions on Microwave Theory and Techniques*, vol. 62, no. 4, pp. 1022–1030, 2014.

[49] L. Rizo, M. Ruiz, and J. García, "Device characterization and modeling for the design of uhf class-e inverters and synchronous rectifiers," in *2014 IEEE 15th Workshop on Control and Modeling for Power Electronics (COMPEL)*. IEEE, 2014, pp. 1–5.

[50] M. Litchfield *et al.*, "High-efficiency x-band mmic gan power amplifiers operating as rectifiers," in *2014 IEEE MTT-S International Microwave Symposium (IMS2014)*. IEEE, 2014, pp. 1–4.

[51] M. Ruiz and J. García, "An e-phemt self-biased and self-synchronous class e rectifier," in *2014 IEEE MTT-S International Microwave Symposium (IMS2014)*. IEEE, 2014, pp. 1–4.

[52] J.-W. Yang and H.-L. Do, "High-efficiency zvs ac-dc led driver using a self-driven synchronous rectifier," *IEEE Transactions on Circuits and Systems I: Regular Papers*, vol. 61, no. 8, pp. 2505–2512, 2014.

[53] C. H. P. Lorenz, S. Hemour, and K. Wu, "Physical mechanism and theoretical foundation of ambient rf power harvesting using zero-bias diodes," *IEEE Transactions on Microwave Theory and Techniques*, vol. 64, no. 7, pp. 2146–2158, 2016.

[54] "An-288 system-oriented dc-dc conversion techniques," *Texas Instruments2013.*

[55] Y. Huang, N. Shinohara, and T. Mitani, "A constant efficiency of rectifying circuit in an extremely wide load range," *IEEE Transactions on Microwave Theory and Techniques*, vol. 62, no. 4, pp. 986–993, 2013.

[56] G. F. Engen, "The six-port reflectometer: An alternative network analyzer," *IEEE Transactions on microwave theory and techniques*, vol. 25, no. 12, pp. 1075–1080, 1977.

[57] C. A. Hoer, "The six-port coupler: A new approach to measuring voltage, current, power, impedance, and phase," *IEEE Transactions on Instrumentation and Measurement*, vol. 21, no. 4, pp. 466–470, 1972.

[58] G. F. Engen, "The six-port measurement technique-a status report," *Microwave Journal*, vol. 21, pp. 18–89, 1978.

[59] F. Ghannouchi, Y. Xu, and R. Bosisio, "One-step connection method for the measurement of n-port microwave networks using six-port techniques," *IEE Proceedings-Microwaves, Antennas and Propagation*, vol. 141, no. 4, pp. 285–289, 1994.

[60] T. Oishi and W. K. Kahn, "Stokes vector representation of the six-port network analyzer: Calibration and measurement," in *1985 IEEE MTT-S International Microwave Symposium Digest*. IEEE, 1985, pp. 503–506.

[61] C. G. Miguelez *et al.*, "A new automobile radar based on the six-port phase/frequency discriminator," *IEEE Transactions on vehicular technology*, vol. 49, no. 4, pp. 1416–1423, 2000.

[62] M. Bialkowski and G. Woods, "Application of a six-port network to a near-field antenna measurement system," *Electronics Letters*, vol. 21, no. 23, pp. 1066–1068, 1985.

[63] T. Yakabe *et al.*, "Six-port based wave-correlator with application to beam direction finding," *IEEE Transactions on instrumentation and Measurement*, vol. 50, no. 2, pp. 377–380, 2001.

[64] F. M. Ghannouchi and R. G. Bosisio, "Measurement of microwave permittivity using a six-port reflectometer with an open-ended coaxial line," *IEEE transactions on instrumentation and measurement*, vol. 38, no. 2, pp. 505–508, 1989.

[65] Y. Zhang *et al.*, "Six-port optical reflectometer," *IEEE transactions on instrumentation and measurement*, vol. 40, no. 5, pp. 869–871, 1991.

[66] S. Bensmida *et al.*, "New time-domain voltage and current waveform measurement setup for power amplifier characterization and optimization," *IEEE transactions on microwave theory and techniques*, vol. 56, no. 1, pp. 224–231, 2008.

[67] J. Li, R. Bosisio, and K. Wu, "A six-port direct digital millimeter wave receiver," in *1994 IEEE MTT-S International Microwave Symposium Digest (Cat. No. 94CH3389-4)*. IEEE, 1994, pp. 1659–1662.

[68] J. Li, R. G. Bosisio, and K. Wu, "Computer and measurement simulation of a new digital receiver operating directly at millimeter-wave frequencies," *IEEE Transactions on Microwave Theory and Techniques*, vol. 43, no. 12, pp. 2766–2772, 1995.

[69] S. O. Tatu *et al.*, "A new direct millimeter-wave six-port receiver," *IEEE Transactions on microwave theory and techniques*, vol. 49, no. 12, pp. 2517–2522, 2001.

[70] R. Bosisio *et al.*, "New-wave radio," *IEEE Microwave Magazine*, vol. 9, no. 1, pp. 89–100, 2008.

[71] T. Eireiner and T. Müller, "Six-port receiver for mm-wave-concept, evaluation and implementation," *Proc. IST Mobile and Wireless CDommunications Summit, Dresden*, vol. 19, p. 23, 2005.

[72] N. Khaddaj Mallat, E. Moldovan, and S. O. Tatu, "Comparative demodulation results for six-port and conventional 60 ghz direct conversion receivers," *Progress In Electromagnetics Research*, vol. 84, pp. 437–449, 2008.

[73] T. Müller, S. Herter, and J. Luy, "Clock generator phase noise in rf sampling receivers," in *Proc. of the 2nd Karlsruhe Workshop on Software Radios*, 2002, pp. 13–18.

[74] H. Packard, "The schottky diode mixer," *The Schottky Diode Mixer*, vol. Application Note 995.

[75] J. Jürgensen *et al.*, "Baseband aspects of a direct conversion receiver concept using five-port technology," in *2nd Karlsruhe Workshop on Software Radio, Karlsruhe, March 2002 Proc*, 2002.

[76] Y. Demers, R. Bosisio, and F. Ghannouchi, "Repetitive and single shot pulse microwave six-port reflectometer," *IEEE transactions on instrumentation and measurement*, vol. 39, no. 1, pp. 195–200, 1990.

[77] M. E. Hines, "The virtues of nonlinearity-detection, frequency conversion, parametric amplification and harmonic generation," *IEEE Transactions on Microwave Theory and Techniques*, vol. 32, no. 9, pp. 1097–1104, 1984.

[78] F. T. Ulaby, R. K. Moore, and A. K. Fung, "Microwave remote sensing: Active and passive. volume 1-microwave remote sensing fundamentals and radiometry," 1981.

[79] S. A. Maas, "Microwave mixers," *ah*, 1986.

[80] D. M. Pozar, *Microwave engineering*. John Wiley & Sons, 2009.

[81] S. M. Sze and K. K. Ng, *Physics of semiconductor devices.* John wiley & sons, 2006.

[82] W. Shockley, "The theory of p-n junctions in semiconductors and p-n junction transistors," *Bell System Technical Journal*, vol. 28, no. 3, pp. 435–489, 1949.

[83] S. Yngvesson, *Microwave semiconductor devices.* Springer Science & Business Media, 2012, vol. 134.

[84] S. A. Maas, *Nonlinear microwave and RF circuits.* Artech house, 2003.

[85] H. C. W. Torrey, C. Austin, and S. A. Goudsmit, *Crystal Rectifiers.* New York, NY, USA: McGraw-Hill,, 1948.

[86] A. Koelpin *et al.*, "The six-port in modern society," *IEEE Microwave Magazine*, vol. 11, no. 7, pp. 35–43, 2010.

[87] S. O. Tatu *et al.*, "Ka-band analog front-end for software-defined direct conversion receiver," *IEEE Transactions on Microwave Theory and Techniques*, vol. 53, no. 9, pp. 2768–2776, 2005.

[88] S. O. Tatu and E. Moldovan, "V-band multiport heterodyne receiver for high-speed communication systems," *EURASIP Journal on Wireless Communications and networking*, vol. 2007, no. 1, p. 034358, 2006.

[89] E. Moldovan, S. Tatu, and S. Affes, "A 60 ghz multi-port receiver with analog carrier recovery for ultra wideband wireless personal area networks," in *2008 European Conference on Wireless Technology.* IEEE, 2008, pp. 358–361.

[90] K. Wu, "Multiport interferometer techniques for innovative transceiver applications," in *2010 IEEE Radio and Wireless Symposium (RWS).* IEEE, 2010, pp. 531–534.

[91] S.-H. Li and R. G. Bosisio, "The automatic measurement of tv-port microwave junctions by means of the six-port technique," *IEEE Transactions on Instrumentation and Measurement*, no. 1, pp. 40–43, 1982.

[92] E. Moldovan *et al.*, "A new 94-ghz six-port collision-avoidance radar sensor," *IEEE Transactions on Microwave Theory and Techniques*, vol. 52, no. 3, pp. 751–759, 2004.

[93] E. Marsan *et al.*, "C-band direct digital receiver mmic," in *2002 9th International Symposium on Antenna Technology and Applied Electromagnetics.* IEEE, 2002, pp. 1–4.

[94] J.-F. Gagne *et al.*, "High-speed low-cost direct conversion digital receiver," in *2001 IEEE MTT-S International Microwave Sympsoium Digest (Cat. No. 01CH37157)*, vol. 2. IEEE, 2001, pp. 1093–1096.

[95] T.-W. Yoo and K. Chang, "Theoretical and experimental development of 10 and 35 ghz rectennas," *IEEE Transactions on Microwave Theory and Techniques*, vol. 40, no. 6, pp. 1259–1266, 1992.

[96] J. O. McSpadden, L. Fan, and K. Chang, "Design and experiments of a high-conversion-efficiency 5.8-ghz rectenna," *IEEE Transactions on Microwave Theory and Techniques*, vol. 46, no. 12, pp. 2053–2060, 1998.

[97] S. Ladan and K. Wu, "35 ghz harmonic harvesting rectifier for wireless power transmission," in *2014 IEEE MTT-S International Microwave Symposium (IMS2014)*. IEEE, 2014, pp. 1–4.

[98] C. R. Valenta and G. D. Durgin, "Harvesting wireless power: Survey of energy-harvester conversion efficiency in far-field, wireless power transfer systems," *IEEE Microwave Magazine*, vol. 15, no. 4, pp. 108–120, 2014.

[99] H. J. Visser and R. J. Vullers, "Rf energy harvesting and transport for wireless sensor network applications: Principles and requirements," *Proceedings of the IEEE*, vol. 101, no. 6, pp. 1410–1423, 2013.

[100] S. Ladan *et al.*, "Highly efficient compact rectenna for wireless energy harvesting application," *IEEE microwave magazine*, vol. 14, no. 1, pp. 117–122, 2013.

[101] H. Sun *et al.*, "Design of a high-efficiency 2.45-ghz rectenna for low-input-power energy harvesting," *IEEE Antennas and Wireless Propagation Letters*, vol. 11, pp. 929–932, 2012.

[102] U. Olgun, C.-C. Chen, and J. L. Volakis, "Investigation of rectenna array configurations for enhanced rf power harvesting," *IEEE antennas and wireless propagation letters*, vol. 10, pp. 262–265, 2011.

[103] H. Sun *et al.*, "A dual-band rectenna using broadband yagi antenna array for ambient rf power harvesting," *IEEE Antennas and Wireless Propagation Letters*, vol. 12, pp. 918–921, 2013.

[104] L. R. Varshney, "Transporting information and energy simultaneously," in *2008 IEEE International Symposium on Information Theory*. IEEE, 2008, pp. 1612–1616.

[105] P. Grover and A. Sahai, "Shannon meets tesla: Wireless information and power transfer," in *2010 IEEE international symposium on information theory*. IEEE, 2010, pp. 2363–2367.

[106] R. Zhang and C. K. Ho, "Mimo broadcasting for simultaneous wireless information and power transfer," *IEEE Transactions on Wireless Communications*, vol. 12, no. 5, pp. 1989–2001, 2013.

[107] K. Huang and E. Larsson, "Simultaneous information and power transfer for broadband wireless systems," *IEEE Transactions on Signal Processing*, vol. 61, no. 23, pp. 5972–5986, 2013.

[108] A. Costanzo and D. Masotti, "Energizing 5g: Near-and far-field wireless energy and data trantransfer as an enabling technology for the 5g iot," *IEEE Microwave Magazine*, vol. 18, no. 3, pp. 125–136, 2017.

[109] S. Claessens *et al.*, "Measurement-based analysis of the throughput-power level trade-off with modulated multisine signals in a swipt system," in *2017 89th ARFTG Microwave Measurement Conference (ARFTG)*. IEEE, 2017, pp. 1–4.